論文 / 著書情報
Article / Book Information

題目(和文)	種々の組成の液晶セグメントを有するブロック共重合体のミクロ相分離構造と液晶相転移挙動
Title(English)	Microdomain structure and phase behavior in block copolymers with various compositions of liquid crystalline segments
著者(和文)	伊藤大道
Author(English)	
出典(和文)	学位:博士(工学), 学位授与機関:東京工業大学, 報告番号:甲第5001号, 授与年月日:2002年3月26日, 学位の種別:課程博士, 審査員:
Citation(English)	Degree:Doctor (Engineering), Conferring organization: Tokyo Institute of Technology, Report number:甲第5001号, Conferred date:2002/3/26, Degree Type:Course doctor, Examiner:
学位種別(和文)	博士論文
Type(English)	Doctoral Thesis

Microdomain Structure and Phase Behavior in Block Copolymers with Various Compositions of Liquid Crystalline Segments

Tomomichi Itoh

2002

Table of Contents

Chapter 2

Chapter 4

Chapter 5

Chapter 6

Interrelation between Microdomain Structure and Liquid Crystalline Phase Behavior in AB Type Block Copolymers Containing Polystyrene and Nematic Side-Chain Liquid Crystalline Segment **106**

Chapter 7

Chapter 1

General Introduction

1.1. Introduction

Nano-technology (NT) is exposed to be a technology of a new era in the world of science and technology, not only researchers, but also politicians and industries hope its potential, which enables to produce high efficient materials such as micro-machine, memory device, quantum device, filter, sensor, biomedical materials, *etc.* Bill Clinton (January 2000) stated that the NT is the most important industry as well as information technology (IT) and biotechnology and the budget supported a major new National Nano-technology Initiative, worth $500 million in the year. He said that the NT is the ability to manipulate matter in the atomic and molecular levels. The latter level, nano-ordered structure can be made by the NT. Many techniques have been revealed for composing the nano-scale structures, such as self-organized organic materials including crystals, liquid crystals, colloids, micelles, emulsions and *etc.*

1.1.1. Microdomain Structures of Block Copolymers

Block copolymers[1] are also categorized in self-organized materials. They form well-ordered microdomains such as lamellae, cylinders, spheres, bicontinuous morphologies, and so on. They have nano-ordered size, depending on volume fractions of the each segment. Control of the morphologies and these sizes is necessary to prepare tailor-made nano-ordered structures. We can prepare tailor-made morphologies and sizes with controlling the molecular weight of each segment by living polymerizations. Additionally, the size and morphologies can be controlled by temperature. In 1980 Leibler drew a morphological diagram in which the morphologies depended on the volume fractions of each segment, degree of polymerization, and Flory χ parameter. Interestingly, the morphological diagram predicted that not only order-disorder transition (ODT) but also order-order transition (OOT) took place. ODT is a transition between microphase segregated structure (orderd phase) and homogeneous

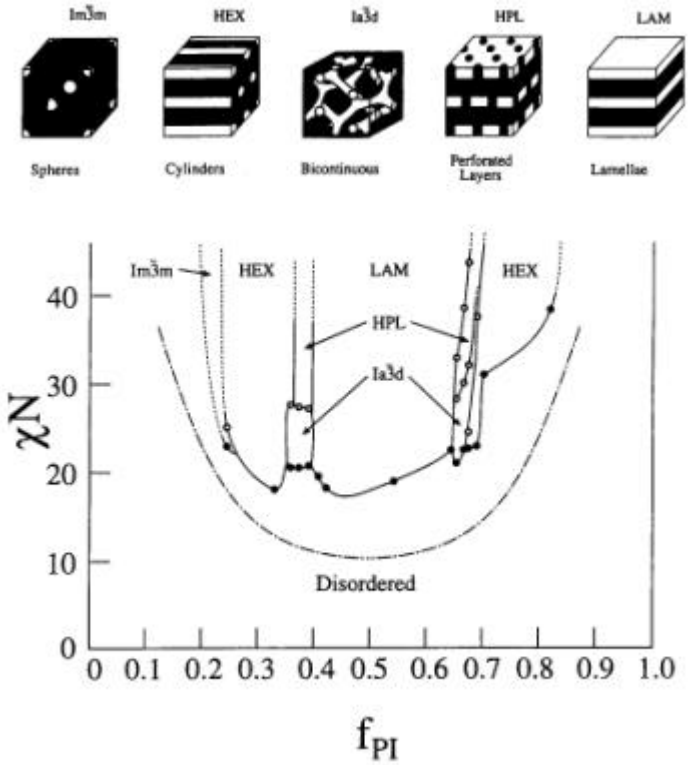

Figure 1.1. A morphological diagram which was determined experimentally for PS-*b*-PI (A. K. Khandpur, *et al.*, *Macromolecules* **28**, 8796 (1995))

(disordered state), while OOT is a transition between different morphologies, for example[3], cylinders and spheres, lamellae and hexagonal performed layers (HPL), HPL and gyroid, and so on. We cannot change the degree of polymerization and the volume fractions in synthesized block copolymer, but we are allowed to change c of the each segment because of a temperature dependency of c. In order to change the morphologies, we change the temperature of the materials. Many researchers are investigating OOT, after Hashimoto *et al.* found thermoreversible OOT in poly(styrene-*b*-isoprene) diblock copolymer[4].

1.1.2. Crystalline Block Copolymers

We can apply phase transitions to OOT. Crystalline block copolymers[1] containing amorphous (coil) polymer segment and crystalline one show crystalline-isotropic phase transitions with some changes of their microdomain morphologies. Crystalline block copolymers form some microphase segregated structure in the isotropic phase of the

crystalline segment as well as amorphous-amorphous block copolymers. In weak segregated region (low molecular weight), the microdomains are broken and reorganize crystalline lamellar structure with transforming to the crystalline phase. In strong segregated region (high molecular weight), crystalline block copolymers form some microdomain morphology in the isotropic phase, and then crystallize in the microdomains with some reforming their shape to packing the crystalline polymer segment. When the amorphous segment has a glass transition temperature above the crystallizing temperature, it drives a little crystallization or vitrescents in the microdomain. In these cases, interesting interrelations between the microphase segregated structure and the phase transition of crystalline polymer segment can be seen.

1.1.3. Liquid Crystalline Block Copolymers

Liquid crystal (LC) also shows phase transitions. LC materials have variable phases including nematic, smectic, cholesteric, chiral smectic, LC glass, crystal, and isotropic, while conventional crystalline materials have only two phases and structures of crystal and isotropic. Each phase has characteristic structures. Nematic phase has one-dimensional oriented structure. Smectic phase has one-dimensional oriented structure and one-dimensional positional ordered structure. Cholesteric and chiral smectic phases have helical structures. Of course crystalline phase has three-dimensional positional ordered structure and isotropic phase has no ordered structure. We believe that these variable phases and structures can change the microdomain morphologies and sizes.

On the other hand, it can be considered that the LC phase behavior and structure are also strongly affected by the microdomain structures. Simply as can be considered, nematic director distribution is not stable in and out of spherical microdomain because of its elastic energy. In the case of smectic phase, LC polymer has anisotropic chain conformation. On the assumption of the most anisotropic chain conformation of extended form, spheres and cylinders can not stow the extended chain stably.

We expect interesting interrelationships between LC phase behaviors and microdomain morphologies because the two different structures of LC and microdomain do not exist individually. Thus LC block copolymers containing amorphous segment and LC segment[5-7] are studied in this thesis.

LC block copolymers must be studied in three parts of synthesis, effect of block copolymer on LC phase behavior, and effect of LC phase behavior on microdomain structure, respectively.

Synthesis LC block copolymers are synthesized by some methods, but each method has both remarkable advantages and fatal disadvantages. Recently, a new method to synthesize living polymers namely living radical polymerization (LRP) is established. At the first, we must investigate better synthesizing method including LRP.

Effect of Block Copolymer on LC Phase Behavior Secondly, the LC phase behavior in LC block copolymer has some differences compared with corresponding LC homopolymer. Block copolymers compose microphase segregated structures. LC structure exists in restrict space with tens nanometers ordered structure in characteristic morphologies. Moreover, main-chain behavior in LC segment has some differences because one or each end of the main-chain is bound to the interface of microdomain, while each end of LC homopolymer is free.

Effect of LC Phase Behavior on Microdomain Structure Finally, LC phase behaviors and structures can change the microdomain structure. Some researches and we found morphological transformation in microdomain structures induced by LC phase transitions. Clarifying their mechanism enables us to control the microdomain morphologies.

In this thesis, we investigate the three points by using smectic A_d (SmA_d) or nematic LC block copolymer in neat LC block copolymer or in LC block copolymer/corresponding homopolymer blend. Finally we will discuss the interrelations between LC phase behavior and microdomain structures.

1.2. Synthesis of LC Block Copolymers

Several methods to introduce LC moiety into block copolymers have been reported as described below. Side-chain LC polymer (SCLCP) is widely used as a LC segment in LC block copolymers.

1.2.1. Polymer Analogous Reaction

Adams and Gronski first synthesized a LC block copolymer[8] by polymer analogous reaction. Some researchers[9,10] used this method to obtain LC block copolymers. A precursor of block copolymers with some functional groups was obtained by living polymerization and then combined mesogenic materials to prepare LC block copolymer.

1.2.2. GTP, Living Cationic, ROMP, and Living Anionic

Some direct block copolymerizations of mesogenic monomer including group transfer polymerization (GTP)[11], living cationic polymerization[12], and ring opening metathesis polymerization (ROMP)[13] were carried out to synthesize LC block copolymers with (rather) narrow molecular weight distribution (MWD, M_w/M_n). Living anionic polymerization is the best method to obtain well-defined methacrylic LC block copolymers with controlling molecular weights, various compositions and very narrow MWD ($\leq$ 1.05 in some case)[14-18]. Some functional groups such as cyano groups can be used in the living anionic polymerization[16].

1.2.3. LRP in Synthesis of SCLCP and LC Block Copolymer

Living radical polymerization (LRP) has been studied incandescently in this decade[19-32]. LRP retains advantages of conventional radical polymerization, *i.e.*, simplicity, robustness, and versatility, and allows fine control of polymer structures owing to the living system. Polymers with complicated topologies such as block, graft, star, and comb-shaped structures can also be tailored by LRP. With these attractive features, LRP is expected to synthesize new advanced materials that have not achieved by either conventional radical polymerization or other living polymerizations.

Gomes *et al.*[33,34] and Ober *et al.*[35] synthesized LC block copolymers with styrenic

derivatives as its LC segment by nitroxide mediated radical polymerization (NMP) with 2,2,6,6-tetramethyl-piperidinyl-1-oxy (TEMPO). Pugh *et al.* synthesized acrylic SCLCP and heteroarm SCLCP by atom transfer radical polymerization (ATRP) and discussed the thermotropic behavior and its relation to MWD and topology[36].

LRP is now developing method and little SCLCPs or LC block copolymers synthesized by LRP have been reported. We believe that LRP is one of the best method to synthesize LC block copolymer, because many monomers including include styrenic, acrylic, and methacrylic SCLCPs which have been reported till now by conventional radical polymerization, can be polymerized and prepare these block copolymers. This method must be a break through of the study in LC block copolymer. Thus we synthesized SCLCP and LC block copolymer by LRP in Chapter 2.

1.3. LC Phase Behavior and Structure in Microphase-Segregated Structures

LC block copolymers generally have a SCLCP segment. Adams and Gronski first synthesized LC block copolymer by polymer analogous reaction[8], and then many researchers synthesized LC block copolymers. However, most of these investigations were limited in the phase sequences in their microdomain. On the other hand, Fischer *et al.*[37], Ober *et al.*[38], Yamada *et al.*[16,39-40], and Hammond *et al.*[41] have discussed interrelations between microdomain structures and LC phase behaviors.

LC phase behavior in microdomains is very complicated but obviously depends on the microphase segregated structure and its morphologies. More studies are needed to clarify the effect of microdomain structure on phase transitions in LC block copolymers.

1.3.1. Differences of the Phase Behavior between LC Block Copolymer and Corresponding SCLCP

LC phase behavior in LC block copolymer is some different from corresponding SCLCP. One or each end of the LC segment in block copolymer is constrained by interface of the microdomains, thus chain mobility is different from homoSCLCP. Moreover the phase transition occurs restrict space in the microdomain.

Yamada synthesized LC block copolymer (PS-*b*-Poly(***lc1***)) containing polystyrene (PS) segment as an amorphous segment and poly(6-[4-(4-methoxyphenyl) phenoxy hexyl] methacrylate) (Poly(***lc1***)) as a LC segment by living anionic polymerization[15]. All block copolymers with narrow MWD, various molecular weights, and a composition of each segment around 50wt% exhibit lamellar type microphase segregation. The LC segment in the lamellar microdomain forms crystalline, SmA_d, and isotropic phases as well as corresponding LC homopolymer, Poly(***lc1***). But their enthalpy changes via their phase transitions are lower than those of Poly(***lc1***). Crystalline-SmA_d phase transition temperatures also are lower. These indicate that the Poly(***lc1***) segment of PS-*b*-Poly(***lc1***) is more difficult to construct LC and crystalline structures than homoPoly(***lc1***). LC block copolymers containing Poly(***lc1***) segment and poly(*a*-methylstyrene) segment instead of PS segment composed vitrificated microdomains above the isotropization temperature of Poly(***lc1***) segment[40]. This leads further decrease of crystallinity, liquid crystallinity and the crystalline-SmA_d phase transition

temperature of Poly(***lc1***) segment than those of PS-*b*-Poly(***lc1***).

1.3.2. LC Phase Transitions in Microphase-Segregated Structure

Fischer *et al.*[37], Yamada *et al.*[16], and Ober *et al.*[38] discussed the phase behavior in various microdomain morphologies. Fischer *et al.*[37] synthesized LC block copolymer containing polystyrene and poly(2-(3-cholesteryloxycarbonyloxy) ethyl methacrylate) (PS-*b*-PChEMA) by polymer analogous reaction. The PS-*b*-PChEMA shows smectic A phase in alternative lamellae, PChEMA-matrix of PS-cylinders, and that of PS-spheres, while only nematic phase in PChEMA-spheres. PChEMA-cylinders was not be observed. This interesting phenomenon was explained by arguing that the thermodynamically stable smectic A layered structure cannot be formed within cylindrical or spherical microdomains. Counter results, on the other hand, have been reported. Yamada *et al.*[16] reported that LC block copolymer containing PS and poly(6-[4-(4'-cyanophenyl)phenoxy]hexyl methacryrate), which showed smactic A_2 phase, composed not only lamellae but also cylinders even if the weight fraction of LC segment was very close to 0.50. Ober *et al.*[38] reported that LC block copolymers containing PS and hydrogenerated polyisoprene derivative of smectic SCLCP containing cyano groups also showed cylinders. Interestingly, they observed the smectic-isotropic phase transition temperature in cylinders was 20°C higher than that in lamellae. These results indicate that the smectic structure was stabilized within cylinders rather than lamellae. The reason for these counter results have not been cleared yet.

1.3.3. Analysis of Phase Transitions in Block Copolymers

On the other hand, crystalline block copolymers containing amorphous segment and crystalline segment crystallize as well as corresponding homopolymers. Avrami equation is usually used for isothermal crystallizations of the homopolymers and the crystalline block copolymers to investigate nucleation and propagation in their whole crystallization.[42] When the molecular weights of each segment are small, Avrami exponents are not different between crystalline block copolymers and corresponding homopolymers, which means that each mechanism of the crystallization is the same and indicates that the driving force of the crystallization is enough dominant to neglect the microdomain morphologies. Increasing the

molecular weight, a rate of crystallization is slower and the crystallinity also lower in their crystalline microdomains. When T_g of its counter amorphous segment is higher than the crystallizing temperature or vitrified, the crystallization does not occur or is hardly observed.

PS-*b*-Poly(***lc1***) also crystallizes from LC phase, while other crystalline block copolymers crystallize from the isotropic phase. For SCLCP, crystallization kinetics has not been studied. In Chapter 4, crystallization kinetics of Poly(***lc1***) homopolymer, PS-*b*-Poly(***lc1***) and these blends are studied by Avrami equation to clear the phase transition.

1.3.4. LC Structure in Oriented Fibers

Oriented fibers of smectic LC polymer were widely used to investigate smectic layered structure. In a case of main-chain type LC polymer [43], smectic layers orient parallel to the direction of stress in fibers drawn from the LC phase, while they align perpendicular to the stress if fibers are drawn from the isotropic phase because of the elongation of the main-chain along the fiber axis. In the case of SCLCP, homoPoly(***lc1***), on the other hand, splayed axis of the main-chain backbone and smectic layer normal are parallel, thus the mesogenic layers orient parallel to the fiber axis drawn both from the isotropic phase and smectic phase. On the other hand, the lamellar microdomains were drawn from the isotropic phase in smectic LC block copolymer, PS-*b*-Poly(***lc1***), and then the layered structures of mesogenic crystal and SmA_d are formed with a preferential orientation lying perpendicular to the microdomain. Interestingly the mesogenic layer in PS-*b*-Poly(***lc1***) is perpendicular to that in Poly(***lc1***) homopolymer due to the microphase segregated structure[15-16,39]. Hammond *et al.* reported, on the other hand, a parallel orientation of smectic layers in a fiber drawn from smectic phase of the smectic LC block copolymer with decyl spacer, which is explained that mesogenic groups decoupled with the main-chain backbone by the long spacer and the smectic layer as well as lamellar microdomain was drawn[44].

We study the orientational behavior of homoPoly(***lc1***), PS-*b*-Poly(***lc1***), and these blends. In Chapter 4, it is found that not only microdomains but also composition fluctuations play an important role.

1.3.5. Composition fluctuation in LC block copolymer

Most of researchers are interested in LC phase behavior in microphase segregated structures. When segmental composition deviates from symmetry, on the other hand, the microdomains were finally disordered. If the weight fraction of LC segment is larger than its counter segment, disordered state is homogeneous with filled LC structure at a glance. But the counter segment must exist and disturb it. We expect the counter segment in homogeneous LC structure, namely composition fluctuation, affect the LC phase behavior.

1.4. Changes in Microdomain Structure by LC Phase Behavior

Some researchers found that LC phase behaviors can change size and morphology of microphase segregated structures in LC block copolymers.

1.4.1. Domain Size Dependency of Temperature.

For symmetric PS-*b*-Poly(***lc1***), Poly(***lc1***) segment in the lamellar microdomain forms crystalline, SmA_d and isotropic phases. The mesogenic layered structures in the crystalline and SmA_d phases are formed with a preferential orientation of side-chain mesogens lying parallel to the microdomain interface. The lamellar thickness depends on the SmA_d temperature[15,39]. With increasing temperature, it decreases from the lamellar thickness of the crystalline phase to that of isotropic phase, and no jump can be seen on the crystal-SmA_d and SmA_d-isotropic transitions. The overall change is completely reversible on heating and cooling cycles, indicating that it proceeds at a thermodynamic equilibrium (Figure 1.2). The reduction is about 20-25%, which can be caused by the conformational change in the main-chain of LC segment from the random coil in the isotropic phase to the extended form in the crystalline phase. The temperature dependence of the main-chain conformational change is considered to arise as a result of the counterbalance between energetic cost of the side-chain mesogenic layerd structure (Figure 1.3) and entropic gain of the main-chain conformation (Figure 1.4). This large characteristic change of the microdomain spacings should enforce a density changes on the counter PS segment. So we expect that this change causes OOT. In reality, OOT induced by the LC phase transition and behavior is found in this thesis.

1.4.2. Order-Order Transitions of Domain Morphology in LC Block Copolymers

In LC block copolymers, OOT induced by LC phase transition was observed in nematic and smectic LC block copolymers. Singer *et al.*[45] reported for ABA triblock copolymers where A is PS segment (12vol%) and B is a nematic SCLCP segment composed PS-spheres in the isotropic phase, while PS-cylinders were composed in the nematic phase. This could be explained that elastic energy of the mesogenic directors induced the microdomain director. Finkelmann *et al.* found an alteration from lamellae to LC-gyroid in a smectic diblock copolymers[46]. Hammond *et al.* also observed an alteration from lamellae to PS-cylinders

through the isotropic to smectic phase transition in a smectic block copolymer[44]. These data indicate that the LC phase transitions are available to change the morphologies of microdomains.

There are interesting phenomena of the morphological transformation in LC block copolymers. However, these driving forces have not been clear yet. It is one of the most important purpose of this thesis to clarify the driving forces, which will be discussed in Chapter 3-6.

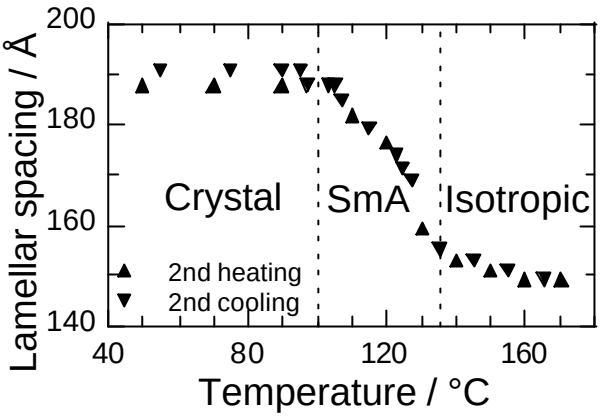

Figure 1.2. Temperature dependence of the microdomain spacings for PS-*b*-Poly(***lc1***) with lamellar type microphase segregated structure on 2nd heating and cooling. No jump can be seen at the phase transitions but continuous change with thermotropically equilibrium in the SmA_d phase.

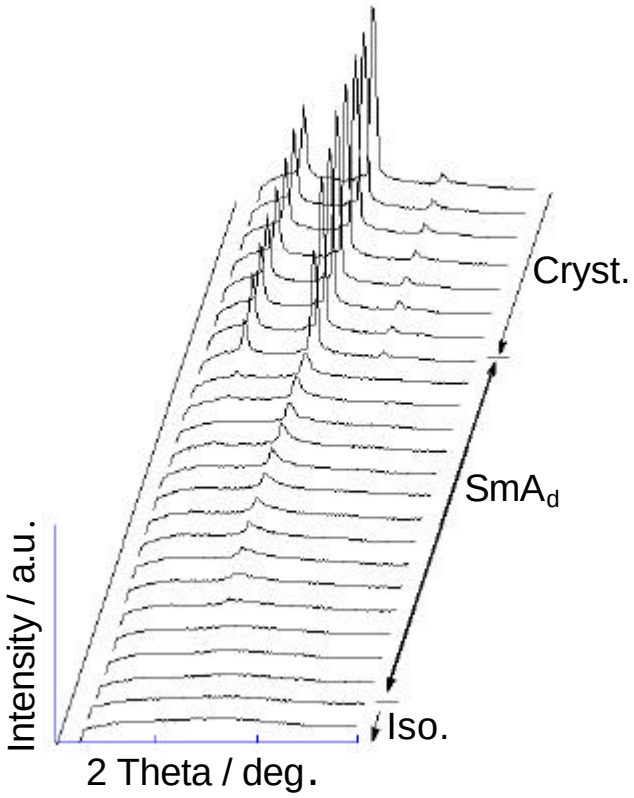

Figure 1.3. Temperature dependence of WAXS profiles for the same PS-*b*-Poly(***lc1***) in Figure1.2. Smectic layered reflection gradually changes in the SmA_d temperature region.

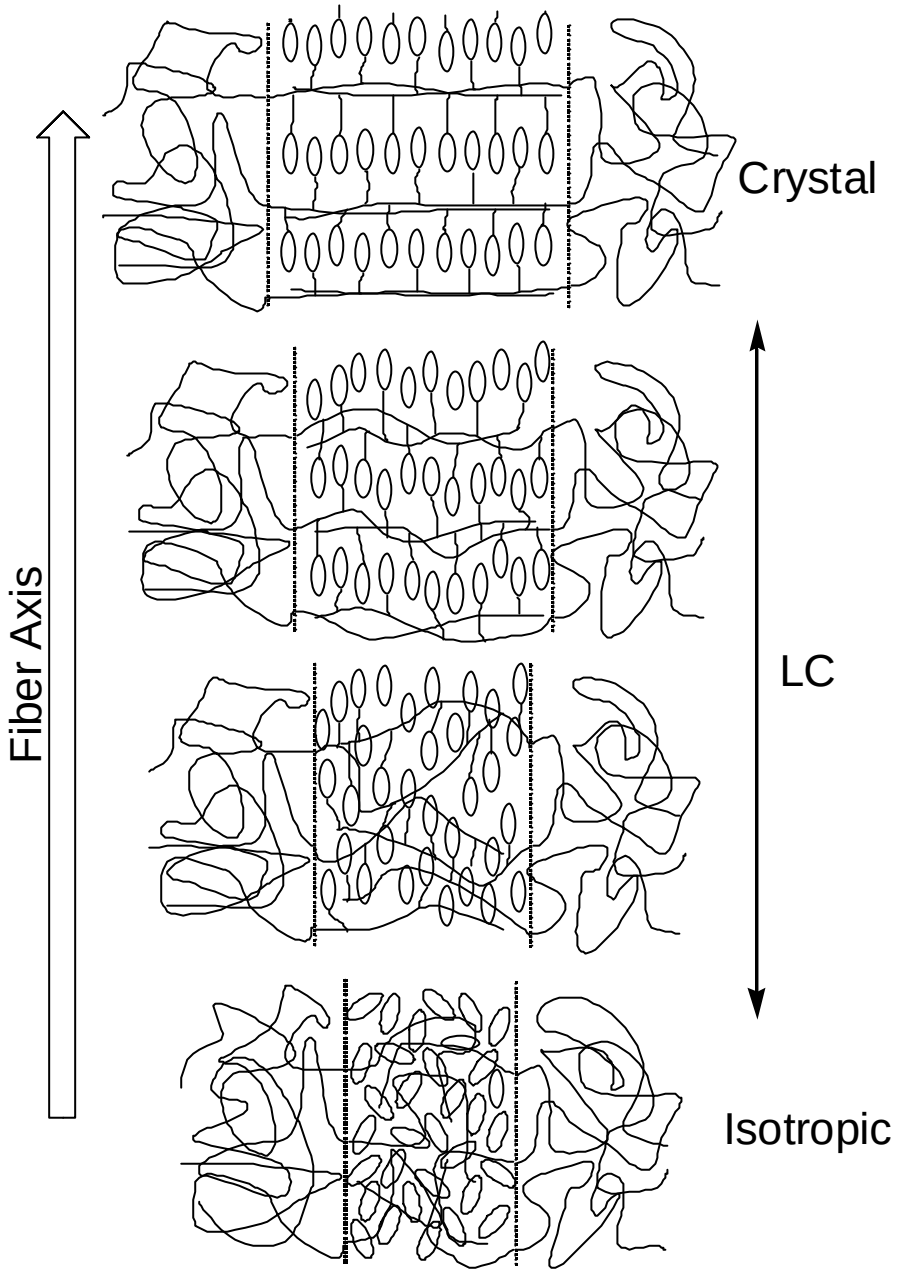

Figure 1.4. Schematic illustration of the conformational change of Poly(***lc1***) segment in the PS-*b*-Poly(***lc1***) with lamellar type microdomain.

1.5. Purpose and Outlines of This Thesis

Now, this thesis aims clearing the driving forces of interrelation between LC phase behavior and microdomain structure, and proposes using LC phase behavior to control nano-ordered structures of microdomain morphology in block copolymers.

In this thesis, three parts have been studied. (i) Synthesis of LC block copolymers is studied at first. Some techniques preparing LC block copolymers are shown and compared. Obtained LC block copolymers have microphase segregated structures and LC structures. Those two structures are not independent but interplay each other. Thus the LC block copolymer must be investigated by two points of view. (ii) One is effects of microdomain morphologies on LC phase behavior, and (iii) the other is those of LC phase behavior on microdomain morphology. For the purpose, we use two LC species of smectic A_d and nematic in study of neat LC block copolymers and blends of LC block copolymer/corresponding homopolymer. Finally we reconstruct obtaining results and discuss factors of the interrelations between LC phase behavior and microdomain structures.

Chapter 2

LC block copolymers containing PS as a coil segment and SCLCP as a LC segment are synthesized by living anionic and living radical polymerizations. Generally, living anionic polymerization produces well-defined polymers, but available monomers are limited. On the other hand, LRP is available various monomers and functional groups, and then LC block copolymer can show variable LC phase behaviors. LRP is successfully carried out to prepare SCLCP and LC block copolymers.

Chapter 3

Microdomain morphologies in neat smectic A_d LC block copolymer with various segmental compositions have been studied. The LC block copolymers with the weight fraction of each segment around 0.50 showed lamellar type microphase segregated structure, while the those with the small weight fraction of smectic SCLCP segment composed LC-cylinders. Interestingly, the lamellae in the isotropic phase were altered into LC-cylinders at the smectic A_d phase temperature in the LC block copolymers with the weight fraction of 0.30 and 0.32.

Conventional block copolymers show OOT by changing temperatures. However, the considerable morphologies are lamellae at the low temperature and cylinders at the high temperature. The LC block copolymer showed counter OOT, which must be induced the LC phase transition.

Chapter 4

Microdomain morphologies, orientational behavior, and isothermal crystallization kinetics of smectic SCLCP, its LC block copolymer, and blends of them have been studied. It clarified that the composition fluctuation strongly affects the mechanical properties and phase behavior of LC in Chapter 4.

Adding the smectic SCLCP to the symmetric smectic LC block copolymer, lamellar type microdomains were altered in cylinders and were disordered. For the smectic SCLCP, Avrami exponents continuously changed within 1 unit depending on the crystallization temperatures. It was considered to be caused by its conformational change from random-coil to extended chain at the crystallization temperature. For the blends of the smectic SCLCP and corresponding LC block copolymer, which composed LC-matrix with coil segmental cylinders, Avrami exponents changed continuously within 1 unit depended on their crystallizing temperature as well as the SCLCP, while they were smaller than those of SCLCP by 1 unit even if the microdomain structures disordered. This indicates that not only the microdomain interface but also composition fluctuation were the nuclei of the crystallites. The LC block copolymer which had lamellar type microdomains showed further smaller Avrami exponents by 1 unit. These results obviously indicate that the morphology of the microdomains strongly depended on the crystallization behaviors.

Orientational behaviors also have been studied in them. For the smectic SCLCP, mesogenic layer lied parallel to its fiber axis which was drawn from the isotropic or smectic phase. On the other hand, the mesogenic layer lied perpendicular in the LC block copolymer which composed lamellar type microphase segregated structure. This can be considered that the microdomain was drawn along the fiber. Blends of the SCLCP and the LC block copolymer were also showed perpendicular orientation of the mesogenic layers in LC-matrix of amorphous-cylinders and even in disordered state. The composition fluctuation was also

aligned along the fiber axis.

Chapter 5

Microdomain morphologies in the blends of a symmetric smectic A_d LC block copolymer with lamellar type microphase segregated structure and corresponding amorphous homoPS have been studied. Three homoPSs with different molecular weight were prepared because swelling type of the homoPS in the LC block copolymer depended on its molecular weight[47]. The blends of LC block copolymer and homoPS with large molecular weight showed 'dry-brush' type swelling behavior and did not changed the lamellae in whole temperature region. On the other hand, 'wet-brush' type one was observed in the blends of the LC block copolymer and two homoPSs with small and middle molecular weight and changed the lamellae to LC-cylinders and LC-spheres in its isotropic phase. At the large composition of the homoPS with middle molecular weight in the 'wet-brush' regime, the LC-spheres were altered in LC-cylinders or lamellae on the isotropic-smectic phase transition, which can be considered to be induced by the director field of the mesogens. On the other hand, the homoPS with small molecular weight altered the LC-spheres in LC-lamellae. This can be considered to be induced by chain extension of the smectic segment in the smectic A_d phase, which is required from the packing of the extended smectic segment in microdomains.

Chapter 6

Microdomain morphologies of nematic LC block copolymers with various molecular weights and segmental compositions have been studied. Microdomain spacings did not change between the isotropic phase and the nematic phase, indicating that the conformation of the nematic SCLCP segment is the same between its isotropic and nematic phases. Some copolymers showed morphological transformation from spheres to cylinders on the isotropic-nematic phase transition, which can be considered that the mesogenic director field in the nematic phase rearranged the microdomain along the same direction. Transition temperature with cylinders was higher than that with spheres due to the difficulty of composing nematic phase. However, nematic phase can be taken place with spheres as 'transparent nematic' phase.

References in This Chapter

1. I. W. Hamley, "The Physics of Block Copolymers", Oxford University Press, Inc., New York, N. Y., 1998.
2. L. Leibler, *Macromolecules*, **13**, 1602 (1980).
3. A. K. Khandpur, S. Föster, F. S. Bates, I. W. Hamley, A. J. Ryan, W. Bras, K. Almdal, and K. Mortensen, *Macromolecules*, **28**, 8796 (1995).
4. S. Sakurai, H. Kawada, T. Hashimoto, and L. J. Fetters, *Macromolecules*, **26**, 5796 (1993).
5. M. Walther and H. Finkelmann, *Prog. Polym. Sci*., **21**, 951 (1996).
6. G. Mao and C. K. Ober, *Acta Polym*., **48**, 205 (1997).
7. S. Poser, H. Fischer, and M. Arnold, *Prog. Polym. Sci.*, **23**, 1337 (1998).
8. J. Adams and W. Gronski, *Makromol. Chem., Rapid Commun*., **10**, 553 (1989).
9. B. Zaschke, W. Frank, H. Fischer, K. Schmutzler, and M. Arnold, *Polym. Bull.*, **27**, 1 (1991).
10. D. R. Iyenger, S. M. Perutz, C. Dai, C. K. Ober, and E. J. Kramer, *Macromolecules*, **29**, 1229 (1996).
11. B. R. Maughon, M. Weck, B. Mohr, and R. H. Grubbs, *Macromolecules*, **30**, 257 (1997).
12. V. Percec and M. Lee, *J. Macromol. Sci., Pure Appl. Chem*., **A29**, 723 (1992).
13. Z. Komiya and R. R. Schrock, *Macromolecules*, **26**, 1387 (1993).
14. R. Bohnert and H. Finkelmann, *Macromol. Chem. Phys.*, **195**, 689 (1994).
15. M. Yamada, T. Iguchi, A. Hirao, S. Nakahama, and J. Watanabe, *Macromolecules*, **28**, 50 (1995).
16. M. Yamada, T. Itoh, R. Nakagawa, A. Hirao, S. Nakahama, and J. Watanabe, *Macromolecules*, **32**, 282 (1999).
17. W. Y. Zheng and P. T. Hammond, *Macromol. Rapid Commun*., **17**, 813 (1996).
18. O. Lehmann, S. Förster, and J. Springer, *Macromol. Rapid Commun*., **21**, 133 (2000).
19. K. Matyjaszewski, S. Gaynor, D. Greszta, D. Maedare, and T. Shigemoto, *J. Phys. Org. Chem.*, **8**, 306 (1995).
20. K. Matyjaszewski, *Macromol. Symp.*, **174**, 51 (2001).
21. K. Matyjaszewski, Ed, "Contorolled / Living Radical Polymerization: Progress in ATRP, NMP, and RAFT", American Chemical Society, Washington, D. C., 2000, Vol. 768.

22. D. H. Solomon, E. Rizzardo, and P. Cacioli, Eur. Pat. Appl., EP 0 135 280 (Jul. 11, 1984) (*Chem. Abstr.* 102, 221335q (1985)).
23. M. K. Georges, R. P. N. Veregin, P. M. Kazmaier, and G. K. Hamer, *Macromolecules*, **26**, 2987 (1993).
24. A. Goto and T. Fukuda, *Macromolecules*, **32**, 618 (1999).
25. D. Benoit, S. Grimaldi, S. Robin, J. P. Finet, P. Tordo, and Y. Gnanou, *J. Am. Chem. Soc.*, **122**, 5929 (2000).
26. J. S. Wang and K. Matyjaszewski, *J. Am. Chem. Soc.*, **117**, 5614 (1995).
27. T. E. Patten, J. Xia, T. Abernathy, and K. Matyjaszewski, *Science*, **272**, 866 (1996).
28. B. Yu and E. Ruckenstein, *J. Polym. Sci., Part A: Polym. Chem.*, **37**, 4191 (1999).
29. V. Coessens, T. Pintauer, and K. Matyjaszewski, *Prog. Polym. Sci.*, **26**, 337 (2001).
30. K. Matyjaszewski and J. Xia, *Chem. Rev.*, **101**, 2921 (2001).
31. T. P. Le, G. Moad, E. Rizzardo, and S. H. Thang, Int. Pat. Appl., WO 98 001 478 (Jan. 15, 1998) (*Chem. Abstr.* **128**, 115390 (1998)).
32. J. Chiefari, Y. K. (B.) Chong, F. Ercole, J. Krstina, J. Jeffery, T. P. T. Le, R. T. A. Mayadunne, G. F. Meijs, C. L. Moad, G. Moad, E. Rizzardo, and S. H. Thang, *Macromolecules*, **31**, 5559 (1998).
33. C. A. Barbosa and A. S. Gomes, *Polym. Bull.*, **41**, 15 (1998).
34. A. S. Gomes, C. A. Barbosa, and M. R. Pinto, *Polym. Int*., **48**, 713 (1999).
35. M. C. Bignozzi, C. K. Ober, and M. Laus, *Macromol. Rapid Commun*., **20**, 622 (1999).
36. A. M. Kasko, A. M. Heintz, and C. Pugh, *Macromolecules*, **31**, 356 (1998).
37. H. Fischer, S. Poser, and M. Arnold, *Liq. Cryst*., **18**, 503 (1995).
38. a) G. Mao, J. Wang, S. R. Clingman, C. K. Ober, J. T. Chen, and E. L. Thomas, *Macromolecules*, **30**, 2556 (1997).
    b) C. O. Osuji, J. T. Chen, G. Mao, C. K. Ober, and E. L. Thomas, *Polymer*, **41**, 8897 (2000).
39. M. Yamada, T. Iguchi. A. Hirao, S. Nakahama, and J. Watanabe, *Polym. J*,. **30**, 23 (1998).
40. M. Yamada, T. Itoh, A. Hirao, S. Nakahama, and J. Watanabe, *High Perform. Polym*., **10**, 131 (1998).
41. a) W. Y. Zheng, R. J. Albalak, and P. T. Hammond, *Macromolecules*, **31**, 2686 (1998).

b) M. Anthamatten, W. Y. Zheng, and P. T. Hammond, *Macromolecules*, **32**, 4838 (1999).

42. Y. Long, R. A. Shanks, and Z. H. Stachurski, *Prog. Polym. Sci.*, **20**, 651 (1995).
43. M. Tokita, K. Osada, S. Kawauchi, and J. Watanabe, *Polym. J.*, **30**, 687 (1998).
44. M. Anthamatten and P. T. Hammond, *Macromolecules*, **32**, 8066 (1999).
45. J. Sänger, W. Gronski, S. Maas, B. Stühn, and B. Heck, *Macromolecules*, **30**, 6783 (1997).
46. A. Schneider, J. J. Zanna, M. Yamada, H. Finkelmann, and R. Thomann, *Macromolecules*, **33**, 649 (2000).
47. a) H. Hasegawa and T. Hashimoto, 'Self-Assembly and Morphology of Block Copolymer System' in "Comprehensive Polymer Science", S. L. Aggarwal and S. Russo, Ed., Pergamon Press, Ltd., Oxford, 1996, Suppl. 2.

    b) T. Hashimoto, H. Tanaka, and H. Hasegawa, *Macromolecules*, **23**, 4378 (1990).

    c) S. Koizumi, H. Hasegawa, and T. Hashimoto, *Makromol. Chem., Macromol. Symp.*, **62**, 75 (1992).

Chapter 2

Synthesis of Side-Chain Liquid Crystalline Polymers and Their Diblock Copolymers with Polystyrene by Sequential Living Anionic and Radical Polymerizations

Abstract: LC block copolymers containing side-chain liquid crystalline polymer segment and amorphous polymer segment were synthesized. The currently best method to obtain LC block copolymer was discussed. Living anionic polymerization of the LC block copolymer containing poly(6-[4-(4'-methoxyphenyl)phenoxy]hexyl methacrylate) and polystyrene with various segmental compositions and narrow molecular weight distributions was successfully carried out. Living radical polymerization was also successfully carried out to synthesize poly(6-[4-(4'-cyanophenyl)phenoxy]hexyl acrylate) homopolymer by three methods; nitroxide mediated radical polymerization (NMP), reversible addition-fragmentation chain transfer (RAFT), and atom transfer radical polymerization (ATRP). Its block copolymer with polystyrene was prepared with various molecular weights and segmental compositions by NMP and ATRP. The best method in LRP for preparing LC block copolymers was also discussed.

2.1. Introduction

At first we synthesized LC block copolymers containing an amorphous polymer segment and a side-chain liquid crystalline polymer (SCLCP) segment. Several methods to synthesize LC block copolymers have been reported. However, all of the methods have some problems. Advantages and disadvantages are summarized in Table 2.1. What method is the best?

2.1.1. Polymer Analogous Reaction

Adams and Gronski first synthesized a LC block copolymer by polymer analogous reaction[1]. A precursor of polystyrene-*b*-(1,2-polybutadiene) (PS-*b*-PB) was obtained by living anionic polymerization, and then PB segment was converted into poly(2-hydroxyethylethylene). The functionalized segment in block copolymers combined mesogenic materials to prepare LC block copolymer. Fisher *et al.*[2] and Ober *et al.*[3] also used polymer analogous reaction to obtain LC block copolymers. Hammond *et al.* synthesized a LC block copolymer containing PS and SCLCP segment with polysiloxane backbone, which had a very low glass transition temperature (T_g) at -23°C[4].

Well-controlled LC block copolymers with wide range of molecular weights and narrow molecular weight distributions (MWDs) can be obtained by this method. However a fateful problem of this method is the incomplete conversion of introducing side-chain mesogenic groups. Hence, obtaining LC block copolymer does not have well-defined structure, and some defects remain in the LC segment. Thus we cannot discuss conformation of the main-chain backbone in the LC segment, which is an important factor to compose microdomain morphologies.

This problem can be solved by direct living polymerizations of mesogenic monomers.

2.1.2. GTP

Hefft and Springer reported LC block copolymers which were synthesized by living group transfer polymerization (GTP)[5]. They obtained LC block copolymers with MWD < 1.1 and with moderate degree of polymerization (DP) of 16-22. They could obtain LC block copolymers, although one of the monomers containing cyano groups was failed.

2.1.3. Living Cationic Polymerization

Percec and Lee synthesized LC block copolymers by living cationic polymerization. However, the DP was limited to very low around 7-12 for each segment[6].

2.1.4. ROMP

Living ring-opening metathesis polymerization (ROMP) was the first employed direct polymerization to synthesize well-defined LC block copolymers by Komiya and Schrock[7]. A novel ruthenium catalyst can tolerate functional groups[8]. However, special ringed monomer was needed in this method.

2.1.5. Living Anionic Polymerization

Finkelmann *et al.* first reported LC block copolymer with mesogenic methacrylates by living anionic polymerization[9]. Yamada *et al.*[10,11], Hammond *et al.*[12] and Springer *et al.*[13] also synthesized LC block copolymers by living anionic polymerization. Yamada *et al.* investigated in detail and obtained well-defined LC block copolymers with controlling DP and narrow MWDs (especially MWD < 1.05[10,11]). Additionally, some functional groups such as a cyano group can be used[11]. Living anionic polymerization is one of the best method to synthesized well-defined LC block copolymer.

However, this method needs tough purification of monomers with special technique. Moreover, Yamada reported that the DP of LC segment was moderate in some case because the polymerization became heterogeneous in large DP[11]. Furthermore, it can be prepare styrenic and methacrylic polymers. SCLCP generally has acrylic or methacrylic main-chain back bone. Few references were reported for conventional acrylic polymers, but acrylic SCLCP have not been reported.

2.1.6. LRP

All of the living polymerizations described above have problems of limited monomers, limited functional groups, moderate DP, necessity of tough purification, and necessity of special technique.

On the other hand, living radical polymerization (LRP)[14,15] has been studied vigorously in

Table 2.1. Comparison of different synthetic methods for LC block copolymers.

Method	Advantages	Disadvantages
Polymer analogous	Wide range of M_n Narrow MWD	Small defect in LC segment
GTP, ROMP, Living cationic	Good control of M_n Narrow MWD	Moderate M_n Limited functional groups Special monomers
Living anionic	Good control of M_n Narrow MWD Control of tacticity	Moderate M_n Limited functional groups Tough monomer purification
Living radical	Good control of M_n Rather narrow MWD Tolerate functional groups	(Need more study)

this decade. LRP retains the advantages of conventional radical polymerization, *i.e.*, simplicity, robustness, and versatility, and allows fine control of polymer structures owing to the living system. Styrenic, acrylic, methacrylic, and functional polymers can be synthesized by LRP. Polymers with complicated topologies such as block, graft, star and comb-shaped structures can also be tailored by LRP. With these attractive features, LRP is expected to synthesize new advanced materials that have not achieved by either conventional radical polymerization or other living polymerizations.

Currently three most efficient methods in LRP are nitroxide mediated radical polymerization (NMP)[16-19], atom transfer radical polymerization (ATRP)[20-24], and reversible addition-fragmentation chain transfer (RAFT)[25,26]. The mechanisms of LRP are described in Appendix.

Ober *et al.*[27] and Gomes *et al.*[28,29] synthesized LC block copolymers by NMP with 2,2,6,6-tetramethyl-piperidinyl-1-oxy (TEMPO[16,17]). However, only styrenic polymer can be obtained with TEMPO. Some other nitroxides which enable to synthesize acrylic polymers were developed[18,19], while acrylic SCLCP have not been synthesized by NMP. Methacrylic polymers have not been prepared by NMP because fast extraction of β-hydrogen at

propagating end comes about. Pugh *et al.* synthesized linear and heteroarm SCLCPs by ATRP and discussed the thermotropic behavior and its relation to MWD and topology[30]. RAFT has not been reported to synthesize SCLCP and LC block copolymer yet.

LRP is now developing method, and a little SCLCPs or LC block copolymers synthesized by LRP have been reported. We believe that LRP is one of the best method to synthesize SCLCP and LC block copolymers because acrylic, methacrylic, and functionalized SCLCPs, which were synthesized by conventional radical polymerization before now, and their block copolymers can be obtained. LRP must be a break through of the study in LC block copolymer field.

The disadvantage of LRP is that obtaining polymers have rather wide MWDs compared with living anionic polymerization. However, the MWD in LRP is appropriate to investigate structures and phase behaviors of the LC block copolymers because of MWD~1.2 as described later, and associations of the molecules in order to construct the structures allow such MWD.

In this chapter, living anionic polymerization and LRP are carried out to obtain well-defined two species of LC block copolymers, respectively.

2.2. Synthesis of Monomers

Monomers, ***lc1***[31] and ***lc2***[32], were synthesized according to references.

2.2.1. Purification

Triethylamine (TEA) Received TEA was stirred over CaH_2 overnight and vacuum distilled before use.

Tetrahydrofuran (THF) Received THF was refluxed over CaH_2 for several hours and distilled before use.

Styrene Received styrene was washed two times with 5% $NaOH_{aq}$. and two times with water, stirred over anhydrous $MgSO_4$ overnight, filtered, stirred over CaH_2 overnight, and vacuum distilled before use.

Other materials were used without further purification.

2.2.2. Monomer *lc1*

4-methoxy-4'-hydroxybiphenyl Methyl iodide 7.62mL (120mmol) was added dropwise over 15 minutes to solution of 4,4'-biphenol 22.3g (120mmol) and NaOH 5.16g (120mmol) in ethanol 250mL. The reaction was stirred for 2h, filtered to eliminate 4,4'-dimethoxybiphenyl, evaporated, and vacuumed. The residue was further purified by column chromatography with CH_2Cl_2 to yield 10.82g (54.1mmol, 45.1%) of 4-methoxy-4'-hydroxybiphenyl as white crystal.

<^{1}H-NMR> solvent: $CDCl_3$ reference: TMS (σ=0.00)

σ=3.75 (s, 1H, -O*H*), 3.83 (s, 3H, -O*CH*$_3$), 6.89 (d, 2H, aromatic *ortho* to OCH_3), 6.94 (d, 2H, aromatic *ortho* to OH), 7.39 (d, 2H, aromatic *meta* to OH), 7.42 (d, 2H, aromatic *meta* to OCH_3)

4-methoxy-4'-(6-hydroxyhexyloxy)biphenyl Ethanol 250mL was added 4-methoxy-4'-hydroxybiphenyl 13.3g (66.8mmol), 6-chloro-1-hexyanol 9.8mL (70mmol), and KOH 4.6g (70mmol), refluxed at 95°C for 24h, cooled to room temperature, and filtered to obtain crystals. The crystals dissolved in chloroform, washed with water, and evaporated. The residue was recrystallized from ethanol to yield 10.5g (54.1mmol, 45.7%) of

4-methoxy-4'-(6-hydroxyhexyloxy)biphenyl as white crystal.

<^{1}H-NMR> solvent: $CDCl_3$ reference: TMS (σ=0.00)

σ=1.4-1.9 (m, 8H, -*CH_2*-), 3.68 (t, 2H, -*CH_2*-OH), 3.85 (s, 3H, -O*CH_3*), 4.00 (t, 2H, -*CH_2*-OPh), 6.92 (dd, 4H, aromatic *ortho* to OCH_2 and OCH_3), 7.44 (dd, 4H, aromatic *meta* to OCH_2 and OCH_3)

6-[4-(4'-methoxyphenyl)phenoxy]hexyl methacrylate A solution of methacryloyl chloride 2.9mL (30mmol) in THF 20mL was added dropwise over 2h to an ice-cooled solution of 4-methoxy-4'-(6-hydroxyhexyloxy)biphenyl 8.05g (26.8mmol) and TEA 4.2mL (30mmol) in THF 200mL. The reaction was warmed to room temperature, stirred for 24h and vacuum distilled to remove THF. The resulting residue was dissolved in diethyether 200mL, washed two times with 2N $HCl_{aq.}$ and two times with water, stirred over anhydrous $MgSO_4$ overnight, filtered, and evaporated to remove diethylether. It was further purified by column chromatography with hexane/diethylether = 20/1. The resulting precipitate was collected and recrystallized from hexane/diethylether = 10/1 to yield 5.31g (14.4mmol, 54%) of 6-[4-(4'-methoxyphenyl)phenoxy]hexyl methacrylate (***lc1***) as white crystal.

<^{1}H-NMR> solvent: $CDCl_3$ reference: TMS (σ=0.00)

σ=1.4-1.9 (m, 8H, -*CH_2*-), 1.94 (dd, 3H, =C-*CH_3*), 3.84 (s, 3H, -O*CH_3*), 3.99 (t, 2H, -*CH_2*-OPh), 4.16 (t, 2H, -COO-*CH_2*-), 5.54 (d of q, 1H, olefinic *trans* to COO), 6.10 (d of q, 1H, olefinic *cis* to COO), 6.89 (dd, 4H, aromatic *ortho* to OCH_2 and OCH_3), 7.42 (dd, 4H, aromatic *meta* to OCH_2 and OCH_3)

Obtaining ***lc1*** was well dried under vacuum, then polymerized.

2.2.3. Monomer *lc2*

4-cyano-4'-(6-hydroxyhexyloxy)biphenyl *N,N'*-dimethylformamide (DMF) 100mL was added 4-cyano-4'-hydroxybiphenyl 9.86g (51mmol), 6-chloro-1-hexanol 8.8mL (66mmol), K_2CO_3 9.74g (66mmol), and small amount of KI (ligand), refluxed at 130°C for 24h, eliminated with vacuum distillation. The resulting residue was dissolved with chloroform, washed with water, stirred over anhydrous $MgSO_4$, filtered, and evaporated. It was further

purified by column chromatography with hexane/ethylacetate (EtAc) = 4/1. The resulting precipitate was collected and recrystallized from hexane/EtAc = 10/1 to yield 11.61g (41mmol, 77%) of 4-cyano-4'-(6-hydroxyhexyloxy)biphenyl as white crystals.

<^{1}H-NMR> solvent: $CDCl_3$ reference: TMS (σ=0.00)

σ=1.3-1.6 (m, 4H, -*CH*$_2$-), 1.67 (m, 2H, *CH*$_2$-CH$_2$-OPh), 1.86 (m, 2H, *CH*$_2$-CH$_2$-OH), 3.67 (t, 2H, *CH*$_2$-OH), 4.02 (t, 2H, *CH*$_2$-OPh), 6.95 (d, 2H, aromatic *ortho* to OCH_2), 7.52 (d, 2H, aromatic *meta* to OCH_2), 7.63 (dd, 4H, aromatic *ortho* and *meta* to CN)

6-[4-(4'-cyanophenyl)phenoxy]hexyl acrylate A solution of acryloyl chloride 3.2mL (39mmol) in THF 20mL was added dropwise over 2h to an ice-cooled solution of 4-cyano-4'-(6-hydroxyhexyloxy)biphenyl 10.45g (35.4mmol) and TEA 5.5mL (40mmol) in THF 250mL. The reaction was warmed to room temperature, stirred for 24h, and vacuum distilled to remove THF. The resulting residue was dissolved in diethyether 200mL, washed two times with 2N HCl_{aq}. and two times with water, stirred over anhydrous $MgSO_4$ overnight, filtered, and vacuum distilled to remove dhiethylether. It was further purified by column chromatography with hexane/EtAc = 10/1. The resulting precipitate was collected and recrystallized from hexane/EtAc = 15/1 to yield 6.42g (18.4mmol, 52%) of 6-[4-(4'-cyanophenyl)phenoxy]hexyl acrylate (***lc2***) as white crystals.

<^{1}H-NMR> solvent: $CDCl_3$ reference: TMS (σ=0.00)

σ=1.3-1.6 (m, 4H, -*CH*$_2$-), 1.72 (m, 2H, *CH*$_2$-CH$_2$-OPh), 1.83 (m, 2H, *CH*$_2$-CH$_2$-OCO), 4.01 (t, 2H, *CH*$_2$-OPh), 4.18 (t, 2H, *CH*$_2$-OCO), 5.83 (d, 1H, olefinic *trans* to COO), 6.13 (dd, 1H, olefinic *gem* to COO), 6.43 (d, 1H, olefinic *cis* to COO), 6.98 (d, 2H, aromatic *ortho* to OCH_2), 7.51 (d, 2H, aromatic *meta* to OCH_2), 7.62 (dd, 4H, aromatic *ortho* and *meta* to CN)

Obtaining ***lc2*** was well dried under vacuum, then polymerized.

2.3. Living Anionic Polymerization of PS-*b*-Poly(***lc1***)

Living anionic polymerization of Poly(***lc1***) with polystyrene (PS) was carried out according to a reference[10]. Monomer ***lc1*** was dried over P_2O_5 for 48h under a high vacuum condition (10^{-6}mmHg), diluted with dry THF to result 0.05M solutions, and placed in glass ampules. Styrene and 1,1-diphenylethlene were purified according to the standard method. Commercially available *sec*-butyllithium (*s*-BuLi) was diluted with heptane in glass ampules. All of the living anionic polymerization were carried out with shaking under high vacuum conditions in all the glass apparatus equipped with break-seals.

Living PS was first prepared with *s*-BuLi in THF at -78°C for 10min and then 1,1-dhiphenylethlene was added to cap the highly reactive PS anion. The sequential polymerization of ***lc1*** was then carried out with this polymeric anion in the presence of LiCl in THF at -40°C for 2h. The polymerization mixtures were poured into methanol to precipitate the polymer. It was purified by reprecipitation from THF to methanol, Soxhlet extraction with methylcyclohexane, which is a Θ solvent for PS but a poor solvent for Poly(***lc1***), to remove terminated PS, and reprecipitation again.

The molecular weight (M_n) and MWD (M_w/M_n) were determined by a GPC profile based on the calibration of standard PS. The composition of each segment was determined by ^{1}H NMR.

All of the living anionic polymerization were carried out quantitatively, and well-defined polymers with various M_n (= 47000-67000), compositions (= 0.24-0.45 of the weight fraction of the Poly(***lc1***) segment), and narrow MWDs (≤ 1.05) could be obtained (Table 2.2).

Table 2.2. Block copolymerization of styrene and ***lc1***

M_n [a]	M_w/M_n [a]	Weight fraction of Poly(***lc1***) segment [b]
47000	1.03	0.45
55000	1.05	0.41
52000	1.03	0.35
55000	1.04	0.32
57000	1.04	0.30
67000	1.04	0.24

a) Determined by GPC. b) Determined by ^{1}H NMR.

2.4. LRP of Poly(*lc2*) and PS-*b*-Poly(*lc2*)

Three methods of NMP, RAFT, and ATRP, which are now most efficient methods in LRP, are carried out to synthesize Poly(***lc2***). LC block copolymer containing PS segment and Poly(***lc2***) segment is also synthesized by NMP and ATRP. Acrylic monomer commonly cannot be polymerized by sequential anionic polymerization because of an inactivation of anion by extraction of *a*-hydrogen at propagating anion. Thus ***lc2*** was polymerized by LRP.

2.4.1. Materials

1-phenylethyl-DEPN (S-DEPN[19]) and 2-phenylprop-2-yl dithiobenzonate[26,27] were kindly proffered from Fukuda Lab. in Institute for Chemical Research, Kyoto University. PS precursors, PS-DEPN and PS-Br, were synthesized by NMP and ATRP as described below, respectively.

2.4.2. Technique of the LRP and Characterization of Polymers.

Mixture of monomer, initiator, ligand, and solvent were charged in a glass tube, degassed with several freeze-pump-thaw cycles, and sealed off under vacuum because of the essential requirement of deoxygenation for the reaction mixtures. The mixture was heated at predetermined temperature for appropriate hours. Then the obtained polymer was purified by reprecipitation with methanol and thoroughly dried. Block copolymers were further purified by Soxhlet extraction with methylcyclohexane, which is a Θ solvent for PS but a poor solvent for Poly(***lc2***), to eliminate remaining precursors and dead PS. M_n and MWD were determined with GPC measurement based on the calibration of standard PS.

2.4.3. Homopolymerization of *lc2*

Homopolymerizations of ***lc2*** were carried out by NMP, RAFT, and ATRP, respectively. Characters of the homopolymers are summarized in Table 2.3-2.5.

NMP First, we synthesized Poly(***lc2***) by NMP with S-DEPN as an initiator in toluene. $[\mathbf{lc2}]_0/[\text{S-DEPN}]_0$ and concentration of ***lc2*** in the solution are summarized in Table 2.3. Then the system was heated at 120°C for several hours. The polymerization underwent. In some

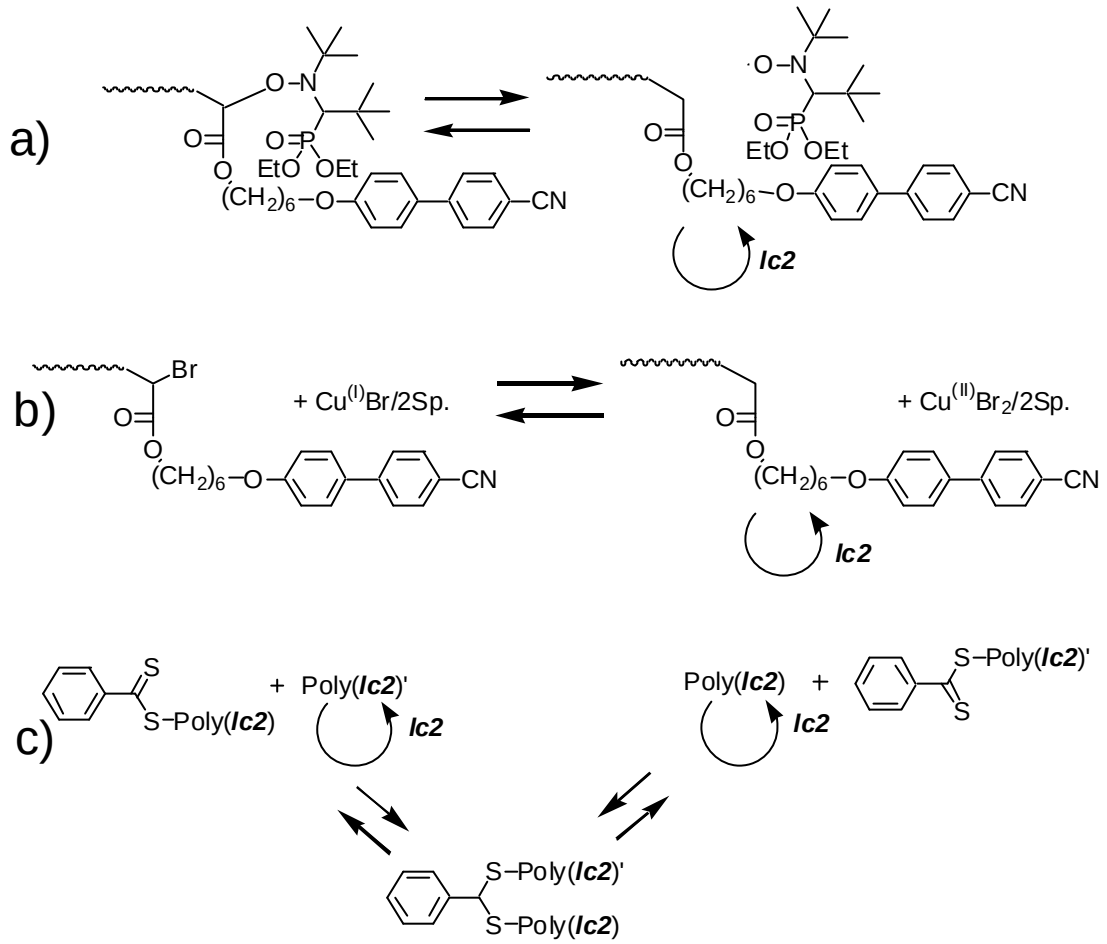

Scheme 2.1. LRP of side-chain liquid crystalline polymer (Poly(***lc2***)) of (a) NMP with DEPN, (b) ATRP with CuBr and sparteine and (c) RAFT.

case, the M_w/M_n is smaller than 2. On the other hand, SCLCP had the $M_w/M_n < 1.3$ in anionic system[10,11]. The reason for the wide MWD is considerable. Inappropriate temperature was too high, thus the equilibrium of the activation-deactivation process largely lied to activation. This can be corrected by decreasing temperature of the reaction system. In early stage of the reaction, moreover, deactivation was small until the activation-deactivation process reaches equilibrium, which can be corrected by adding DEPN at first to enlarge the deactivation. At all events, the condition of polymerization system must be further improved.

Table 2.3. Results of homopolymerization by NMP [a)]

$[M]_0/[S\text{-}DEPN]$	Conc. [b)]	Time	M_n [c)]	M_w/M_n [c)]
100/1	25wt%	2.0h	7600	1.79
100/1	50wt%	1.3h	19200	3.04

a) Polymerization temperature at 120°C. b) Weight fraction of ***lc2*** in the solution diluted with toluene.
c) Determined by GPC.

Table 2.4. Results of homopolymerization by RAFT [a)]

$[M]_0/[AIBN]/[dithioester^{b)}]$	Conc. [c)]	Time	M_n [d)]	M_w/M_n [d)]
100/0.6/1	30wt%	8.0h	18300	1.29
100/0.6/1	30wt%	22h	20200	1.34

a) Polymerization temperature at 60°C. b) 2-Phenylprop-2-yl dithiobenzonate. c) Weight fraction of ***lc2*** in the solution diluted with toluene. d) Determined by GPC.

Table 2.5. Results of homopolymerization by ATRP [a)]

$[M]_0/[I^{b)}]/[CuBr]/[Sp.^{c)}]$	Conc. [d)]	Time	M_n [e)]	M_w/M_n [e)]
50/1/1/2	25wt%	5.0h	5800	1.11
100/1/1/2	25wt%	10.0h	11100	1.13
160/1/1/2	50wt%	2.5h	12600	1.20
200/1/1/2	25wt%	20.0h	14300	1.26

a) Polymerization temperature at 90°C. b) Ethyl 2-bromopropionate as initiator. c) Sparteine as a ligand.
d) Weight fraction of ***lc2*** in the solution diluted with anisole. e) Determined by GPC.

RAFT A toluene solution of ***lc2***, 2-phenylprop-2-dithiobenzonate, and AIBN as an initiator charged into a glass tube, which degassed and sealed off under vacuum. $[\boldsymbol{lc2}]_0/[I]/[dithioester]$ and weight fraction of ***lc2*** in solution are summarized in Table 2.4. Then the system was heated at 60°C for several hours. The polymerization underwent. Obtained Poly(***lc2***) has M_w/M_n about 1.3 which is a rather narrow MWD.

ATRP Poly(***lc2***) was synthesized by ATRP. A glass tube was charged with the appropriate ***lc2***, ethyl 2-bromoprorionate as initiator, $Cu^{(I)}Br$, sparteine (Sp.)[22] as ligand, and anisole as solvent, degassed, and sealed off in vacuum. $[\boldsymbol{lc2}]_0/[I]/[Cu]/[Sp.]$ and concentration of ***lc2*** in the solution are summarized in Table 2.5. Then the system was heated at 90°C for several hours. The polymerization carried out successfully to obtain Poly(***lc2***)s with $M_w/M_n < 1.3$.

2.4.4. Block Copolymerizations of *lc2* with PS

Block copolymerizations of ***lc2*** were carried out by using precursor with transfer agent

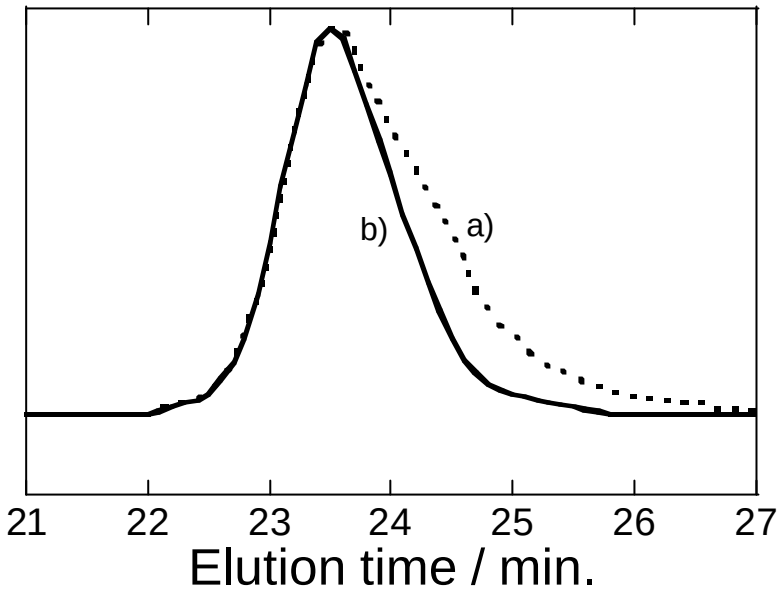

Figure 2.1. GPC charts of PS-*b*-Poly(***lc2***) a) before (M_n = 25000, M_w/M_n = 1.22) and b) after (M_n = 32200, M_w/M_n = 1.15) Soxhlet extraction with methylcyclohexane. The PS-*b*-Poly(***lc2***) was prepared by ATRP.

such as PS-DEPN (NMP) and PS-Br (ATRP) as initiators.

2.4.4.1. Consideration of Appropriate Precursor

Producing PS-*b*-Poly(***lc2***) diblock copolymer, it is able to use both PS-X and Poly(***lc2***)-X where X is a transfer agent as initiators. Which precursor is better to use, PS-X or Poly(***lc2***)-X?

A consideration of an efficiency of initiation selects Poly(***lc2***)-X as appropriate initiator. The dissociation of polyacrylates-X is commonly larger than that of PS-X, which enables to obtain narrower MWD. However, if the Poly(***lc2***)-X used as initiator, propagating end is PS radical, which is easier to break out bimolecular termination than polyacrylic radical, and then it produces Poly(***lc2***)-*b*-PS-*b*-Poly(***lc2***) triblock copolymer. The triblock copolymer must be prevented because of possibility of different characters and properties compared with the diblocks. In early stage of the polymerization, moreover, bimolecular terminations come about until the activation-deactivation process reaches equilibrium. Hence, Poly(***lc2***) with bimolecular weight is produced. The triblock copolymer and Poly(***lc2***) homopolymer cannot

be eliminated out of the polymeric system.

On the other hand, using PS-X precursor hardly produce PS-*b*-Poly(***lc2***)-*b*-PS triblock copolymer in an appropriate condition, and then terminated PS-PS and remaining PS-X can be removed by Soxhlet extraction with methylcyclohexane which is a Θ solvent for PS but a poor solvent for Poly(***lc2***) (see in Figure 2.1). The efficiency of the initiation is a little wrong compared with using Poly(***lc2***)-X. However, purer PS-*b*-Poly(***lc2***) can be obtained by using PS-X precursor.

Thus the block copolymerization was carried out only with PS-X precursors in this study.

2.4.4.2. Preparing PS-X Adducts

PS-DEPN and PS-Br were prepared as follow.

PS-DEPN A styrene solution of appropriate S-DEPN and BPO in a glass tube was degassed, sealed off under vacuum, and heated. After purification, a PS-DEPN was obtained with M_n of 3600 and $M_w/M_n \sim 1.1$, according to a GPC measurement calibrated by PS standard.

PS-Br An anisole solution of styrene 2640mg (25.4mmol), 2-bromoethylbenzene 25.5mg (0.138mmol), CuBr 38.7mg (0.270mmol), and Sp. 132mg (0.562mmol) in a glass tube was degassed, sealed off under vacuum, and heated at 120°C for 3h. After purification, 760mg of PS-Br was obtained with M_n of 6200 and M_w/M_n of 1.15.

2.4.4.3. Block Copolymerizations of *lc2* with PS-X Precursors

Block copolymerizations of ***lc2*** by NMP with PS-DEPN and by ATRP with PS-Br were carried out as described below. Characters of obtained polymers are summarized in Table 2.6-2.7.

NMP PS-DEPN precursor which had the $M_n = 3600$ was used. The PS-DEPN, ***lc2*** monomer, and toluene were pored in a glass tube, degassed, sealed off under vacuum, and heated at 120°C for several hours. Block copolymerization was carried out. However, MWD was wide at this condition. The reaction condition is needed more study as same as described in

Table 2.6. Results of block copolymerization by NMP [a)]

$[M]_0/[PS\text{-}DEPN]$ [b)]	Conc. [c)]	Time	M_n [d)]	Weight fraction of Poly(***lc2***) [e)]	M_w/M_n [d)]
100/1	25wt%	3.0h	11500	0.69	1.79
100/1	50wt%	2.3h	23200	0.84	2.24

a) Polymerization temperature at 120°C. b) Using PS-DEPN (M_n = 3600, M_w/M_n=1.1). c) Weight fraction of ***lc2*** in the solution diluted with toluene. d) Determined by GPC. e) Determined by ^{1}H NMR.

Table 2.7. Results of block copolymerization by ATRP [a)]

$[M]_0/[PS\text{-}Br]$ /[CuBr]/[Sp.]	Conc. [d)]	Time	M_n [e)]	Weight fraction of Poly(***lc2***) [f)]	M_w/M_n [e)]
15/1/1/2 [b)]	9.1wt%	18h	16400	0.10	1.14
22/1/1/2 [b)]	18wt%	6.8h	17800	0.17	1.13
80/1/1/2 [b)]	32wt%	7.5h	32200	0.54	1.15
235/1/1/2 [b)]	33wt%	19h	43500	0.65	1.22
480/1/1/2 [b)]	33wt%	41h	53900	0.73	1.38
225/1/1/2 [c)]	33wt%	19h	20200	0.69	1.19
220/1/1/2 [c)]	31wt%	40h	23200	0.73	1.34

a) Polymerization temperature at 90°C. b) Using PS-Br (M_n = 14700, M_w/M_n = 1.13). c) Using PS-Br (M_n = 6200, M_w/M_n = 1.15). d) Weight fraction of ***lc2*** in the solution diluted with toluene. e) Determined by GPC. f) Determined by ^{1}H NMR.

homopolymerization.

ATRP A glass tube was charged with the appropriate amount of ***lc2***, PS-Br which had the M_n = 14700 or 6200, $Cu^{(I)}Br$, Sp., and anisole, degassed, and sealed off under vacuum. $[\textbf{\textit{lc2}}]_0/[PS\text{-}Br]/[Cu]/[Sp.]$ and concentration of ***lc2*** in the solution are summarized in Table 2.7. Then the system was heated at 90°C for several hours. The polymerization underwent. After purification, the PS-*b*-Poly(***lc2***)s with various M_n of 16400-53900, compositions of Poly(***lc2***) segment at 0.10-0.73, and narrow MWDs (=1.1-1.3) as listed in Table 2.7. However, the PS-*b*-Poly(***lc2***)s with large M_n showed rather large MWDs. This needs more studies to improve.

RAFT was not demonstrated because a block copolymerization of acrylates with PS-dithioester cannot be carried out. By using PS-dithioester, an intermeditiate of PS-(dithioester radical)-acrylates only back to PS-dithioester, thus PS-*b*-Poly(***lc2***) cannot be obtained. If the Poly(***lc2***)-dithioester adduct is used, PS-*b*-Poly(***lc2***) will be obtained but

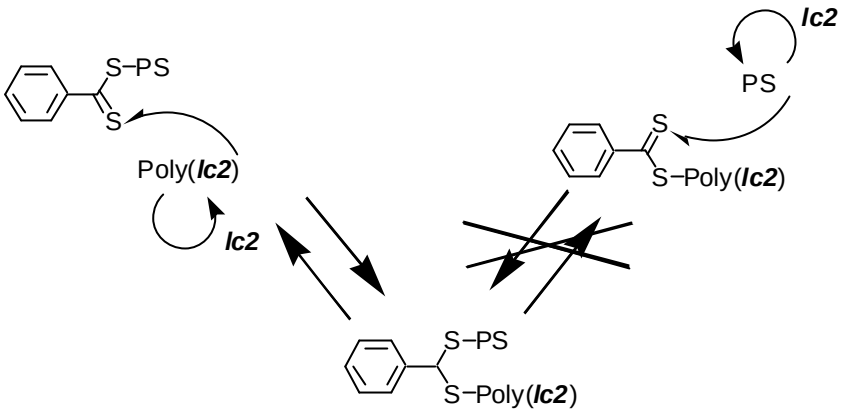

Scheme 2.2. RAFT process with PS-dithioester and Poly(***lc2***) radical.

contain side-reacted polymers as described above.

2.4.5. Comparison of NMP, RAFT, and ATRP

The three efficient methods of LRP including NMP, RAFT, and ATRP for synthesis of Poly(***lc2***)s are successfully carried out, while NMP and ATRP are also available for synthesis of PS-*b*-Poly(***lc2***)s with PS precursors. The three methods are compared in Table 2.8. Which is the best system in LRP for synthesis of SCLCP and LC block copolymer?

In order to investigate thermotropic phase behaviors, polymers must be thermally stable. With this requirement in mind, NMP, RAFT, and ATRP are compared.

NMP After purification, living polymers terminated with nitroxide are obtained. This nitroxide dissociates thermally, and then polymer radical appears. The polymer radical is killed by oxygen in atmosphere or produces bimolecular terminated polymer in bulk. The polymers are heated above the reaction temperature to investigate thermotropic phase behavior and structures at several temperature. Particularly a differential scanning calorimetric measurement is carried out under nitrogen. Thus Poly(***lc2***) and PS-*b*-Poly(***lc2***) can produce bimolecular terminated polymers during the investigation. The polymers obtained by NMP are thermally irrelevant without something to kill the nitroxides. Even if the nitroxides are transformed into thermally stable ends, moreover, methacrylic side-chain polymers can not be synthesized currently due to fast extraction of *b*-hydrogen.

RAFT The dithio compound can dissociate photochemically or thermochemically. Thus RAFT is not also appropriate to obtain thermotropically stable polymer. Even if the dithio compound is transformed into thermally stable ends, moreover, the polymerization in RAFT is very slow, thus inaptitude to obtain polymers with large M_n. Furthermore, block copolymerization of acrylic and methacrylic monomers with PS precursor can not be available as described above. On the other hand, RAFT can be applied to the polymerization of many unreactive monomers in NMP and ATRP such as vinyl and acidic monomers.

ATRP Now, ATRP is a universal method to obtain thermotropic polymers with eliminating the catalyst and the ligand. Halogens at the end of chain is not dissociated without the catalyst and the ligand. Moreover, obtaining polymers have an inexpensive halogen at the chain end. Hence the PS-*b*-Poly(***lc2***)s obtained by ATRP are used in Chapter 6.

ATRP is limited to the polymerization without acidic monomers, which can protonate the ligands and complex with copper. However, most of SCLCPs do not need acidic functional groups.

Table 2.8. Comparison of NMP, RAFT, and ATRP in synthesis of acrylic LC block copolymers.

Method	Monomer	Block copolymerization with PS precursor	End group
NMP	○Styrenes ×Acrylates with TEMPO ○Acrylates with DEPN ×Methacrylates	Available	Relatively expensive Thermally unstable
RAFT	○Nearly all monomers	Not available	Relatively expensive Thermally less stable
ATRP	○Nearly all monomers ×Acidic monomers ×Alkyl-substituted olefins	Available	Inexpensive Thermally stable

2.5. Concluding Remarks

Side-chain liquid crystalline polymers and their block copolymers with polystyrene (PS) were synthesized by living anionic polymerization and living radical polymerization. Living anionic polymerization is the best method to synthesize well-defined polymers. However, it has some limitations of monomer species and molecular weight. On the other hand, a new living polymerization, namely living radical polymerization, does not have these limitations. Hence, variable liquid crystalline species can be introduce into block copolymers.

Living anionic polymerization was successfully carried out to obtain well-defined liquid crystalline (LC) diblock copolymers containing poly(6-[4-(4'-methoxyphenyl)phenoxy]hexyl methacrylate) as a LC segment and polystyrene as an amorphous segment with various molecular weights and compositions and with narrow molecular weight distributions ($M_w/M_n \leq 1.05$).

Living radical polymerization was performed to prepare a series of side-chain liquid crystalline poly(6-[4-(4'-cyanophenyl)phenoxy]hexyl acrylate) by nitroxide-mediated radical polymerization (NMP), reversible addition-fragmentation chain transfer (RAFT), and atom transfer radical polymerization (ATRP). The three methods were successfully carried out to obtain living poly(6-[4-(4'-cyanophenyl)phenoxy]hexyl acrylate). Its block copolymerizations with PS precursor were also carried out by NMP and ATRP. Obtaining block copolymers have various molecular weights, compositions and narrow molecular weight distributions (M_w/M_n = 1.1-1.3 by ATRP). ATRP is considered to be currently the best method to obtain thermostable polymers in LRP.

References in This Chapter

1. J. Adams and W. Gronski, *Makromol. Chem., Rapid Commun.*, **10**, 553 (1989).
2. B. Zaschke, W. Frank, H. Fischer, K. Schmutzler, and M. Arnold, *Polym. Bull.*, **27**, 1 (1991).
3. D. R. Iyenger, S. M. Perutz, C. Dai, C. K. Ober, and E. J. Kramer, *Macromolecules*, **29**, 1229 (1996).
4. A. Moment, R. Miranda, and P. T. Hammond, *Macromol. Rapid Commun.*, **19**, 573

(1998).

5. M. Hefft and J. Springer, *Makromol. Chem. Rapid Commun*., **11**, 397 (1990).
6. V. Percec and M. Lee, *J. Macromol. Sci., Pure Appl. Chem*., **A29**, 723 (1992).
7. Z. Komiya and R. R. Schrock, *Macromolecules*, **26**, 1387 (1993).
8. B. R. Maughon, M. Weck, B. Mohr, and R. H. Grubbs, *Macromolecules*, **30**, 257 (1997).
9. R. Bohnert and H. Finkelmann, *Macromol. Chem. Phys.*, **195**, 689 (1994).
10. M. Yamada, T. Iguchi, A. Hirao, S. Nakahama. and J. Watanabe, *Macromolecules*, **28**, 50 (1995).
11. M. Yamada, T. Itoh, R. Nakagawa, A. Hirao, S. Nakahama, and J. Watanabe, *Macromolecules*, **32**, 282 (1999).
12. W. Y. Zheng and P. T. Hammond, *Macromol. Rapid Commun*., **17**, 813 (1996).
13. O. Lehmann, S. Förster, and J. Springer, *Macromol. Rapid Commun*., **21**, 133 (2000).
14. K. Matyjaszewski, S. Gaynor, D. Greszta, D. Maedare, and T. Shigemoto, *J. Phys. Org. Chem.*, **8**, 306 (1995).
15. K. Matyjaszewski, Ed, "Contorolled / Living Radical Polymerization: Progress in ATRP, NMP, and RAFT", American Chemical Society, Washington, D. C., 2000, Vol. 768.
16. D. H. Solomon, E. Rizzardo, and P. Cacioli, Eur. Pat. Appl., EP 0 135 280 (Jul. 11, 1984) (*Chem. Abstr.* 102, 221335q (1985)).
17. M. K. Georges, R. P. N. Veregin, P. M. Kazmaier, and G. K. Hamer, *Macromolecules*, **26**, 2987 (1993).
18. A. Goto and T. Fukuda, *Macromolecules*, **32**, 618 (1999).
19. D. Benoit, S. Grimaldi, S. Robin, J. P. Finet, P. Tordo, and Y. Gnanou, *J. Am. Chem. Soc.*, **122**, 5929 (2000).
20. J. S. Wang and K. Matyjaszewski, *J. Am. Chem. Soc.*, **117**, 5614 (1995).
21. T. E. Patten, J. Xia, T. Abernathy, and K. Matyjaszewski, *Science*, **272**, 866 (1996).
22. B. Yu and E. Ruckenstein, *J. Polym. Sci., Part A: Polym. Chem.*, **37**, 4191 (1999).
23. V. Coessens, T. Pintauer, and K. Matyjaszewski, *Prog. Polym. Sci.*, **26**, 337 (2001).
24. K. Matyjaszewski and J. Xia, *Chem. Rev.* **101**, 2921 (2001).
25. T. P. Le, G. Moad, E. Rizzardo, and S. H. Thang, Int. Pat. Appl., WO 98 001 478 (Jan. 15, 1998) (*Chem. Abstr.* **128**, 115390 (1998)).

26. J. Chiefari, Y. K. (B.) Chong, F. Ercole, J. Krstina, J. Jeffery, T. P. T. Le, R. T. A. Mayadunne, G. F. Meijs, C. L. Moad, G. Moad, E. Rizzardo, and S. H. Thang, *Macromolecules*, **31**, 5559 (1998).
27. M. C. Bignozzi, C. K. Ober, and M. Laus, *Macromol. Rapid Commun*., **20**, 622 (1999).
28. C. A. Barbosa and A. S. Gomes, *Polym. Bull.*, **41**, 15 (1998).
29. A. S. Gomes, C. A. Barbosa, and M. R. Pinto, *Polym. Int*., **48**, 713 (1999).
30. A. M. Kasko, A. M. Heintz, and C. Pugh, *Macromolecules*, **31**, 356 (1998).
31. H. Finkelmann, M. Happ, M. Portugal, and H. Ringsdorf, *Makromol. Chem*. **179**, 2541 (1978).
32. J. C. Dubois, G. Decobert, P. L. Barny, S. Esselin, C. Friedrich, and C. Noël, *Mol. Cryst. Liq. Cryst*., **137**, 349 (1986).

Appendix

NMP, ATRP, and RAFT in Living Radical Polymerization

A1. Introduction

The past few years have witnessed the rapid growth in the development and understanding of the new living radical polymerization (LRP) methods[1-3]. We need to describe its outline in this thesis. Details are described in some reviews[3,12]. Three methods are currently standard; nitroxide-mediated radical polymerization (NMP)[4-7], atom transfer radical polymerization (ATRP)[8-12], and reversible addition-fragmentation chain transfer (RAFT)[13,14]. LRP retains the advantages of conventional radical polymerization, *i.e.*, simplicity, robustness, and versatility, and allows fine control of polymer structures owing to the living system. Styrenic, acrylic, methacrylic, olefinic, and functionallized polymers can be synthesized by LRP. Polymers with complicated topologies such as block, graft, star, and comb-shaped structures can also be tailored by LRP. With these attractive features, LRP is expected to synthesize new advanced materials that have not achieved by either conventional radical polymerization or other living polymerizations.

A2. Requirements for LRP

The basic mechanism common to all the variants of LRP is the alternating activation-deactivation process [1,2], in which P-X (dormant species) is supposed to be activated to polymer radical (P•, active species) by thermal, photochemical, and/or chemical stimuli. In the presence of monomer (M), polymer radical undergo propagation until it is deactivated to P-X (Scheme A1-A3).

On the other hand, possible elementary reactions other than reversible activation process are described in Scheme A4. Irreversible chain transfer and decomposition of P-X hardly occur except for special systems. Livingness is possible in a chain growth polymerization when nearly all the chains are initiated at the same time and the contribution of chain breaking reactions such as transfer and termination can be neglect in comparison to propagation.

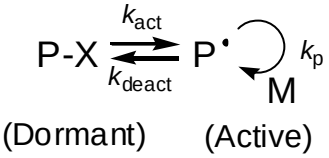

Scheme A1. A general scheme of reversible activation.

Dissociation-Combination

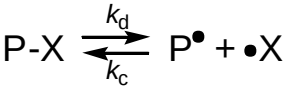

Degenerative Chain Transfer

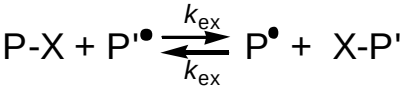

Atom Transfer

Scheme A2. Three main mechanisms of reversible activation.

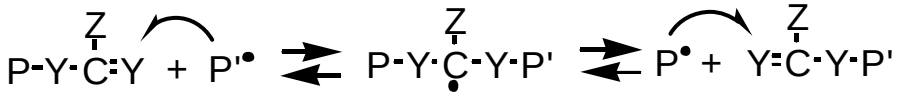

Scheme A3. Reversible addition-fragmentation chain transfer (RAFT).

Initiation

$$R_i = k_i[M]^3 + k_I[I]$$

Propagation

$$P^{\cdot} + M \longrightarrow P^{\cdot}$$

Termination

$$P^{\cdot} + P^{\cdot} \longrightarrow \text{dead polym.}$$

Chain Transfer

$$P^{\cdot} + RH \longrightarrow PH + R^{\cdot}$$

Decomposition of P-X

$$P\text{-}X \longrightarrow \text{dead polym.} + XH$$

Scheme A4. Possible elementary reactions except for reversible activation.

Conventional initiation is usually induced by initiator such as azoisobuthylonitrile (AIBN), benzoyl peroxide (BPO), thermally, and decomposition of polymers. It needs to be careful the experimental conditions such as concentrations, temperature, and reaction time. Relatively noteworthiness is propagation and bimolecular termination. When the concentration of M is large, propagation is dominant in the system, while bimolecular termination cannot be neglected in small concentration of M. The break through of LRP, concentration of $P^{\bullet}$ is very small to neglect actually the bimolecular termination with the activation-deactivation process. In order to keep this condition, it is usually holds that $[P^{\bullet}]/[P\text{-}X] \leq 10^{-5}$ and the polymerization is stopped within the large concentration of M, in other words, polymerization is not complete. Moreover, the activation-deactivation cycle is supposed to be repeated enough times to give every chain an almost equal chance to grow. In this way, LRP process come about the narrow molecular weight distribution (MWD) product, a linear molecular weight-conversion profile, the predictability of the molecular weight from the ratio of monomer consumed to transfer agents, and the ability to produce blocks or higher molecular weight polymers by further monomer addition.

LRP is separated by process of the deactivation of P-X; dissociation-combination, degenerative chain transfer, and atom transfer as illustrated in Scheme A2.

A3. NMP

NMP is categorized in the dissociation-combination mechanism. NMP was first succeeded with 2,2,6,6-tetramethyl-piperidinyl-1-oxy (TEMPO) as a transfer agent of X affording well-defined polymers with low MWD (M_w/M_n ~ 1.1-1.3)[4,5]. PS-TEMPO is dissociated with increasing temperature of the system and the polymerization undergo until decrement of temperature.

TEMPO can be used for the polymerization of styrene and styrenic derivatives. Other nitroxide such as di-*tert*-buthyl nitroxide (DBN)[6] and *N*-*tert*-butyl-1-diethylphosphono-2,2-dimethylpropyl nitroxide (DEPN)[7] enable to polymerize acrylate and acrylic derivatives. Polymerizations of methacrylates and *a*-methylstyrene, on the other hand, have not been succeeded with nitroxide because the nitroxides come about side-reaction with *a*-methylene at the end of propagation.

The end group of nitroxide is retained in the polymeric product, and then block copolymerization can be carried out by further monomer addition.

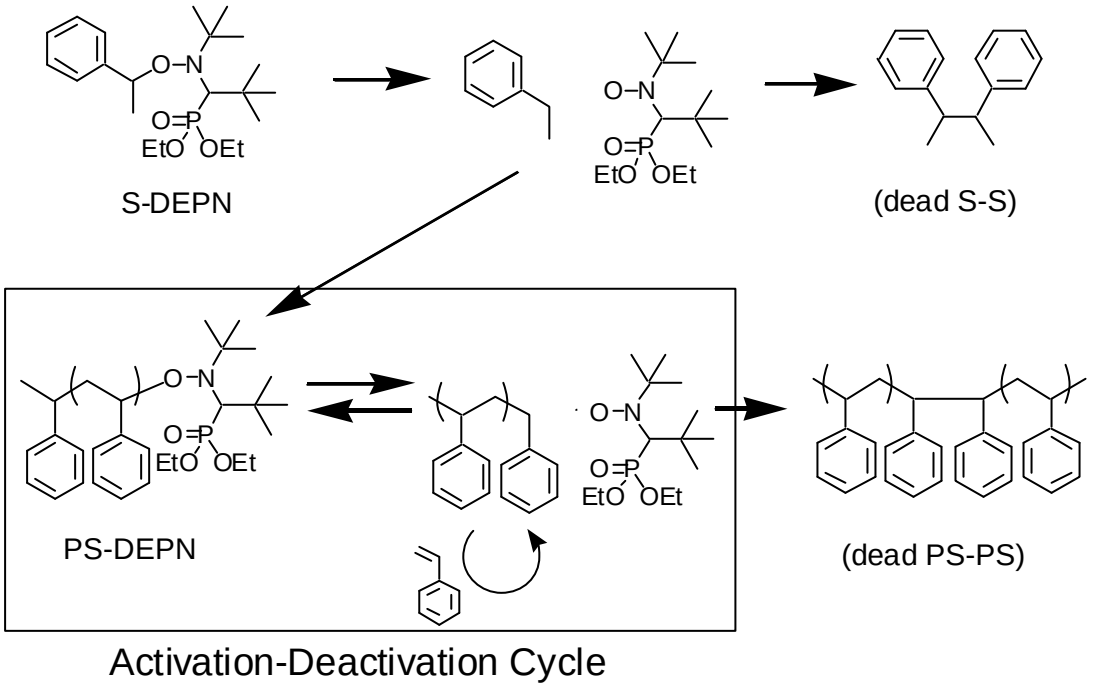

Scheme A5. Nitroxide mediated radical polymerization (NMP) of polystyrene.

A4. RAFT

RAFT[13,14] with dithioester is a branch of degenerative chain transfer (Scheme A3). Polymer radical attacks the dithioester which is a capping agent of polymer, and then an intermeditiate A-(dithio radical moiety)-A is produced. The intermaditiate is rapidly back to the past P-X or alters to new P'-X.

The experimental condition is allowed in bulk, solution, emulsion, or suspension. There appear to be no limitations on solvent or reaction temperature. A major advantage of the RAFT process over other LRP is that it is compatible with a very wide range of monomers including functional groups. The dithioester end group is retained in the polymeric product.

It can be carried out block copolymerizations with further monomer addition. However, the A-(dithio radical moiety)-B intermediate in RAFT process prepares selectively A-dithio moiety and B radical because the bond between dithio moiety and B is weaker than that with A (for example A is styrene and B is acrylate). Hence, a precursor in block copolymerization is necessary to select.

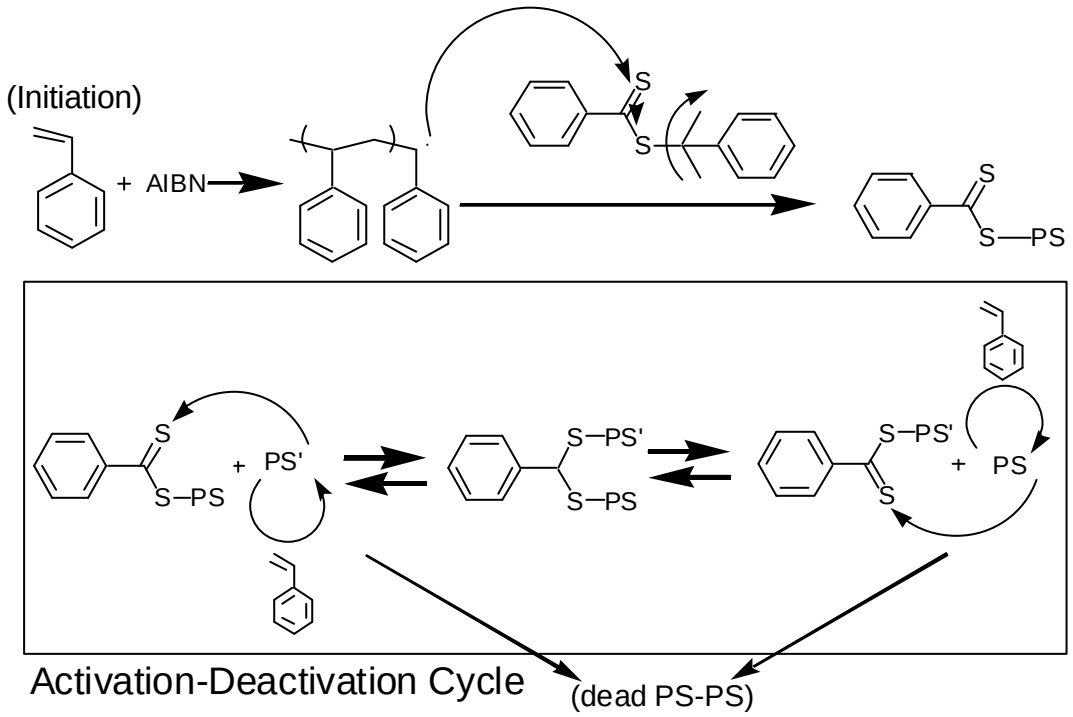

Scheme A6. RAFT process of polystyrene.

A5. ATRP

In ATRP, a redox reaction of transition metals activates reversibly the dormant polymer chains via halogen atom transfer reaction. As reported[12], the homogeneous ATRP of styrene, acrylates, methacrylates, acrylonitrile, vinylpyridine, and many other monomers can yield polymers with predetermined molecular weights and narrow MWD. A list of suitable transition metals includes Cu, Fe, Ru, Ni, Pd and some others. Some suitable ligand is needed to compose a metal complex, which enables the reaction system to be homogeneous. For example, the bulk polymerization of styrene catalyzed by CuBr/2dNbpy (dNbpy = 4,4'-di(nonan-5-yl)-2,2'-bipyridine) prepared well-defined PS (sometimes the MWD < 1.05)[9]. Block copolymerization is also carried out by halogen-mediated prepolymer as initiator. The ligand is commonly used some appropriate base. Hence, acidic monomers such as neat acrylate can not be available because they can protonate the ligand and make complexes with the metals.

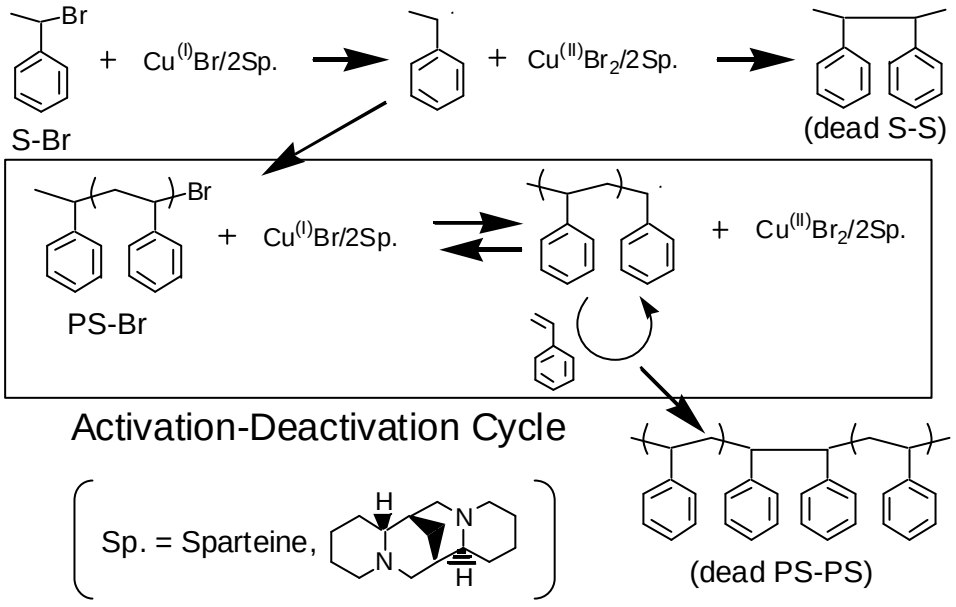

Scheme A7. Atom transfer radical polymerization (ATRP) of polystyrene.

References

1. K. Matyjaszewski, S. Gaynor, D. Greszta, D. Maedare, and T. Shigemoto, *J. Phys. Org. Chem.*, **8**, 306 (1995).
2. K. Matyjaszewski, *Macromol. Symp.*, **174**, 51 (2001).
3. K. Matyjaszewski, Ed, "Contorolled / Living Radical Polymerization: Progress in ATRP, NMP, and RAFT", American Chemical Society, Washington, D. C., 2000, Vol. 768.
4. D. H. Solomon, E. Rizzardo, and P. Cacioli, Eur. Pat. Appl., EP 0 135 280 (Jul. 11, 1984) (*Chem. Abstr.* 102, 221335q (1985)).
5. M. K. Georges, R. P. N. Veregin, P. M. Kazmaier, and G. K. Hamer, *Macromolecules*, **26**, 2987 (1993).
6. A. Goto and T. Fukuda, *Macromolecules*, **32**, 618 (1999).
7. D. Benoit, S. Grimaldi, S. Robin, J. P. Finet, P. Tordo, and Y. Gnanou, *J. Am. Chem. Soc.*, **122**, 5929 (2000).
8. J. S. Wang and K. Matyjaszewski, *J. Am. Chem. Soc.*, **117**, 5614 (1995).
9. T. E. Patten, J. Xia, T. Abernathy, and K. Matyjaszewski, *Science*, **272**, 866 (1996).
10. B. Yu and E. Ruckenstein, *J. Polym. Sci., Part A: Polym. Chem.*, **37**, 4191 (1999).
11. V. Coessens, T. Pintauer, and K. Matyjaszewski, *Prog. Polym. Sci.*, **26**, 337 (2001).
12. K. Matyjaszewski and J. Xia, *Chem. Rev.*, **101**, 2921 (2001).
13. T. P. Le, G. Moad, E. Rizzardo, and S. H. Thang, Int. Pat. Appl., WO 98 001 478 (Jan. 15, 1998) (*Chem. Abstr.* **128**, 115390 (1998)).
14. J. Chiefari, Y. K. (B.) Chong, F. Ercole, J. Krstina, J. Jeffery, T. P. T. Le, R. T. A. Mayadunne, G. F. Meijs, C. L. Moad, G. Moad, E. Rizzardo, and S. H. Thang, *Macromolecules*, **31**, 5559 (1998).

Chapter 3

Morphological Transformation Induced by Liquid Crystalline Phase Transition in Diblock Copolymers Containing Polystyrene and Smectic Side-Chain Liquid Crystalline Segment

Abstract: We have synthesized well-defined AB type diblock copolymers, which have polystyrene as an amorphous segment and poly(6-[4-(4'-methoxyphenyl)phenoxy]hexyl methacryrate) as a liquid crystalline (LC) segment with various compositions and narrow molecular weight distributions, by sequential living anionic polymerization. The thermotropic phase behavior and structures were examined for six copolymers with the weight fraction of LC segments from 0.24 to 0.45. All copolymers exhibit crystalline-smectic A_d and the smectic A_d-isotropic phase transitions. With the weight fraction of the LC segment deviating from 0.5, the block copolymers form cylindrical microdomain as expected in the isotropic phase, whereas the lamellar microdomains are formed for the copolymer with the weight fraction of the LC segment around 0.5. Some block copolymers reorganize extraordinarily the microdomain structure by the phase transition. Factors to determine microdomain morphology are discussed.

3.1. Introduction

Block copolymers containing liquid crystalline (LC) segment have two different ordering structures of microdomain structure and LC phase structure. In other words, the LC segment has to take the phase transitions in a restricted space of the microdomain with various sizes and shapes. Hence, when they form a highly anisotropic microstructure in the LC and crystal, the microdomain morphology may be altered from that in the isotropic phase. Conversely, if the microdomain morphology is tightly maintained, the transitional behavior of the LC segment may be strongly affected. It is one of the interesting subjects in not only the LC polymer field but also block copolymer field to clarify this relationship between two different ordering structures.

In previous studies[1], we prepared block copolymers (PS-*b*-Poly(***lc1***)) composed of polystyrene (PS) and poly(6-[4-(4'-methoxyphenyl)phenoxy]hexyl methacrylate) (Poly(***lc1***)) segments by sequential living anionic polymerization.

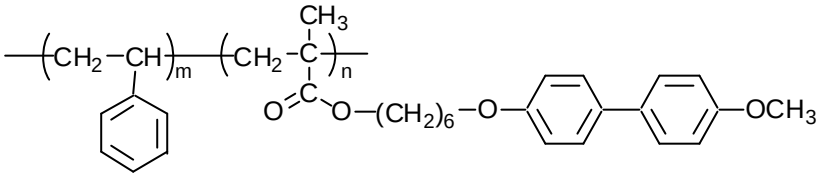

PS-*b*-Poly(***lc1***)s with various molecular weights and segmental compositions of around 50wt% exhibited lamellar type microphase segregations, and their Poly(***lc1***) segments formed crystalline, smectic A_d (SmA_d), and isotropic phases like in Poly(***lc1***) homopolymer. The mesogenic layered structures of the crystal and the SmA_d were formed with the side-chain mesogens lying parallel to the microdomain interface, *i.e.*, with the mesogenic layers perpendicular to the interface. A most interesting feature is that the lamellar thickness depended on the SmA_d temperature (see Figure 1.2 in Chapter 1). With increasing temperature, it decreased continuously from the value in the crystalline phase to that of the isotropic phase; no jump could not be seen on both the crystalline-SmA_d and SmA_d-isotropic phase transitions. The overall change was completely reversible on heating and cooling cycles, indicating that it proceeds at a thermodynamic equilibrium. The reduction was about 20-25%, which is associated with the conformational change of Poly(***lc1***) segment from the extended form in the crystalline phase to the random coil in the isotropic phase. Such a conformational change

was considered to arise as a result of the counterbalance between conformational entropic gain of the main-chain and energetic cost due to the layer ordering of side-chain mesogens.

Several other type microdomains, cylinder, sphere, and bicontinuous morphology, have been reported in other LC block copolymers, and interesting relationships between the microdomain morphology and LC phase structure have been discussed[2,3]. Sänger *et al.* observed a order-order transition (OOT)[4,5] from PS-spheres above the clearing temperature to the PS-cylinders in the nematic phase in PS-*b*-LC-*b*-PS triblock copolymer with 12vol% of the PS segment[6]. Hammond *et al.*[7] and Finkelmann *et al.*[8] reported OOT followed by the LC phase transition in smectic LC-coil diblock copolymers. So we study OOT induced by LC phase transition in following chapters with various composition in the case of neat LC block copolymer (current Chapter and Chapter 6) and of its blend with corresponding homopolymer (Chapter 5).

Moreover, LC phase behavior is affected by microdomain morphology. Fisher and coworkers reported[9] a morphology diagram for smectic LC-coil block copolymers (PS-*b*-PChEMA) synthesized by polymer analogous reaction. In their morphology diagram, PS-spheres, PS-cylinders, lamellae, and LC-spheres were observed. LC-cylinders were not observed. The LC phase in the spherical microdomain only showed nematic phase rather than smectic phase that appeared in other morphologies and corresponding LC homopolymer. This indicated that a thermodynamically stable smectic layered structure could not be formed in a cylindrical and spherical microdomains. Recently, on the other hand, Yamada *et al.* observed[10] that the smectic temperature region is broadened in the LC-cylinders for a LC-coil diblock copolymer composed with PS and poly(6-[4-(4'-cyanophenyl)phenoxy]hexyl methacrylate) which showed SmA_2 phase. Ober *et al.* also reported the same phenomena[11]. Interestingly, Yamada's observation and Ober's are in contrast to Fischer's. It needs more experimental results and discussion for the interrelations between morphologies and phase transitions of LC-coil block copolymers. In this chapter, we investigate the interrelations in PS-*b*-Poly(***lc1***) which had various segmental compositions.

3.2. Experimental Section

Materials PS-*b*-Poly(***lc1***)s were prepared by sequential living anionic polymerization, namely **S1**-**S6** as shown in Table 3.1 (see Chapter 2). Their molecular weights of Poly(***lc1***) segment in this study were around 20000 with the segmental composition from 24wt% to 45wt%. The composition of each segment was finally determined by ^{1}H NMR. Molecular weight (M_n) and molecular weight distribution (M_w/M_n) values were estimated from GPC profile based on the standard polystyrene calibration. The characteristics of PS-*b*-Poly(***lc1***)s are summarized in Table 3.1.

Methods Differential scanning calorimetric (DSC) measurements were carried out with a Perkin-Elmer DSC Model II at a scanning rate of 2°C·min^{-1}. X-ray measurements were performed by using Rigaku Denki X-ray generator with Ni-filtered Cu-Kα radiation. Reflection spacings were calibrated by using silicon standard. Temperatures of the sample were regulated within 1°C by using Mettler FP-82 hot stage. Transmission electron microscopic (TEM) observations to clarify the morphology of PS-*b*-Poly(***lc1***)s were performed by Hitachi H-500 transmission electron microscope with 75kV of accelerating voltage. For this observation, the PS-*b*-Poly(***lc1***)s were cut into ultrathin sections (700-1000Å) by ultramicrotome with a glass knife. The sectioned specimens were stained with vapor of ruthenium tetraoxide (RuO_4) for 10min before observation.

Table 3.1. Block Copolymerization of styrene and LC monomer ***lc1*** [a)]

	M_n [b)]		M_w/M_n [c)]	Weight fraction
	PS segment	Poly(***lc1***) segment		of Poly(***lc1***)
S1	26000	21000	1.03	0.45
S2	34000	21000	1.05	0.41
S3	34000	18000	1.03	0.35
S4	36000	17000	1.04	0.32
S5	40000	17000	1.04	0.30
S6	51000	16000	1.04	0.24

a) Block copolymerization was carried out by sequental addition of styrene at first and then ***lc1*** in THF at -40°C with *sec*-BuLi as an initiator. Yields of polymers were quantitative in all runs. b) Determined by GPC and ^{1}H NMR. c) Determined by GPC.

3.3. Results and Discussion

3.3.1. Phase Transitions

Transition temperatures and enthalpies measured by DSC are summarized in Table 3.2. All PS-*b*-Poly(***lc1***)s exhibited two transitions, similarly as corresponding homopolymers of Poly(***lc1***) and PS-*b*-Poly(***lc1***)s composed of both segments around 50wt%[1]. The phase sequence was also similar; crystal-SmA_d and SmA_d-isotropic phase transitions took place. The SmA_d-isotropic phase transition temperatures varied depending on the composition of the LC segment, whereas the crystal-SmA_d phase transition temperatures did not vary.

3.3.2. Microdomain Structures in the Isotropic Phase

We expected that the block copolymers in the isotropic phase form the microphase segregated structure as same as conventional coil-coil block copolymers form the lamellar, cylindrical, and spherical microdomains depending on the weight fraction of the two segments. Figures 3.1a-c show TEM photographs for ultrathin section cut out of PS-*b*-Poly(***lc1***)s which are annealed in the isotropic phase at 150°C overnight and then quenched. The Poly(***lc1***) microdomains appear dark due to staining RuO_4, and dark Poly(***lc1***)-lamellar domain is narrower than blight PS-domains as expected from the segmental composition of Poly(***lc1***) segment. The lamellar type morphology is observed for **S1**-**S5** containing Poly(***lc1***) segment from 30wt% to 45wt%. Dark lines and circles can be observed for **S6**, which indicated Poly(***lc1***)-cylinders as expected from 24wt% of the Poly(***lc1***) segment.

Table 3.2. DSC data of PS-*b*-Poly(***lc1***)s [a)]

	Transition temperature / °C (Enthalpy changes / kcal·mol^{-1} [b)])			
	Heating		Cooling	
	T_1 (DH_1)	T_2 (DH_2)	T_1 (DH_1)	T_2 (DH_2)
S1	108.2 (1.03)	132.6 (0.52)	102.8 (0.99)	133.4 (0.52)
S2	105.6 (0.84)	126.9 (0.40)	99.8 (0.81)	125.5 (0.39)
S3	104.8 (0.74)	133.2 (0.38)	100.3 (0.71)	132.5 (0.33)
S4	103.0 (0.74)	124.9 (0.27)	98.2 (0.74)	124.4 (0.30)
S5	103.4 (0.68)	128.5 (0.35)	98.9 (0.74)	127.8 (0.35)
S6	105.9 (0.62)	132.9 (0.37)	101.4 (0.74)	131.6 (0.26)

a) Determined by DSC measurement on 2nd heating and cooling at the rate of 2°C·min.$^{-1}$.
b) Estimated per mole of Poly(***lc1***) segment.

3.3.3. Morphological Transformation Induced by Phase Transition

According to the Leibler's theory for a AB block copolymer[12], the microdomain morphology is determined by the fraction of A (or B) segment in the AB diblock copolymer and cN where N is the polymerization index and c is the Flory parameter characterizing the effective interaction of segments AB. Generally c depends on the inverse of temperature. As the segmental composition deviates from 50wt%, decrement of temperature causes morphological reorganizations, for example, from spheres to cylinders and from cylinders to lamellae. These OOTs have been experimentally observed in conventional block copolymers[4,5]. LC block copolymers also showed OOT. However, they had some differences from conventional block copolymers. The OOTs were induced by LC phase transition[6-8]. Although their driving forces have not been clear yet, LC microdomain in the LC-coil diblock copolymer including PS-*b*-Poly(***lc1***) is also expected the morphological reorganization by the phase transition.

Figure 3.2 shows the temperature dependence of domain spacing for **S1**-**S6** by small angle X-ray scattering (SAXS) measurements on cooling (reversibly on heating). The spacings reduce remarkably through the SmA_d temperature region from the size in the isotropic phase to that in the crystalline phase for **S1**-**S6**. This can be explained to be caused by conformational change of Poly(***lc1***) segment from the extended form to the random coil. In current study, the reduction lengths of the spacing were expected the same degree because of similar M_n of the Poly(***lc1***) segment around 20000 for **S1**-**S6**, and the reductions were nearly same about 80Å for **S1**-**S5**. However, the drastic reduction of the spacing near the SmA_d-isotropic phase transition temperature could be observed for **S4** and **S5**. Furthermore, the reduction length of the domain spacing was only 35Å for **S6** which formed cylindrical microdomains in the isotropic phase.

The most distinct feature here is that extraordinary morphological transformations could be observed from lamellae to cylinders by decrement of temperature. Figures 3.1d-f show the TEM photographs for ultrathin section cut out of **S1**-**S6** which were quenched from smectic phase temperature region at 120°C. The lamellar morphology is observed for **S1**, **S2**, and **S3** and the cylindrical morphology for **S4**, **S5**, and **S6**. The morphology remains lamellae for **S1**, **S2**, and **S3**, and cylinders for **S6** through the isotropic-SmA_d transition. On the other hand, it

changes from lamellae to cylinders through the phase transition from the isotopic phase to the SmA_d phase for **S4** and **S5**. The two block copolymers show the drastic reduction of the spacing near the SmA_d-isotropic phase transition temperature as described above (see Figure 3.2). This indicates that the microphase segregated structure reorganizes from lamellae to cylinders on the isotropic-SmA_d phase transition in the two PS-*b*-Poly(***lc1***)s. This OOT was unexpected according to Leibler's theory[12] and experimental results[4,5] in conventional block copolymers, in which cylinders at high temperature altered into lamellae at low temperature. Hence, the OOT in this study must be induced by the LC phase transition. This result indicate that the smectic structure is stable in cylinders rather than lamellae.

This can be explained as follow. In the isotropic phase of Poly(***lc1***) segment, PS-*b*-Poly(***lc1***) was regarded as conventional block copolymers such as PS-*b*-PI, and showed appropriate morphology depending on the segmental composition. When Poly(***lc1***) segment composed smectic structure in the lamellar microdomain, anisotropic expansion of the Poly(***lc1***) segment due to smectic layered packing structure constrained the anisotropy to its counter PS segment. If the PS segment can not hold the anisotropy in PS-lamellae, a relaxation of the conformational entropy in the PS segment induced an interfacial curvature of the microdomains, resulting in Poly(***lc1***)-cylinders as illustrated in Figure 3.4. Hence, the OOT took place in narrow region of segmental composition around 30wt% of Poly(***lc1***) segment.

3.3.4. Determination of Microdomain Morphology in LC Block Copolymer

Previously it was found that order-disorder transition (ODT) induced by LC phase transition, in which disordered state of the microdomain at the isotropic phase in LC segment transformed ordered state of microdomain (lamellae) at the smectic phase. Hammond *et al*. explained that smectic structure led discontinuous increment of c[13]. Symmetric PS-*b*-Poly(***lc1***)s with low molecular weight also showed the same ODT[1]. But the transformation from lamellae at the isotropic phase to cylinders at the smectic phase in current study means that decrement of c was led by smectic structure. Same PS-*b*-Poly(***lc1***)s but different molecular weight showed antinomic c behavior with composing same smectic structure. We must note that microdomain morphology simply depends on c for conventional

block copolymers but not simply for LC block copolymer.

The microdomain structure can be simply considered in strong segregated limited theory by Helfand[3]. Chain conformational free energy in block copolymers depends on four terms of interfacial free energy between each microdomain, placement of the each segment in a restricted microdomain, localization of chemical junction of each segment at the microdomain interface, and demixing enthalpy of each segment. For LC block copolymer, the last two terms can be considered as same as conventional block copolymers. E. L. Thomas noted[14] that the interfacial free energy and conformational changes in the LC segment affected the microdomain morphology. The interfacial free energy is drastically changed by the LC phase transition because of the elasticity coefficients of mesogenic director. Moreover, the result in current study strongly suggests the importance of anisotropic chain conformation of LC segment inducement of anisotropy for the counter segmental conformation.

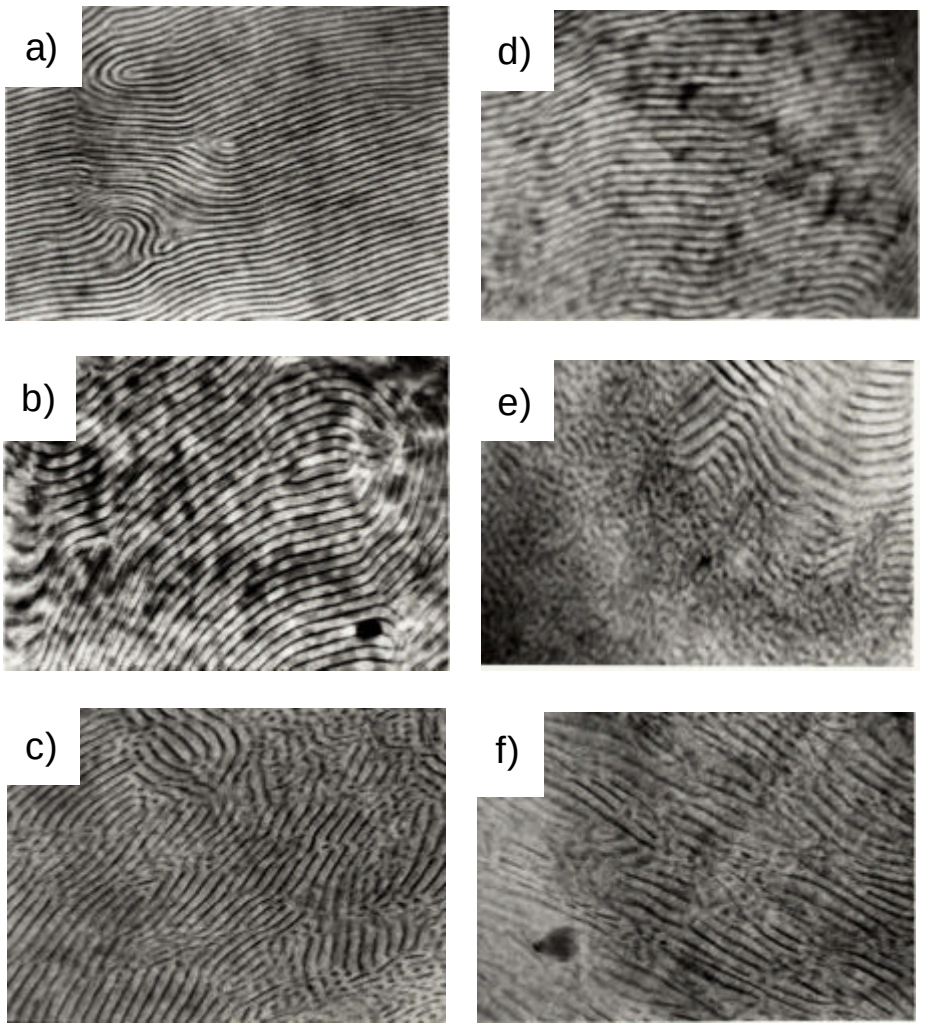

Figure 3.1. Transmission electron microscopic photographs for the ultrathin section cut out of the block copolymers stained by RuO_4. Dark area is the Poly(***lc1***) microdomain. a)**S2**, b)**S4**, c)**S6** were quenched from the isotropic phase, respectively. d)**S2**, e)**S4**, f)**S6** were annealed at the smectic temperature of 120℃, and then quenched to room temperature, respectively.

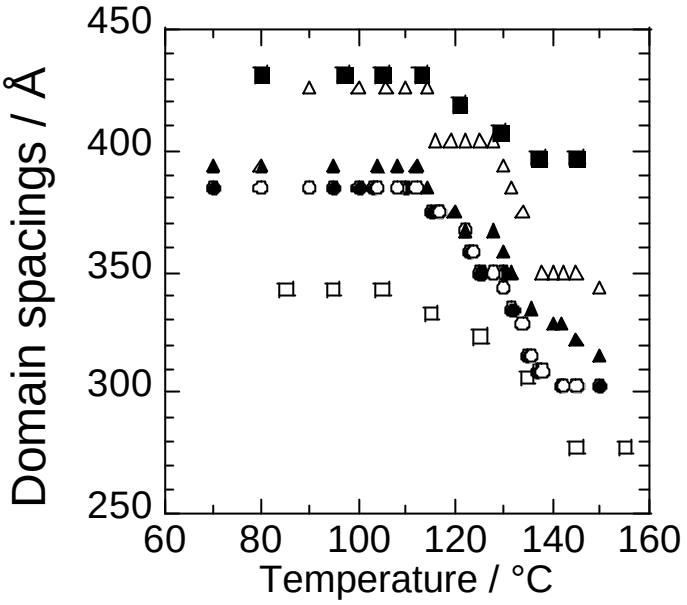

Figure 3.2. Temperature dependence of the microdomain spacings observed for (□)**S1**, (●)**S2**, (○)**S3**, (▲)**S4**, (△)**S5** and (■)**S6**, respectively.

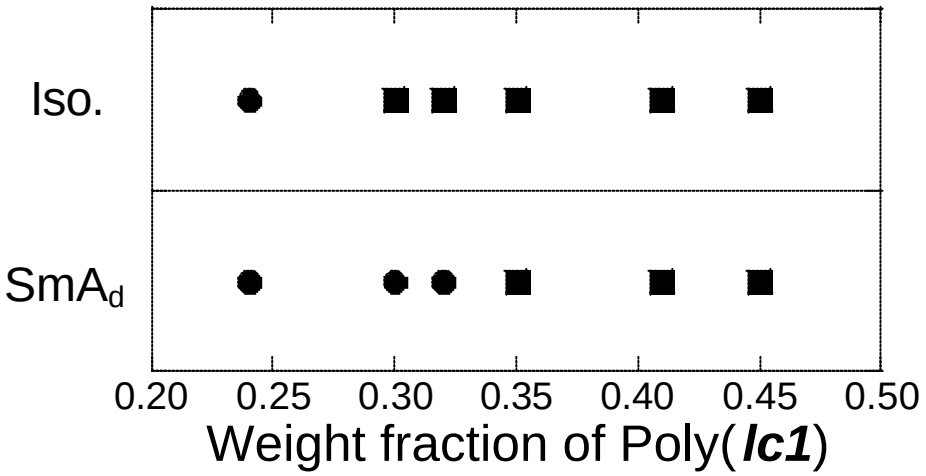

Figure 3.3. Morphological diagram of PS-*b*-Poly(***lc1***). Circles and squares denote cylinders and lamellae, respectively.

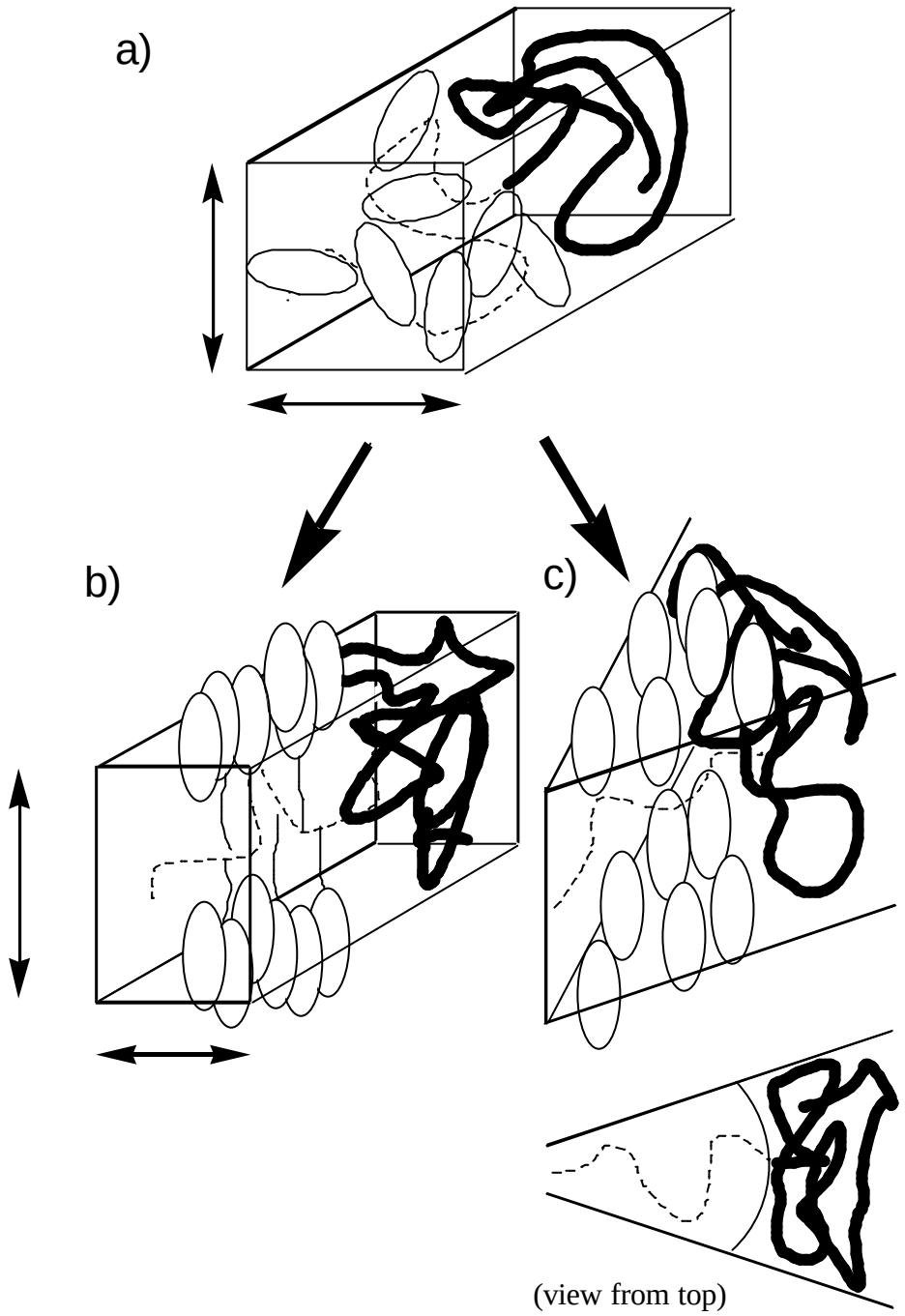

Figure 3.4. Schematic illustration of chain conformation and the morphologies in **S4** and **S5** where a) random coil at the isotropic phase in a lamella, b) anisotropic chain conformation owing to smectic layered packing in the SmA_d phase in a lamella, and c) in a cylinder take place.

3.4. Concluding Remarks

We have synthesized the AB type liquid crystalline (LC) block copolymers with polystyrene as A segment and side-chain LC polymer as B segment by sequential living anionic polymerization. All copolymers with the molecular weight of side-chain LC segment have around 20000 and with the segmental composition from 24wt% to 45wt%, and exhibit crystal, smectic A_d and isotropic phases in their microdomains. The cylindrical microphase segregated structure is formed at 24wt% of the side-chain LC polymer segment. The lamellar type microdomains are formed at 30wt% to 45wt% of the side-chain LC polymer segment in their isotropic phase, as expected from the weight fractions of the each segment. The block copolymers containing 30wt% and 32wt% of the side-chain LC polymer segment form the cylindrical microdomain in their smectic phase, whereas the lamellar one in their isotropic phase. This transformation can be simply explained neither by discontinuous changes of c which induced by smectic structure nor by the temperature dependency of c. The smectic structure of side-chain LC polymer segment enforced the anisotropic chain conformation to the counter PS segment. When a relaxation of the conformational chain entropy is needed, the interface of microdomain is bent, resulting in morphological transformation from lamellae to LC-cylinders.

References in This Chapter

1. a) Chapter 1 in this thesis.
   b) M. Yamada, T. Iguchi, A. Hirao, S. Nakahama, and J. Watanabe, *Macromolecules*, **28**, 50 (1995).
   c) M. Yamada, T. Iguchi, A. Hirao, S. Nakahama, and J. Watanabe, *Polym. J.*, **30**, 23 (1998).
2. G. E. Molau, "Block Copolymers", Plenum Publishing Corporation, New York, N. Y., 1970, 79.
3. I. W. Hamley, "The Physics of Block Copolymers", Oxford University Press, Inc., New York, N. Y., 1998.

4. S. Sakurai, H. Kawada, T. Hashimoto, and L. J. Fetters, *Macromolecules,* **26**, 5796 (1993).
5. A. K. Khandpur, S. Föster, F. S. Bates, I. W. Hamley, A. J. Ryan, W. Bras, K. Almdal, and K. Mortensen, *Macromolecules*, **28**, 8796 (1995).
6. J. Sänger, W. Gronski, S. Maas, B. Stühn, and B. Heck, *Macromolecules*, **30**, 6783 (1997).
7. M. Anthamatten and P. T. Hammond, *Macromolecules*, **32**, 8066 (1999).
8. A. Schneider, J. J. Zanna, M. Yamada, H. Finkelmann, and R. Thomann, *Macromolecules*, **33**, 649 (2000).
9. H. Fisher, S. Poser, and M. Arnold, *Liq. Cryst*., **18**, 503 (1995).
10. M. Yamada, T. Itoh, R. Nakagawa, A. Hirao, S. Nakahama, and J. Watanabe, *Macromolecules*, **32**, 282 (1999).
11. G. Mao, J. Wang, S. R. Clineman, C. K. Ober, J. T. Chen, and E. L. Thomas, *Macromolecules*, **30**, 256 (1997).
12. L. Leibler, *Macromolecules*, **13**, 1602 (1980).
13. W. Y. Zheng, R. J. Albalak, and P. T. Hammond, *Macromolecules*, **31**, 2686 (1998).
14. C. O. Osuji, J. T. Chen, G. Mao, C. K. Ober, and E. L. Thomas, *Polymer*, **41**, 8897 (2000).

Chapter 4

Microphase Morphology in Blends of Diblock Copolymer Containing Polystyrene and Side-Chain Liquid Crystalline (SCLC) Segments and SCLC Homopolymer

Abstract: Microdomain morphologies, orientational behavior, and isothermal crystallization kinetics of side-chain liquid crystalline homopolymer (hPoly(***lc1***)), its symmetric block copolymer with polystyrene (PS-*b*-Poly(***lc1***)), and these blends (PS-*b*-Poly(***lc1***)/hPoly(***lc1***)) were studied. PS-*b*-Poly(***lc1***) and hPoly(***lc1***) showed crystalline, smectic A_d, and isotropic phases. Adding hPoly(***lc1***) to PS-*b*-Poly(***lc1***), PS domain altered from lamellae to cylinders and disordered state. In the disordered region, isotropic-smectic phase transition temperature decreased, which indicates the PS chain reduced the stability of LC phase. Orientational behavior of mesogenic layered structure in a fiber specimen drawn from the isotropic phase of PS-*b*-Poly(***lc1***) was perpendicular to that of hPoly(***lc1***) owing to its microdomain structure. Even if the microdomain disappeared, side-chain mesogenic orientational behavior in fibers of the blends was not same as hPoly(***lc1***) but PS-*b*-Poly(***lc1***) because of the composition fluctuations. By quenching from the liquid crystalline phase to crystallization temperature, Avrami exponents depended on crystallization rate for hPoly(***lc1***) and PS-*b*-Poly(***lc1***)/hPoly(***lc1***), and continuously changed within 1 unit, for which the reason is explained by the conformational changes in Poly(***lc1***) at the crystallization temperature. PS-*b*-Poly(***lc1***)/hPoly(***lc1***) had smaller Avrami exponents than hPoly(***lc1***) by 1 unit. This result was led by the difference of the nucleation between them. Avrami exponent of isothermal crystallization in restricted lamellar microdomains for neat PS-*b*-Poly(***lc1***) was further smaller than that of hPoly(***lc1***) and PS-*b*-Poly(***lc1***)/hPoly(***lc1***). These kinetic results show that the crystallization was strongly affected by not only microdomain structures but also composition fluctuations.

4.1.Introduction

Liquid crystal (LC) - coil block copolymers containing side-chain LC polymer (SCLCP) segment have two different ordering structures; microphase segregated structure and LC structure[1,2]. These two structures are not independent but changeable each other. Thus the copolymer must be investigated by two points of view. One is effects of microdomain morphologies on LC phase behavior and the other is those of LC phase behavior on microdomain morphology.

Side-chain LC homopolymer, poly(6-[4-(4'-methoxyphenyl)phenoxy]hexyl methacryrate) (hPoly(***lc1***)), and its diblock copolymer with polystyrene (PS-*b*-Poly(***lc1***)) were synthesized by sequential anionic living polymerization as described in Chapter 2 and a reference[3].

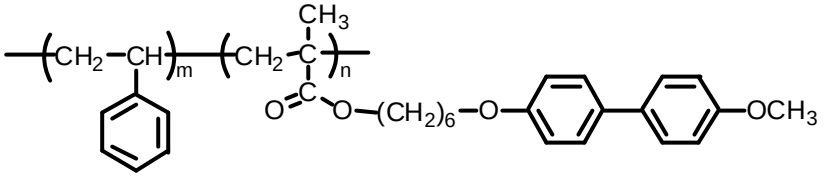

hPoly(***lc1***) and Poly(***lc1***) segment in PS-*b*-Poly(***lc1***) showed two transitions; crystalline-smectic A_d (SmA_d) and SmA_d-isotropic phase transitions. For symmetric PS-*b*-Poly(***lc1***)s which composed lamellar type microdomains, interestingly, its microdomain spacing depended on the SmA_d temperature and its reduction was 20-25%. In PS-*b*-Poly(***lc1***) with low molecular weight, a phase transition from isotropic to SmA_d pulled out the microphase segregated structure from disordered state[4].

PS-*b*-Poly(***lc1***) showed some reduction of transition temperatures and enthalpy changes compared with hPoly(***lc1***). This means that the LC phase behavior was strongly affected by counter PS segment in the PS-*b*-Poly(***lc1***). More study is needed to clarify the effect of microdomain on the LC phase behavior. In current chapter, hence, crystallization kinetics for hPoly(***lc1***), PS-*b*-Poly(***lc1***), and these blends is studied.

hPoly(***lc1***) and PS-*b*-Poly(***lc1***) show not only LC phase but also crystalline phase. In the crystalline phase, hPoly(***lc1***) and PS-*b*-Poly(***lc1***) can be regarded as a crystalline polymer and block copolymer[5], respectively. Kinetics of phase transitions for a number of crystalline homopolymers and block copolymers has been studied using the Avrami equation. The Avrami theory is based on nucleation and growth of crystallites. For heterogeneous

crystallization, it is assumed that all nuclei are formed and start to grow at time $t = 0$, the crystallites then grow at a constant rate until their boundaries meet leading to the formation of spherulites. In homogeneous crystallization, crystallites are nucleates at a constant rate in space and time, while the crystalline growth drives in the same space and time. In the case of crystalline block copolymers, kinetics of crystallization appears to be largely similar to the crystallization dynamics of corresponding homopolymers. Nojima *et al.*[6] have studied the kinetics of crystallization in a number of poly(*e*-caprolactone)-*b*- polybutadiene (PCL-*b*-PB) diblocks and compared to crystallization kinetics in PCL homopolymers. The values of Avrami exponent for PCL-*b*-PB were comparable to those obtained for PCL homopolymer, which indicates that the crystallization of the PCL blocks drives without any influence from the existence of microphase segregated structure. Crystalline homopolymers and block copolymers crystallize from isotropic melt in crystalline segment. On the other hand, hPoly(***lc1***) and PS-*b*-Poly(***lc1***) crystallizes from premonitory structure of SmA_d in LC segment.

The conformational change of the main-chain, which can be seen in Poly(***lc1***) segment of PS-*b*-Poly(***lc1***), is also expected to be seen in hPoly(***lc1***) because the conformational change of the main-chain backbone of Poly(***lc1***) segment in PS-*b*-Poly(***lc1***) is considered to be caused by a counterbalance between entropic gain of the main-chain conformation and energetic cost of the side-chain mesogenic layered structure, not directly by the microdomain structure. The conformational change of the main-chain in hPoly(***lc1***) has not been seen yet, but is easily considered to affect the crystallization behavior.

From a point of above view, we study the crystallization kinetics for hPoly(***lc1***), neat PS-*b*-Poly(***lc1***), and these blends in order to clarify the interrelation between the LC phase behavior and microdomain structure. Throughout this investigation, it is clarified that not only microdomain structure but also composition fluctuation in the PS-*b*-Poly(***lc1***) strongly affects LC phase behavior of transition temperature and LC structure in orientational behavior in their fiber.

4.2. Experimental Section

Materials The side-chain LC homopolymer (hPoly(***lc1***)) and its diblock copolymer (PS-*b*-Poly(***lc1***)) with polystyrene (PS) were prepared by sequential living anionic polymerization. Details of synthesis are described in Chapter 2 and a reference[3]. The characteristics of these polymers are summarized in Table 4.1. The composition of each segment was finally determined by ^{1}H NMR. M_n and M_w/M_n values were estimated from SEC profile based on standard polystyrene calibration.

The PS-*b*-Poly(***lc1***)/hPoly(***lc1***) binary blends (**B1**-**B5**) with their compositions as shown in Table 4.2 were prepared. The neat polymers and blends were prepared by dissolving in 10wt% polymer solution with tetrahydrofuran (THF) and by evaporating the solvent slowly over 1 week at room temperature. The film specimens were further dried in an oven at 60°C until constant weights were attained.

Methods Differential scanning calorimetric (DSC) measurement was carried out with Perkin-Elmer Pyris 1 DSC at a scanning rate of 2°C·min^{-1} to determine transition temperature and corresponding enthalpy change. X-ray measurement was performed by using Rigaku Denki X-ray generator with Ni-filtered Cu-Kα radiation. Reflection spacings were calibrated by using silicon standard or chicken tendon. Transmission electron microscopic (TEM) observation to clarify the morphology of materials was performed by Hitachi H-500 transmission electron microscope with 75kV of accelerating voltage. For this observation, the materials were cut into ultrathin sections (700-1000Å) by ultramicrotome with a glass knife. The sectioned specimens were stained with vapor of ruthenium tetraoxide (RuO_4) for 10min before observation.

Table 4.1. Characterization of LC block copolymer and homopolymer

	M_n [a), b)]		M_w/M_n [a)]	F of LC [b)]
	PS segment	Poly(***lc1***) segment		
PS-*b*-Poly(***lc1***)	12000	16000	1.05	0.57
Poly(***lc1***)	0	11200	1.12	1

a) Determined by GPC calibrated by PS standard. b) Weight fraction of Poly(***lc1***) determined by ^{1}H-NMR.

Isothermal Crystallization Perkin-Elmer Pyris 1 DSC was used to analyze the overall transformation kinetics of the hPoly(***lc1***), PS-*b*-Poly(***lc1***), and these blends. In order to eliminate any thermal history, the materials were placed at the 10°C above the isotropization temperature for 10min before the measurement. After holding the samples at predetermined temperature in the SmA_d phase for 10min, they were rapidly cooled (at a rate of 50°C·min^{-1}) to the temperature at which the crystallization takes place (T_c) and maintained at that temperature until the exotherm was not detected. The heat evolved during the isothermal condition was recorded as a function of time at different transition temperatures.

Analysis of Isothermal Crystallization The isothermal crystallization kinetics was analyzed by evaluating its degree of crystallization (X_t) as a function of time at a constant temperature of T_c. X_t is defined as

$$X_t = \int_0^t (dH/dt)dt \Big/ \int_0^\infty (dH/dt)dt$$

where dH/dt is the rate of heat evolution[7]. The overall kinetics is analyzed with the Avrami equation[7,8]. Avrami equation is described as follow[7,8].

$$1\text{-}X_t = \exp(-K_n t^n)$$

where X_t is a degree of crystallization (not crystallinity), n (so called 'Avrami exponent') depends on the modes of the nucleation and on the geometry of growth of the transforming regions, and K_n is a constant depending on nucleation density and on the growth of the transformation. Then the Avrami equation is reduced to

$$\log\{-\ln(1\text{-}X_t)\} = n\log t + \log K_n$$

From the graphic representation of $\log\{-\ln(1\text{-}X_t)\}$ versus $\log t$ (so called 'Avrami plot'), the Avrami exponent, n, (slope of the straight line) and the crystallization kinetic constant, K_n, (intersection with the y axis) can be calculated. Avrami exponent, n, is explained as follow.

Dimension of growth	Homogeneous nucleation	Heterogeneous nucleation
3 dimension	n=4	3≤n≤4
2 dimension	n=3	2≤n≤3
1 dimension	n=2	1≤n≤2

When the nucleation is homogeneous, nucleation occurs in overall crystallization. Heterogeneous nucleation means that some nuclei readily exist, and then the crystalline

growth drives from the nuclei.

The peak time, t_p, is taken to represent the measure of the transition rate. The reason for this choice is due to the fast transition for some of polymers, and only the peak time can be precisely determined during the experimental equilibration. The t_p^{-1} is proportional to the transition time. The equilibrium melt temperature (T_m^0) was obtained from the t_p^{-1} versus T_c plots which is extrapolated to $t_p^{-1} = 0$.

4.3. Results and Discussion 1: Thermotropic Phase Behavior and Microdomain Structures

4.3.1. Thermotropic Phase Behavior

Thermodynamic data for the hPoly(***lc1***), PS-*b*-Poly(***lc1***), and **B1**-**B5** are summarized in Table 4.2. All the materials in this study showed two clear transitions of crystalline-SmA_d and SmA_d-isotropic phase transitions. On comparison with the hPoly(***lc1***), the PS-*b*-Poly(***lc1***) showed several distinct features with respect to the transition behavior. The transition temperatures and corresponding enthalpy changes of PS-*b*-Poly(***lc1***) were smaller than those of hPoly(***lc1***)[4], and those of **B1**-**B5** increased by adding hPoly(***lc1***) and finally reached those of hPoly(***lc1***). On the other hand, we can also find in Figure 4.1 that SmA_d-isotropic phase transition temperature was lowered in the weight fraction of hPoly(***lc1***) in the blends (w_h) ≥ 0.65. This indicates eutectic temperature and disappearance of microdomains. Hence, it is considered that **B3**, **B4**, and **B5** had some difficulties to construct the LC structure.

Table 4.2. Characterization of the PS-*b*-Poly(***lc1***), Poly(***lc1***) homopolymer and blends [a)]

Sample	*F* of hPoly(***lc1***)[b)]	*F* of LC[c)]	Transition temperature / °C (Enthalpy changes / kcal·mol^{-1} [d)])				Microdomain morphology [e)]
			Heating		Cooling		
			T_1 (DH_1)	T_2 (DH_2)	T_1 (DH_1)	T_2 (DH_2)	
PS-*b*-Poly(***lc1***)	0	0.57	106.1 (0.45)	132.1 (0.23)	101.2 (0.45)	130.9 (0.26)	Lam.
B1	0.30	0.70	111.0 (0.62)	131.8 (0.39)	106.5 (0.64)	131.1 (0.41)	PS-Cyl.
B2	0.53	0.80	117.5 (0.77)	133.4 (0.47)	109.7 (0.76)	131.8 (0.49)	PS-Cyl.
B3	0.65	0.85	120.9 (0.95)	131.8 (0.50)	110.6 (0.92)	130.0 (0.51)	Disorder
B4	0.77	0.90	120.4 (0.94)	129.8 (0.54)	110.6 (0.88)	128.5 (0.57)	Disorder
B5	0.88	0.95	120.9 (1.25)	128.9 (0.64)	111.7 (1.18)	127.1 (0.74)	Disorder
hPoly(***lc1***)	1.00	1.00	123.4 (1.38)	134.3 (0.67)	114.6 (1.19)	132.8 (0.67)	-

a) Determined by DSC measurement at 2nd heating and cooling (2°C·min^{-1}). b) Weight fraction of hPoly(***lc1***) in the blends. c) Weight fraction of total Poly(***lc1***) component in the blends. d) Estimated per mole of LC. e) Determined by TEM observation. Lam. and Cyl. denote lamellae and cylinders, respectively.

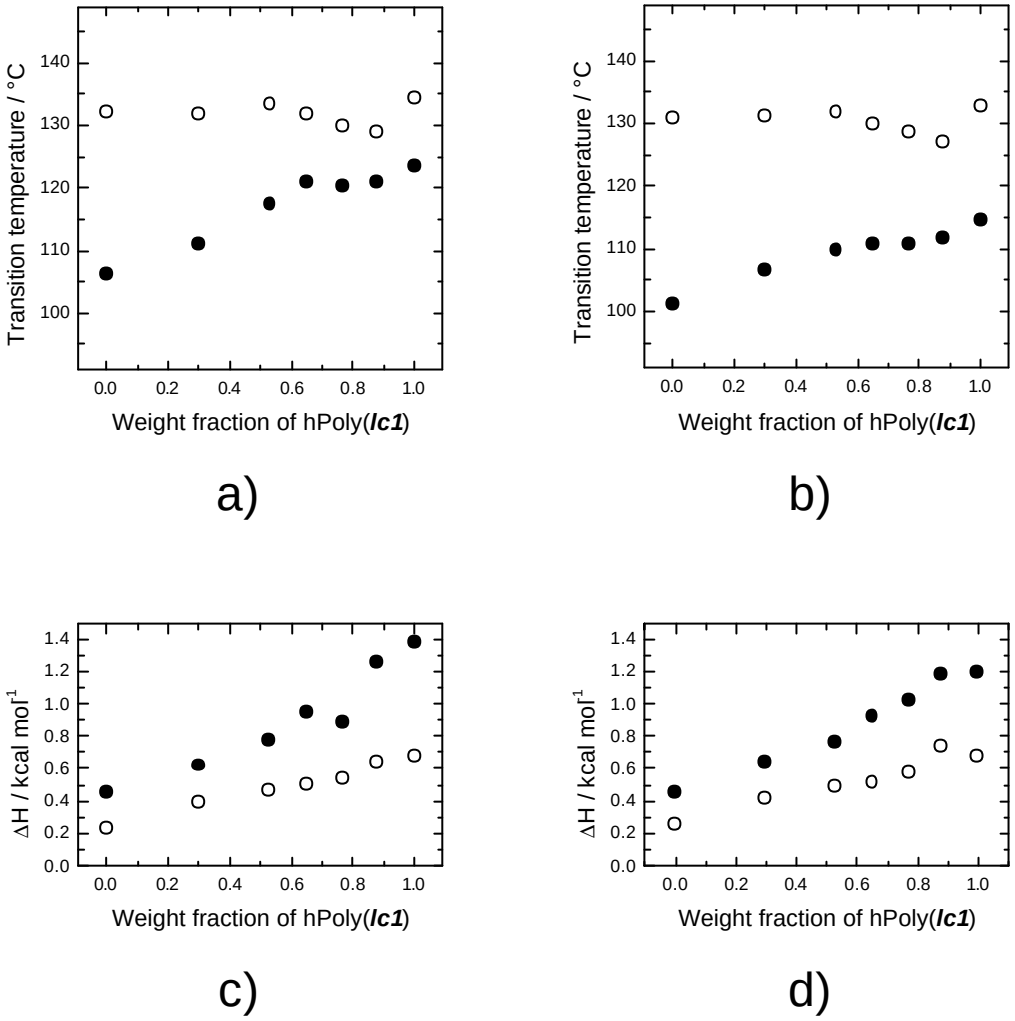

Figure 4.1. Phase diagram for hPoly(***lc1***), PS-*b*-Poly(***lc1***), and **B1**-**B5** in which a) transition temperature and c) corresponding enthalpy change on heating, respectively, and b) transition temperature and d) corresponding enthalpy change on cooling, respectively. Filled circles and open circles denote the crystalline-SmA_d phase transition and the SmA_d-isotropic phase transition, respectively. Enthalpy changes in c) and d) are estimated per mole of Poly(***lc1***).

4.3.2. Microdomain Morphology

Figure 4.2 represents TEM photographs for ultrathin section cut out from **B1**, **B2**, and **B4** (w_h=0.30, 0.53, and 0.77, respectively) which were annealed in the isotropic phase at 150ºC then cooled down into the crystalline phase of room temperature at a rate of 2ºC·min^{-1}. In the micrographs, Poly(***lc1***) microdomain appears dark because of staining with RuO_4. PS-*b*-Poly(***lc1***) shows a clear lamellar type microdomain. Adding hPoly(***lc1***) to

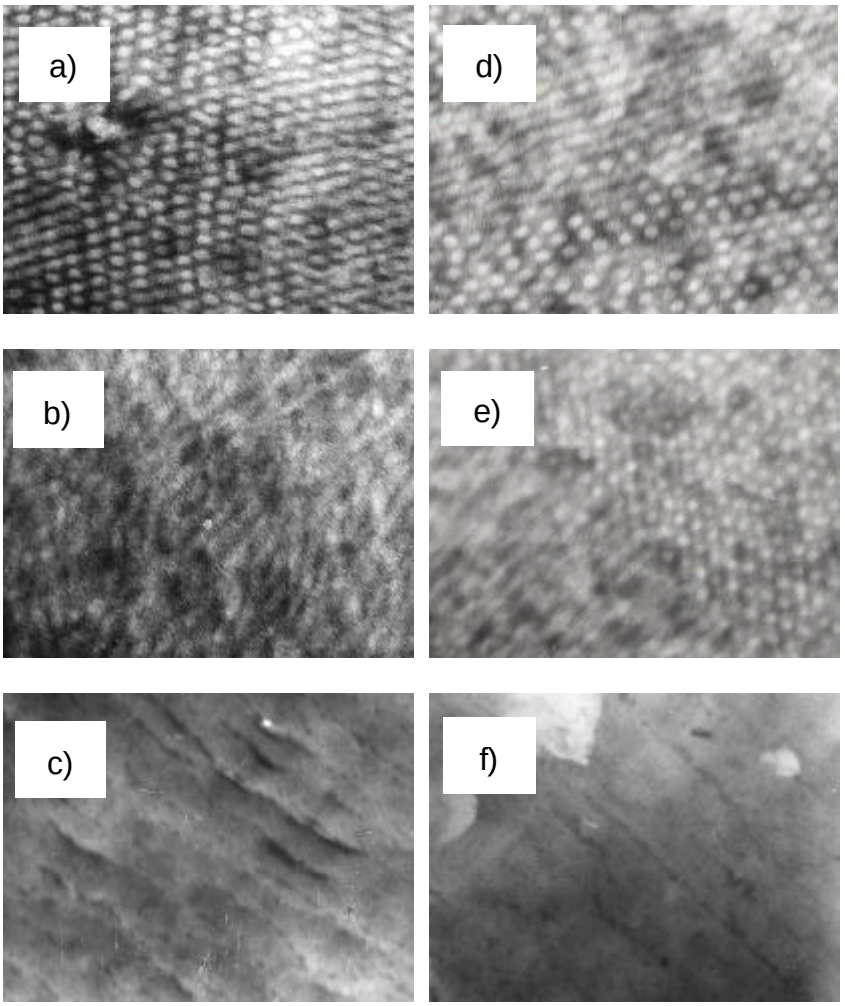

Figure 4.2. TEM Photographs for microphase segregated structure in a), b) and c) of **B1**, **B2**, and **B4** at the crystalline phase, and d), e), and f) of those at the isotropic phase, respectively.

PS-*b*-Poly(***lc1***), microdomain morphology changed from lamellae to PS-cylinders with Poly(***lc1***)-matrix in **B1**, distorted and undulating PS-cylinders in **B2**, and finally disordered in **B4**. In this study, no macroscopic segregation with hPoly(***lc1***) and PS-*b*-Poly(***lc1***) could not be seen because the molecular weight of hPoly(***lc1***) was enough small than Poly(***lc1***) segment in PS-*b*-Poly(***lc1***) (refer in Chapter 5).

Small angle X-ray scattering (SAXS) patterns are shown in Figure 4.3. All materials were drawn from the isotropic phase of Poly(***lc1***) segment to prepare fibers whose axis were placed vertically. Neat PS-*b*-Poly(***lc1***), **B1**, and **B2** showed sharp reflections due to their microphase segregated structure, while those of **B3**, **B4**, and **B5** had broaden and weak reflections (Figure

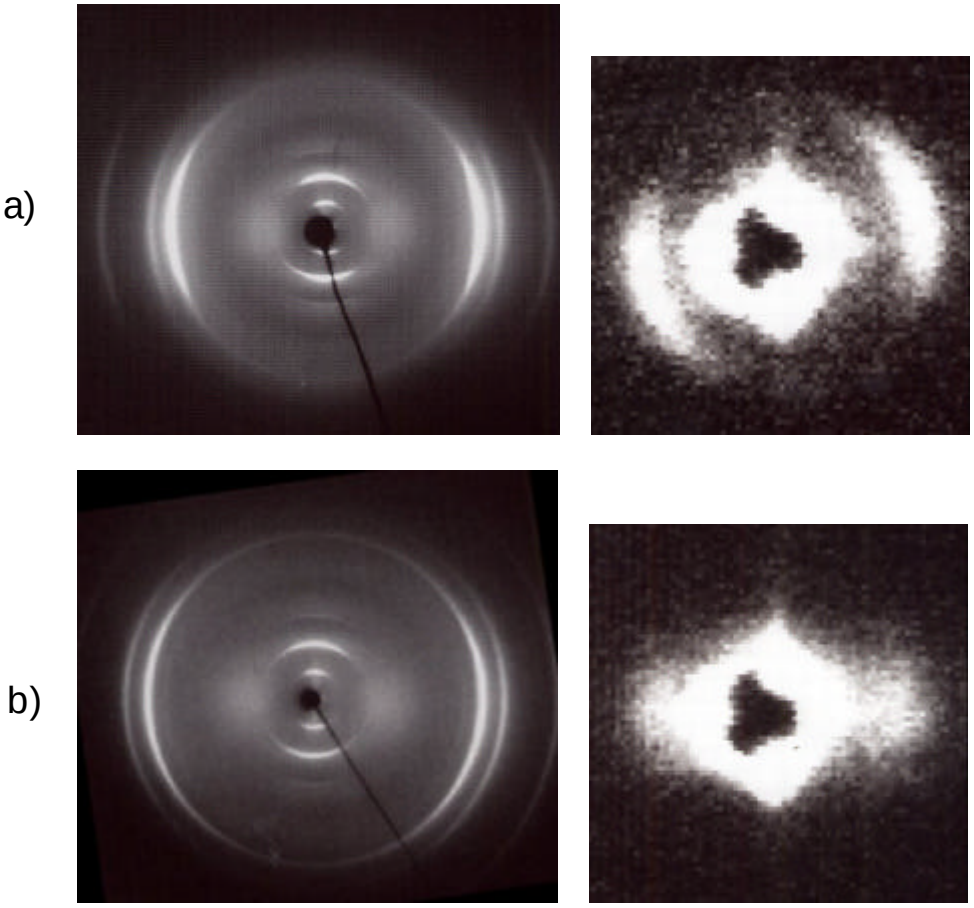

Figure 4.3. WAXS (left) and SAXS (right) photographs for fibers of a) **B1** and b) **B4** drawn from the isotropic phase. The measurement was carried out at room temperature in the crystalline phase. The fiber axis was placed vertical direction. **B1** and **B4** showed that the mesogenic layer was perpendicular to the fiber axis. Not only the microphase segregated structure (in **B1**) but also composition fluctuation (in **B4**) aligned along the fiber.

4.4). Hence, we determined that the microphase segregated structure was disordered in **B3**-**B5** by the TEM and SAXS studies. This result was some relative to the thermotropic phase behavior as discussed below.

The microdomain structure of all samples did not change at whole temperature region, which was observed by TEM using materials quenched from the isotropic phase and compared to the preceding materials at crystalline phase. Some researchers and we found order-disorder transition (ODT) and order-order transition (OOT) induced by LC phase transitions in which the microdomain was disordered in the isotropic phase and ordered in the LC phase, respectively. PS-*b*-Poly(***lc1***) with low molecular weight and with asymmetric

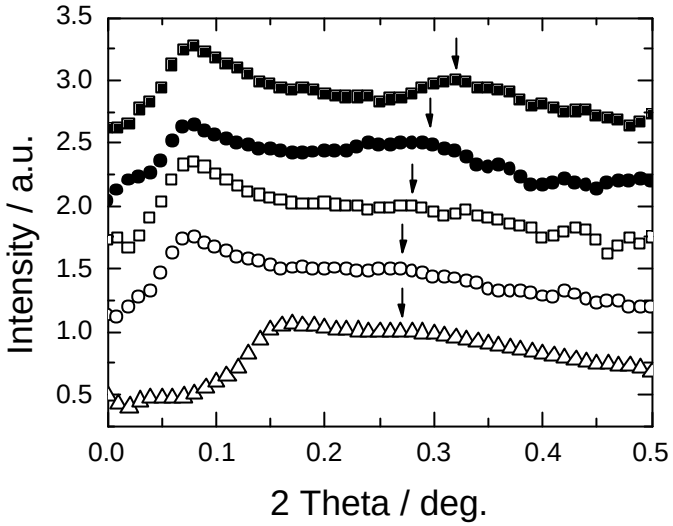

Figure 4.4. Small-angle X-ray profiles for (■)**B1**, (●)**B2**, (□)**B3**, (○)**B4**, and (△)**B5**, respectively. The measurements were driven out at room temperature. The reflection (denoted with arrows) was drastically broaden and weaken above w_h=0.65, which indicates that the microdomains disappeared.

composition also showed the ODT and OOT at the SmA_d-isotropic phase transition temperature, respectively[4]. But in current study, both ODT and OOT could not be seen.

Interestingly, adding hPoly(***lc1***) to PS-*b*-Poly(***lc1***), the morphology clearly changed to PS-cylinders with Poly(***lc1***) matrix in w_h=0.30, 0.53. In Chapter 5, on the other hand, PS-*b*-Poly(***lc1***)/homopolystyrene blend system did not construct Poly(***lc1***)-cylinder but only lamellar type microdomain could be seen at crystalline phase owing to packing of extended main-chain in Poly(***lc1***)-microdomains.

4.3.3. Interrelation between Microdomain Structure and Thermotropic Phase Behavior

The SmA_d-isotropic phase transition temperature decreased above w_h=0.65. This can be explained by microphase segregated behavior. In $w_h \geq 0.65$, the microdomain disappeared and was homogeneous with SmA_d structure of Poly(***lc1***) at a glance. However, PS chain must exist in the SmA_d structure. When the phase transition from the isotropic to the SmA_d occur,

PS chain can be considered to disturb the construction of SmA_d structure. Hence, it was difficult to construct the SmA_d structure compared with pure hPoly(***lc1***), microphase segregated PS-*b*-Poly(***lc1***), and PS-*b*-Poly(***lc1***)/hPoly(***lc1***) with $w_h \leq 0.53$. Thus the isotropic-SmA_d transition temperature was lowered as far as the eutectic temperature by alloying with PS segment.

4.3.4. Orientational Behavior in Fiber

The oriented fibers were prepared by pulling up an isotropic melt of hPoly(***lc1***), PS-*b*-Poly(***lc1***), and PS-*b*-Poly(***lc1***)/hPoly(***lc1***) blends to determine the crystalline and LC structures. Figures 4.3, 4.5, and 4.6 show wide-angle X-ray scattering (WAXS) patterns of the materials in the crystalline phase at room temperature, and their fiber axis were placed vertically. In their crystalline patterns, we observed inner reflections due to mesogenic layer spacings of 25.8Å and several outer reflections owing to crystalline mesogenic unit cell. In the SmA_d phase, the outer reflections broadened and the inner reflections were very weak but its position did not change. The crystalline structure, smectic structure, and their sizes were the same as hPoly(***lc1***) and PS-*b*-Poly(***lc1***) as reported in previous papers[3,4].

Here, we notice the orientational director of their mesogenic layer. For hPoly(***lc1***), inner reflections localized on the horizontal direction. No LC structure was constructed at the drawing isotropic phase. Thus the main-chain backbone of hPoly(***lc1***) was drawn along the fiber axis, and then the mesogens crystallized at room temperature (Figure 4.5). On the other hand, the WAXS pattern of PS-*b*-Poly(***lc1***) shows that the mesogenic layers oriented perpendicular to the fiber axis. Its SAXS pattern indicated parallel orientation of the lamellar microdomains along the fiber axis. This can be explained that the lamellar type micridomains were drawn in the isotropic melt along the fiber axis, the main-chain backbone of the Poly(***lc1***) segment spread perpendicular to the microdomain interface, and then the mesogenic layer oriented perpendicular to the interface of the lamellar microdomain (Figure 4.6).

B1 and **B2** drawn from the isotropic phase showed same orientational behavior as the PS-*b*-Poly(***lc1***) (Figure 4.3a). It is interestingly that the mesogenic layers of not only the Poly(***lc1***) segment in PS-*b*-Poly(***lc1***) but also hPoly(***lc1***) aligned perpendicular to the fiber axis, while the mesogenic layer in neat hPoly(***lc1***) was aligned parallel to the fiber axis owing

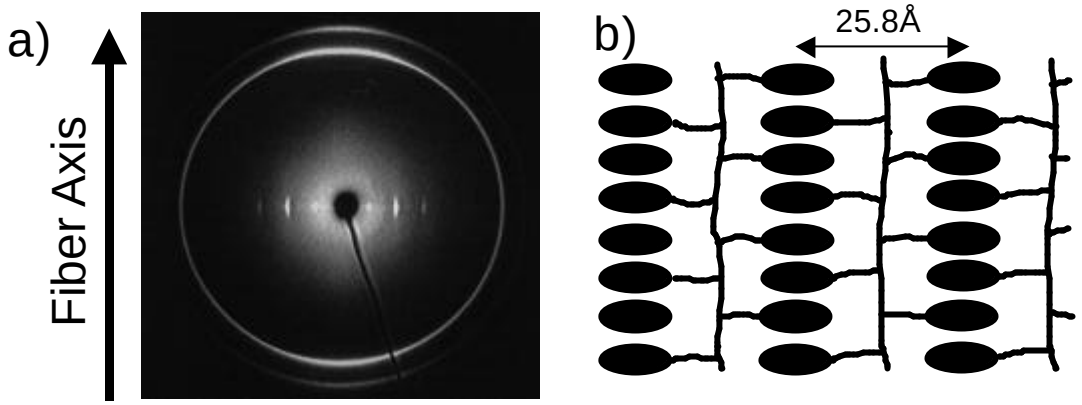

Figure 4.5. The mesogenic layered structure in a fiber of Poly(***lc1***) homopolymer drawn from the isotropic phase. a) WAXS phorograph and b) plausible structure.The mesogenic layered structure was paralell to the fiber axis.

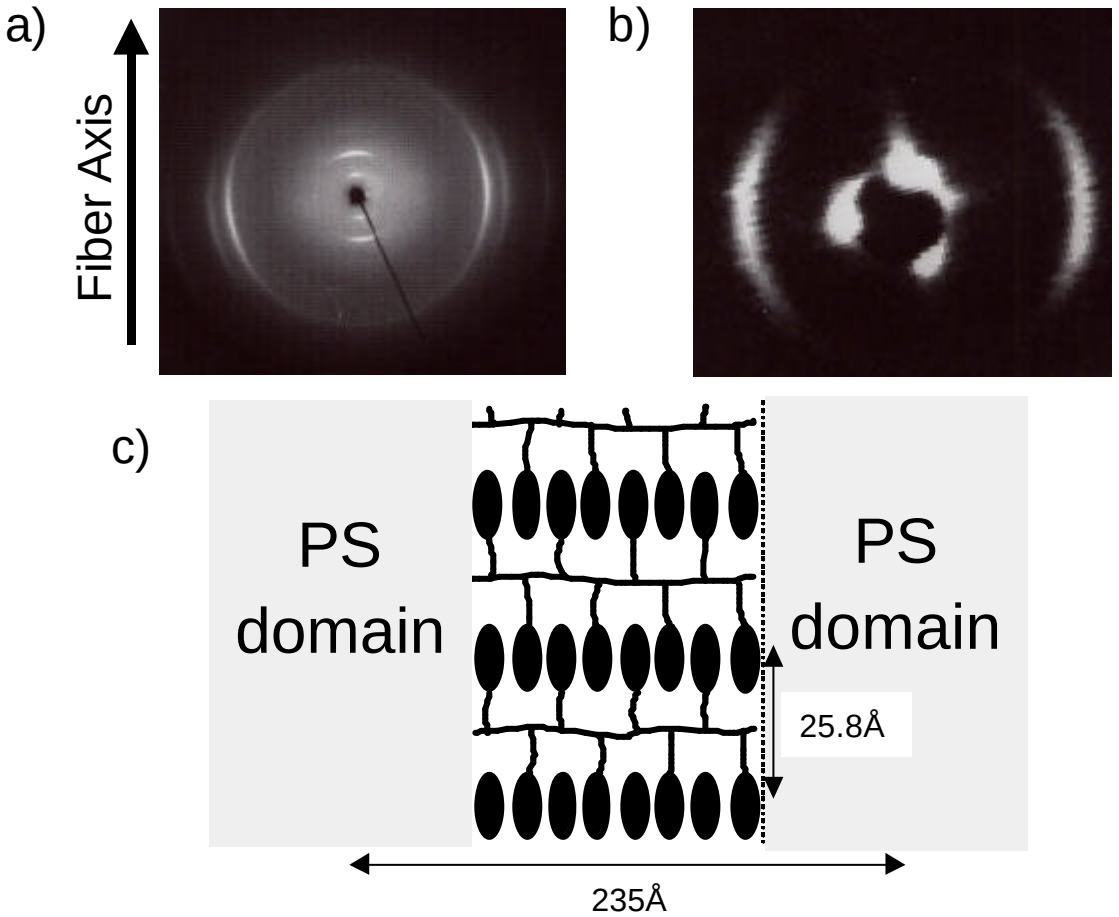

Figure 4.6. The mesogenic layered structure in a fiber of PS-*b*-Poly(***lc1***) drawn from the isotropic phase. a) WAXS phorograph, b) SAXS photograph, and c) plausible structure. Microdomain structure was drawn, and then the mesogenic layered structure was perpendicular to the fiber axis.

to the elongation of its main-chain. This can be considered the same reason in neat PS-*b*-Poly(***lc1***) where the microdomain was aligned by the drawing, and then the mesogenic layers crystallized. Moreover, the mesogenic layer of hPoly(***lc1***) in them also crystallized perpendicular to the fiber axis. This means that liquid crystallization and crystallization of the Poly(***lc1***) segment in PS-*b*-Poly(***lc1***) led those of hPoly(***lc1***). In other words, the liquid crystallization and crystallization started at the Poly(***lc1***) segment in PS-*b*-Poly(***lc1***) rather than hPoly(***lc1***). This is investigated below in detail.

We expected that the mesogenic layers in **B3**-**B5** aligned parallel to the fiber axis because of homogeneous SmA_d structure as same as hPoly(***lc1***). But **B3**-**B5** also showed the same orientational behavior as same as neat PS-*b*-Poly(***lc1***), **B1**, and **B2**. This can be explained only by the effect of the PS segment in the homogeneous SmA_d structure. Even if the microdomain disappeared with no clear interface, composition fluctuations of PS segment must exist. The composition fluctuations in block copolymers show anisotropic reflection under flow [9,10]. Actually, the SAXS reflection was located on the horizontal position along the fiber axis (see in Figure 4.3b). However, we could not see microdomains of the **B4** fiber spun at the isotropic phase. Taking into account that the mesogenic layers at the crystalline phase aligned perpendicular to the fiber axis, not only the microdomains but also the composition fluctuations were drawn along the fiber axis. Then Poly(***lc1***) segment of PS-*b*-Poly(***lc1***) and hPoly(***lc1***) aligned perpendicular to the fiber axis even if the clear interface did not exist.

We note that not only the microdomain interface but also the composition fluctuation strongly affects the orientational behavior of LC structure.

4.4. Results and Discussion 2: Isothermal Crystallization

Crystalline homopolymers and its block copolymers have been widely investigated with Avrami equation. In the case of crystalline block copolymers such as PCL-*b*-PB[6], when the molecular weights of each segment are small, Avrami exponents are not so different from corresponding homopolymers, which means that the mechanism of the crystallization is the same and indicate that the driving force of the crystallization is very dominant to neglect the microdomain morphologies. Increasing the molecular weight, rate of crystallization is slower and the crystallinity also lower. When glass transition temperature of the amorphous segment is higher than the crystallizing temperature, the crystallization does not or hardly drives.

In this section, crystallization behaviors in hPoly(***lc1***), PS-*b*-Poly(***lc1***), and **B1**-**B5** are studied. Some differences of crystallization mechanism among them can be seen due to microdomain structure and composition fluctuation. The effect of block copolymer on the LC phase behavior is investigated through isothermal crystallization with Avrami analysis.

4.4.1. Isothermal Crystallization of Poly(*lc1*) Homopolymer

In order to analyze the effect of crystallization temperatures on hPoly(***lc1***) quenched from SmA_d phase at 125.0°C, the crystallization isotherms at different T_c are represented in Figure 4.7a. At T_c<115.0°C, the crystallization was very fast and started before reaching a constant isothermal temperatures. At T_c>118.0°C, the crystallization could not be observed. So we estimated the X_t only in 115.0°C<T_c<118.0°C. ΔH_∞ was constant at (1.2±0.1) kcal·mol^{-1} independently of T_c.

The Avrami plots at various T_c are presented in Figure 4.8a, where X_t was obtained as described in experimental section. We used the experimental data of 0.05<X_t<0.95 because noises of DSC endothermic line and errors were large in X_t<0.05 and X_t>0.95. For these runs, the slope of the straight lines corresponded to 2.5<n< 3.5 and n increased continuously with decrement of T_c. The values of $-\log K_n$ also changed from 3.8 to 5.1. The kinetic parameters are collected in Table 4.3.

We also examined the isothermal crystallization at T_c=116.0°C with variable quenching temperature at 130.0°C and 120.0°C. But any differences of t_p and n against ΔT (=T_m^0-T_c where T_m^0 is the equilibrium melting temperature of their crystallites) from the isotherms

quenched from 125.0°C could not be seen (Figure 4.9). Hence, we used the experimental data obtained from the isotherms quenched from 125.0°C to discuss below. Moreover, annealing effect at the prenominated quenching temperature at 125.0°C is shown in Figure 4.10. The annealing effect was not observed above 30sec and all of n values were around 3.4±0.1 at T_c=116.0°C. Thus the continuous change of n depended on T_c was not error, and annealing for 10min at quenching temperature was appropriate in this experiment.

4.4.2. Avrami Analysis of Poly(*lc1*) Homopolymer

The Avrami exponents of the isothermal crystallization for hPoly(***lc1***) significantly changed continuously from 2.5 to 3.5 with decreasing T_c. This is not error as described above.

In previous study for symmetric PS-*b*-Poly(***lc1***) [4], Poly(***lc1***) segment in PS-*b*-Poly(***lc1***) showed conformational changes in SmA_d temperature region where random coil conformation took place at near the SmA_d-isotropic phase transition temperature with low order of SmA_d layered structure, while extended form took place at near the crystalline-SmA_d phase transition temperature with high order of SmA_d layered structure. We believe that hPoly(***lc1***)

Table 4.3. Kinetic parameters for overall crystallization

for hPoly(*lc1*) quenched from 125°C

T_c / °C	ΔT / °C	t_p / sec.	n	-logK_n
115.0	4.1	86	3.40	6.08
116.0	3.1	109	3.52	6.76
116.5	2.6	242	3.08	6.96
117.0	2.1	418	2.82	6.99
117.5	1.6	468	2.82	7.14
118.0	1.1	770	2.66	7.28

for B5 quenched from 125°C

T_c / °C	ΔT / °C	t_p / sec.	n	-logK_n
114.0	4.1	57	2.32	3.80
114.5	3.6	89	2.20	4.17
115.0	3.1	129	1.93	4.05
115.5	2.6	185	1.90	4.22
116.0	2.1	292	1.86	4.55
116.5	1.6	496	1.67	4.47
117.0	1.1	739	1.76	5.07

can take place such a conformational change because the conformational change of Poly(***lc1***) segment in PS-*b*-Poly(***lc1***) was raised by the counterbalance between an enthalpic cost of the mesogenic layered structure in side-chain and an entropic gain in main-chain conformation, but not directly by the microdomain structure. As illustrated in Figure 4.10, when the crystallization occurs at three-dimensional position of the side-chain mesogens with low ordered smectic layer order parameter, three-dimensional crystalline growth must drive. On the other hand, two-dimensional crystalline growth in smectic layered plane is necessary to drive when smectic layer order is high because one-dimensional positional order already exists. Immediately after quenching hPoly(***lc1***) from 125.0°C to T_c, it can be considered the main-chain forms near the random-coil. When the rate of crystallization is fast, three-dimensional crystalline growth drives. On the other hand, when the rate of crystallization is slow, the main-chain is gradually extended by annealing effect at T_c. For fully extended main-chain with high ordered smectic layer, two-dimensional crystalline growth can drive. Thus, n changed continuously within 1 unit because of the conformational change of the main-chain by the annealing effect at T_c. The conformational change is continuous. Hence, the Avrami exponent changed continuously from 2.5 to 3.5 with the decrement of T_c.

On the other hand, it can be also considered that the continuous change would be caused by a change of nucleation mechanism from homogeneous to heterogeneous. But it will be denied in comparison with the isothermal crystallization for PS-*b*-Poly(***lc1***)/hPoly(***lc1***) as discussed below.

4.4.3. Overall Features of the Isothermal Crystallization of PS-*b*-Poly(*lc1*)/hPoly(*lc1*)

In order to clarify the effects of block copolymer on the crystallization mechanism, isothermal crystallization of PS-*b*-Poly(***lc1***) and PS-*b*-Poly(***lc1***)/hPoly(***lc1***) blends were studied. In this section, the blends were experienced. **B1**-**B4** showed similar exothermal curves to **B5** in Figure 4.7c. Because of the fast initiation of the transformation, the ΔH_t and ΔH_8 corresponding to X_t and X_8 could not be obtained in **B1**-**B4**. We could evaluate the isothermal crystallization for **B5** by the same process as the hPoly(***lc1***). Thermo dynamic data were collected in Table 4.3. ΔH_∞ is constant at (0.86±0.02) kcal·mol^{-1} independently of the

T_c. We can find similar trends to hPoly(***lc1***), in which n value in the isothermal crystallization for **B5** changed continuously from 1.5 to 2.5. The reason for the continuous change can be explained by the annealing effect at T_c as same as hPoly(***lc1***). We expected n values for **B5** would be comparable to those of hPoly(***lc1***) because microdomains did not exist, filled with homogeneous LC structure at a glance, and crystalline and LC structures are same. But all n values for the **B5** are smaller than those for hPoly(***lc1***) by 1 unit. In order to compare n values for **B5** with those of hPoly(***lc1***), n is plotted against ΔT (Figure 4.11).

It is difficult to consider that the mechanism of crystalline growth of **B5** is not same as hPoly(***lc1***) because of the same homogeneous LC and crystalline phases and structures. We determined the reason for the difference of n values between hPoly(***lc1***) and **B5** was raised not by the difference of mechanism in the crystalline growth but by that in the nucleation in the overall crystallization. The nuclear can be considered to be PS segment in **B5**. PS segment existed as composition fluctuation. It is considered as a defect of the crystalline and LC structure. If the nucleation mechanism had changed continuously from homogeneous to perfect heterogeneous with increment of T_c (decrement of the rate of crystallization), n values would decrease continuously within 1 unit. In such hypothesis, however, we cannot explain the difference of n by 1 unit between hPoly(***lc1***) and **B5**. Hence, the continuous change of n values in **B5** (and hPoly(***lc1***)) is caused by the annealing effect at the crystallization temperature as described above.

For **B1**-**B4**, we could not obtain X_∞ and X_t from isothermal curve and could not analyze the crystallization kinetics in detail because the crystallization started before constant isothermal temperature was obtained (see in Figure 4.7b). But we can roughly estimate n and K_n from the shape of the exothermal curve. Using Avrami equation, we made a graphs with calculating dX_t/dt versus t, which corresponded to exothermal curve, with fitting value of n and K_n. In large n around 3, a peak top of the calculated curve exists medial time in overall transformation. On the other hand, when n is small around 1.5, a calculated curve arises fast and finishes slow, and then the peak top of the curve deviates from the middle of overall transformation. We fitted the experimental exothermal curve with calculated curves, and the estimated the fitting values. This estimation is not so quantitative as the above analysis, but we obtained the fitting values of n around 2 and $-\log K_n \approx 4.0$-5.0 (Figure 4.13a). These values

are comparable to those of **B5**. Hence, we determined the mechanism of the crystallization for all blends of PS-*b*-Poly(***lc1***)/hPoly(***lc1***) drove in heterogeneous nucleation and their nuclei are the microdomains or the composition fluctuation of PS as same as **B5**.

This result means that the crystallization drove from PS-*b*-Poly(***lc1***) chain in the blends as expected from the study of the orientational behavior in section 4.3. We pointed out again that not only the interface between microdomains but also the composition fluctuation in the LC structure strongly affected the LC phase behavior of crystallization as well as orientational behavior.

4.4.4. Overall Features of the Isothermal Crystallization of PS-*b*-Poly(*lc1*)

Isothermal crystallization for neat PS-*b*-Poly(***lc1***) quenched from SmA_d phase at 125.0°C was also investigated. The quenching temperature was near the isotropic-SmA_d phase transition temperature. The crystallization could not be seen at T_c>103.0°C. At T_c<103.0°C, the crystallization started before constant isothermal temperatures (see in Figure 4.7d). Hence, we could not obtain X_∞ and X_t from the isothermal curve, and could not analyze the crystallization kinetics in detail. But we can roughly estimate n value and K_n as described above, and then we obtained the fitting value of $n \approx 1.2$ and $-\log K_n \approx 2.0$-3.0 (Figure 4.13b). The kinetic constant K_n was larger than those of hPoly(***lc1***) and PS-*b*-Poly(***lc1***)/hPoly(***lc1***)s. Interestingly, the n value of isothermal crystallization for neat PS-*b*-Poly(***lc1***) was also different from those for hPoly(***lc1***), in spite of the same crystalline structure and LC structure. This result means that the crystallization of Poly(***lc1***) segment in neat PS-*b*-Poly(***lc1***) drove with strong dependency of the microphase segregated structure, although other crystalline block copolymers such as PCL-*b*-PB do not. The crystallization from isotropic phase of PCL-*b*-PB which was reported by Nojima *et al*.[6] did not show any significant difference from corresponding PCL homopolymer, which was explained by the fact that the crystallization mechanisms in the PCL-*b*-PB and the PCL homopolymer were the same.

Crystalline block copolymers typically show Avrami exponents ranging from 2-4, reflecting growth in two or three dimensions from isolated nuclei. Recently, however, a first-order kinetics was reported in the case of the crystallization confined within individual microdomains in a crystalline block copolymer[11], which was explained that the crystalline

growth from the nuclei of the microdomain interface was essentially instantaneous and only massive homogeneous nucleation drove in them. In our case of neat PS-*b*-Poly(***lc1***), on the other hand, heterogeneous nucleation could be considered, because the interface of the lamellar microdomains could be the nuclei as well as PS-*b*-Poly(***lc1***)/hPoly(***lc1***)s. Immediately after quenching to T_c, the main-chain conformation of Poly(***lc1***) segment was considered to be random coil because the quenching was near the isotropic-SmA_d transition temperature. As described above, **B5** had n=2.5 where the nucleation was heterogeneous and the fast crystalline growth drove from the random coil. However, the crystallization in the neat PS-*b*-Poly(***lc1***) was confined with in individual lamellar microdomains. It can be considered that the crystalline growth was not carried into neighboring Poly(***lc1***)-lamella through PS-lamella (Figure 4.14). Thus the Avrami exponent of PS-*b*-Poly(***lc1***) was smaller than that of **B5** by 1 unit. Furthermore, some annealing effect at the T_c on the smectic layer order could be considered. The n value of 1.2, which was a little smaller than 1.5, was an appropriate value.

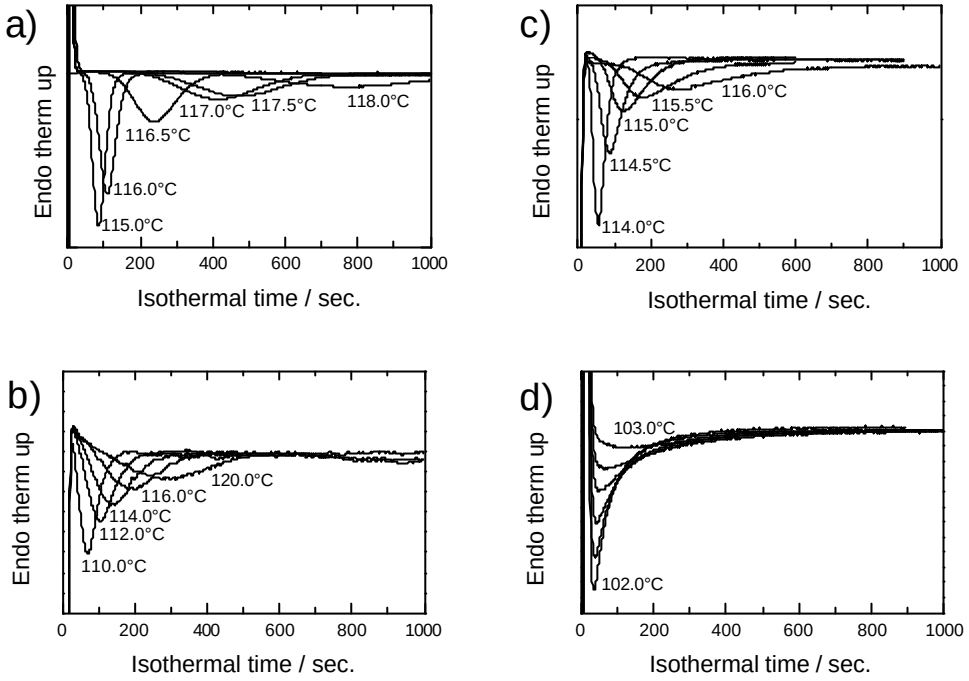

Figure 4.7. DSC thermograms of isothermal crystallization quenched from predetermined temperature at 125.0°C in smectic A_d phase to crystallization temperature for a) hPoly(***lc1***), b) **B1**, c) **B5**, and d) PS-*b*-Poly(***lc1***), respectively. Temperatures in the figures denote crystallization temperature.

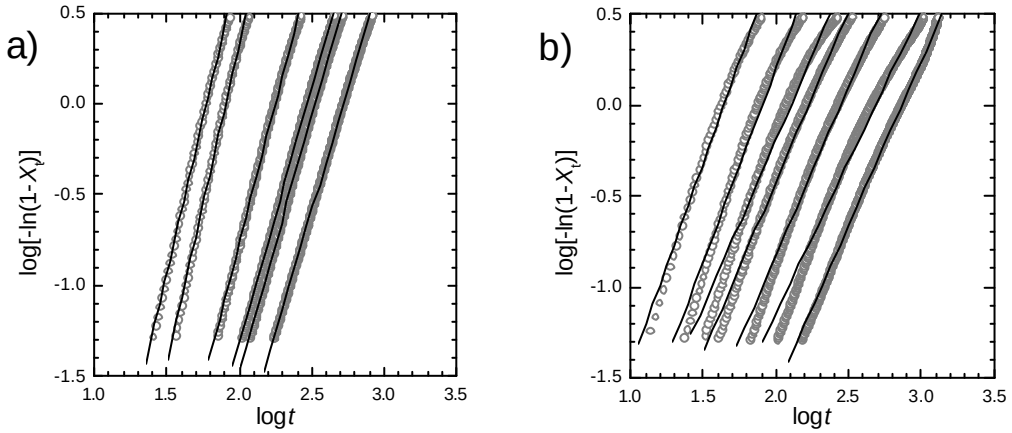

Figure 4.8. Avrami plots of the isothermal crystallization quenched from predetermined temperature at 125.0°C in smectic A_d phase to crystallization temperature for a) hPoly(***lc1***) and b) **B5**, respectively. X_t is a ratio of crystallization calculated from isothermal curve in Figure 4.7.

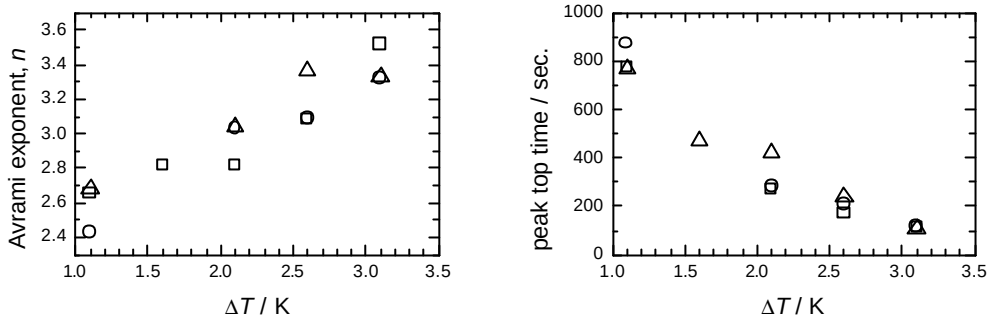

Figure 4.9. Effect of super cooling on (left) Avrami exponent and (right) peak top time of the isothermal crystallization for hPoly(***lc1***) quenched from (○)120℃, (□)125℃, and (△)130℃, respectively.

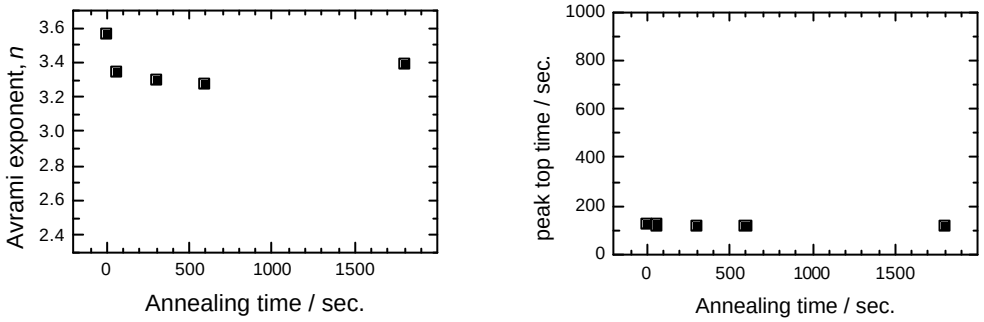

Figure 4.10. Effect of annealing at the quenching temperature of 125.0°C on (left) Avrami exponent and (right) peak top time of the isothermal crystallization for hPoly(***lc1***) at a constant T_c = 116.0°C.

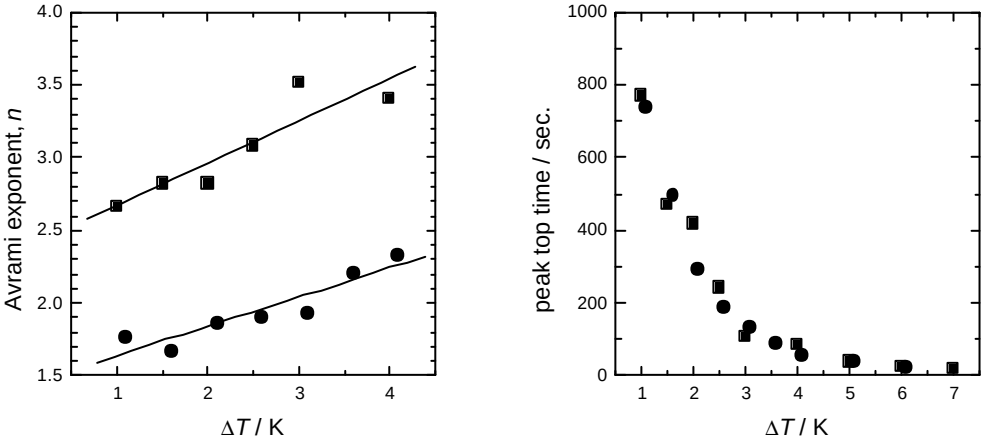

Figure 4.11. (left) Avrami exponent and (right) peak top time of isothermal crystallizations for (■) hPoly(***lc1***) and (●) **B5**, respectively.

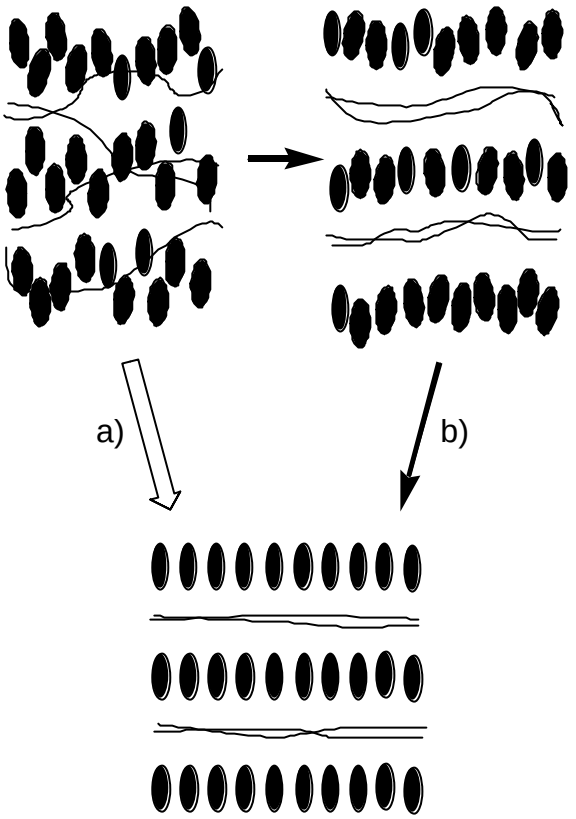

Figure 4.12. Schematic illustration for the mechanism of the isothermal crystallization in hPoly(***lc1***) and **B5**. a) When the crystallization rate is fast with large ΔT, crystalline structure is formed from random position of the mesogens, b) while most of the crystalline growth drives within the smectic layer because annealing at the T_c leads high smectic layered order and then one-dimensional positional order of mesogens already exists when the crystallization rate is slow with small ΔT.

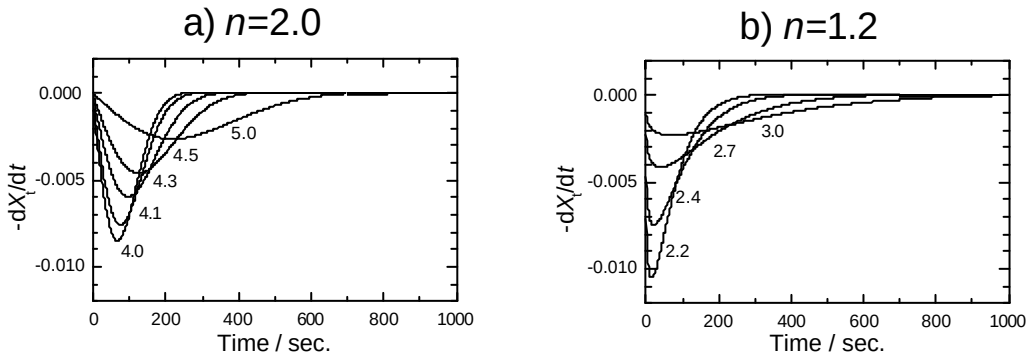

Figure 4.13. Calculated isothermal curves by Avrami equation with a) n=2.0 and b) n=1.2. The values in the figure denote -log K_n. Compare with Figure 4.7.

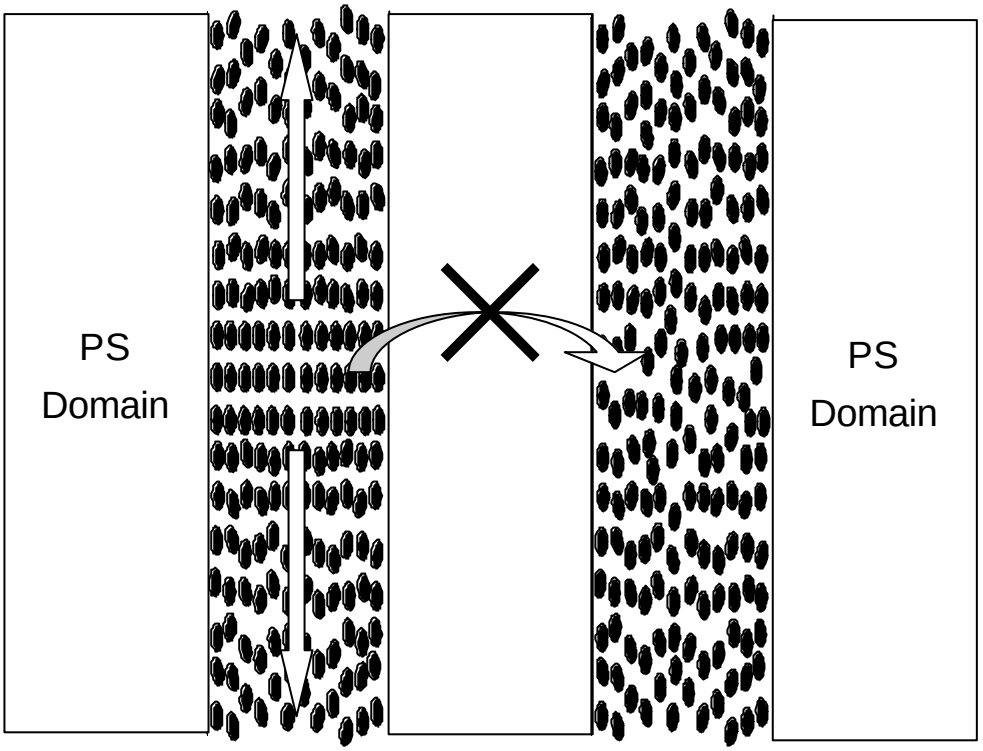

Figure 414. Schematic illustration for the mechanism of crystallization in PS-*b*-Poly(***lc1***) which composed lamellar type microdomain. The crystallization growth drives within each Poly(***lc1***)-lamella, individually.

4.5. Concluding Remarks

Microdomain morphologies and liquid crystalline phase behavior in side-chain liquid crystalline homopolymer, poly(6-[4-(4-methoxyphenoxy)phenyl]hexyl methacrylate (hPoly(***lc1***)), its block copolymer (PS-*b*-Poly(***lc1***)) with polystyrene (PS), and these blends were studied. All samples in this study showed crystalline, smectic A_d, and isotropic phases. The lamellar microdomain in PS-*b*-Poly(***lc1***) with segmental compositions around 0.50 altered into PS-cylinder and disordered state with adding hPoly(***lc1***). In disordered region, the smectic A_d-isotropic phase transition temperatures were lowered, which indicates that the smectic structure was difficult to construct owing to the composition fluctuation of PS.

Orientational behavior was studied. Mesogenic layered structure in a fiber specimen drawn from the isotropic phase of hPoly(***lc1***) was parallel to the fiber axis because the main-chain was elongated. Microdomain structure was drawn and then the mesogenic layered structure was perpendicular to the fiber axis for neat PS-*b*-Poly(***lc1***) and all the blends, even if the microdomain disappeared. Not only the microdomain structure but also its composition fluctuation strongly affected the orientational behavior of the side-chain mesogenic orientation.

We also studied isothermal crystallization kinetics of the materials by DSC. Avrami exponent of the isothermal crystallization quenched from the smectic A_d phase for hPoly(***lc1***) was continuously changed from 2.5 to 3.5 with increment of degree of super cooling. The continuous change is explained by the annealing effect at the crystallization temperature where the smectic layer order parameter gradually enlarged. This indicates that a conformational change, which could be seen in PS-*b*-Poly(***lc1***) with lamellar type of microdomain and could be explained by a counter valance between energetic force of side-chain layered structure and entoropic force of main-chain conformation. PS-*b*-Poly(***lc1***)/hPoly(***lc1***) also showed continuous change in Avrami exponent as well as hPoly(***lc1***). However, the Avrami exponent changed from 1.5 to 2.5, which were smaller than that of hPoly(***lc1***) by 1 unit, even if interface of the microdomains disappeared. The difference between hPoly(***lc1***) and PS-*b*-Poly(***lc1***)/hPoly(***lc1***) was due to a difference of the nucleation mechanism where homogeneous nucleation in hPoly(***lc1***) and heterogeneous nucleation in the blends drove owing to not only the microdomains but also the composition fluctuation. This

means that the crystallization started at the composition fluctuations as well as microdomains. Isothermal crystallization for neat PS-*b*-Poly(***lc1***) with lamellar type microdomain showed further smaller Avrami exponent than that of PS-*b*-Poly(***lc1***)/hPoly(***lc1***) at least by 1 unit because the crystalline growth could not carried into neighbor Poly(***lc1***)-lamella beyond intermediary PS-lamella.

This study points out that not only morphologies of microphase segregated structures but also composition fluctuations are strongly affected by the LC phase behavior in LC block copolymer systems.

References in This Chapter

1. M. Walther and H. Finkelmann, *Prog. Polym. Sci*., **21**, 951 (1996).
2. G. Mao and C. K. Ober, *Acta Polym*., **48**, 405 (1997).
3. M. Yamada, T. Iguchi, A. Hirao, S. Nakahama, and J. Watanabe, *Macromolecules*, **28**, 2556 (1995).
4. M. Yamada, T. Iguchi, A. Hirao, S. Nakahama, and J. Watanabe, *Polym. J*., **30**, 23 (1998).
5. I. W. Hamley, "The Physics of Block Copolymers", Oxford University Press, Inc., New York, N. Y., 1998.
6. S. Nojima, H. Nakano, Y. Takahashi, and T. Ashida, *Polymer*, **35**, 3479 (1994).
7. Y. L. Loo, R. A. Register, and A. J. Ryan, *Phys, Rev. Lett*., **84**, 4120 (2000).
8. M. Avrami, *J. Chem. Phys*., **7**, 1103 (1939).
9. G. H. Fredrickson, *J. Chem. Phys.*, **85**, 5306 (1986).
10. A. Onuki, *J. Chem. Phys.*, **87**, 3692 (1987).
11. Y. Long, R. A. Shanks, and Z. H. Stachurski, *Prog. Polym. Sci.*, **20**, 651 (1995).

Chapter 5

Microphase Morphology in Blends of Diblock Copolymer Containing Polystyrene and Side-Chain Liquid Crystalline Segments and Polystyrene Homopolymer

Abstract: The microdomain structure in blends of liquid crystal (LC)-coil block copolymer with corresponding coil homopolymers was studied. The used LC-coil block copolymer is composed of poly(6-[4-(4'-methoxyphenyl)phenoxy]hexyl methacrylate) as a LC segment and polystyrene as a coil segment. It has the molecular weight M_n = 47000 with the LC segment fraction of 45wt%. As a blended coil homopolymer, three polystyrenes with different molecular weights of 37000, 26000, and 8200 were used. In all the blends with LC segmental fractions of 35wt% to 10wt%, the microphase segregation is clearly recognized and LC segment in resulting microdomain undergoes the well-defined crystal-SmA_d-isotropic phase transitions. The microdomain structure depends on both the molecular weight of blended homopolystyrene and the phase structure of LC segment. When the highest molecular weight of polystyrene with M_n = 37000 was blended (so-called in a 'dry-brush' regime), a lamellar type of morphology is invariably observed even if the composition and temperature varied. In contrast, when the lowest molecular weight of polystyrene with M_n = 8200 was used (in a 'wet-brush' regime), the type of morphology is significantly altered. In the isotropic phase of LC segment, the lamellar morphology is observed for blends with LC contents from 45wt% to 35wt%, but cylindrical or spherical domain becomes predominant with a decrease in the LC content. On the other hand, the lamellar type of morphology is commonly observed at the crystalline phase. In some blends with the lower weight fractions of LC content, hence, there can be seen order-order transition from sphere or cylinder to lamella on decreasing temperature. This morphological transformation is caused by the formation of the layered structure that tends to orient perpendicularly to the interface of microdomain. The results show that the structural order of LC segment affects both the microdomain and the solubility style of the homopolymer into the block copolymer.

5.1. Introduction

Several types of microdomains, lamella, cylinder, sphere, and bicontinuous morphology, have been reported in the LC block copolymers[1-3], and interesting relationships between the morphology and the LC phase structure have been discussed. Some researchers and we (in Chapter 3) observed order-order transition (OOT)[4,5] in microdomain morphologies which were induced by the LC phase transition in nematic LC block copolymer and smectic LC block copolymers[6-9].

Microphase segregated morphologies depend on the weight fraction of the each segment, degree of polymerization (molecular weight) and Flory *c* parameter as described previously. We can not change the weight fraction and the molecular weight in synthesized block copolymers, but the total composition in the system by adding corresponding homopolymers. To extend such morphological studies, we have treated the binary blends of symmetric smectic LC block copolymer (PS-*b*-Poly(***lc1***)), which contains polystyrene (PS) and poly(6-[4-(4'-methoxyphenyl)phenoxy]hexyl methacrylate) (Poly(***lc1***))[10], and PS homopolymer (hPS).

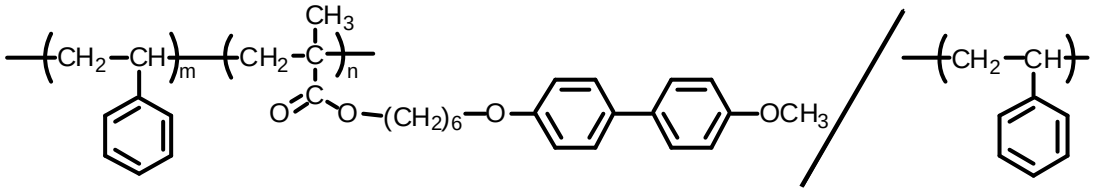

In these blend systems, the effect of the molecular weight of respective homopolymer on the microdomain strucrures must be taken into account. It has been investigated by Hashimoto *et al*. for given volume fractions of block copolymer in the blends comprising polystyrene-*b*-polyisoprene (PS-*b*-PI) and hPS with various molecular weights[11-13]. When hPS has a relatively lower molecular weight giving $r_s << 1$ where $r_s = M_{PS,homo}/M_{PS,block}$, the ratio of number average molecular weight of hPS ($M_{PS,homo}$) to that of corresponding polystyrene segment in the block copolymer ($M_{PS,block}$), the hPS is uniformly dissolved in the PS microdomain. The swelling of PS segment in PS-*b*-PI expands both the interdomain distance and the distance between the neighboring junctions of block chains at the interface. The resulting asymmetry in the effective volume of PS and PI block chains yields the interface curvature. Hence, the morphology may change from lamellae to cylinders and the spheres by

adding the hPS[12]. It is called 'wet-brush' regime. In the case of $r_s \approx 1$, on the other hand, hPS is also soluble in the PS microdomain but it is localized in the middle of the domain to expand only the domain spacing distance[13]. The distance between the neighboring junction of the block chains at the interface is thus unaffected by the hPS so that the type of morphology may not change ('dry-brush' regime). Referring to these basic data on the conventional blend system, we examined the microdomain morphologies in the PS-*b*-Poly(***lc1***)/hPS blends in this chapter. The effects of the molecular weight of hPS, the weight fraction, and the microdomain structure of Poly(***lc1***) segment were considered. In some blends, we found that well-defined OOT took place on the phase behavior of Poly(***lc1***) segment.

5.2. Experimental Section

Materials PS-*b*-Poly(***lc1***) block copolymer, which was the same material as **S1** in Chapter 3, and three polystyrene homopolymers were prepared by a sequential living anionic polymerization. Details of the synthesis are described elswhere[10]. The characteristics of these polymers are summarized in Table 5.1. The composition of each segment was finally determined by ^{1}H NMR. M_n and M_w/M_n values were estimated from GPC profile based on the standard PS calibration and ^{1}H NMR. PS-*b*-Poly(***lc1***) used here is composed of PS segment with M_n=26000 and Poly(***lc1***) segment with M_n=21000 (see Table 5.1). Three polystyrene homopolymers, abbreviated here hPS37, hPS26, and hPS08, have the molecular weights of M_n=37000, 26000, and 8200, respectively. Here, the number following to hPS in the abbreviation is $M_n \times 10^{-3}$.

The mixtures of PS-*b*-Poly(***lc1***) and hPS with the weight fraction of Poly(***lc1***) segment of 0.35 to 0.10 were dissolved in tetrahydrofuran with the total polymer concentration of 10wt%, then cast into the films by slow evaporation of the solvent during one week at room temperature. The resulting films were completely dried in a oven at 60°C until a constant weight was attained.

Methods Differential scanning calorimetric (DSC) measurements were carried out with a Perkin-Elmer DSC II at a scanning rate of 2°C·min.$^{-1}$ X-ray measurements were performed by using a Rigaku Denki RU-200BH X-ray generator with Ni-filtered Cu-Kα radiation. Reflection spacings were calibrated by using a silicon standard. Temperatures of the sample were regulated within 1°C by using a Mettler FP-82 hot stage.

Transmission electron microscopic (TEM) observation was performed with a Hitachi H-500 transmission electron microscope with 75kv of accelerating voltage. The sample was heated to an isotropic phase at 150°C in an effort to prevent a thermal prehistory, cooled to a predetermined temperature, and annealed for the proper period. Then the sample was quenched to the room temperature and cut into ultrathin sections with a thickness around 700-1000Å by ultramicrotome with a glass knife. The sectioned specimens were stained with the vapor of ruthenium tertaoxide (RuO_4) for 10 min before observation.

5.3. Results and Discussion

5.3.1. Characterization and Thermal Behavior of Neat PS-*b*-Poly(***lc1***)

DSC thermograms of the neat PS-*b*-Poly(***lc1***) are shown in curve a of Figure 5.1. Two transitions taking place on the Poly(***lc1***) segment, crystalline-SmA_d phase transition at 107°C and SmA_d-isotropic ones at 126°C, were observed together with the glass transition of PS segment at 90°C. Figure 5.2 represents a TEM photograph for ultrathin section of it which was slowly cooled from the isotropic phase at 150°C to the crystalline phase at room temperature. It clearly demonstrated the lamellar type of microphase segregated structure with the Poly(***lc1***) microdomains appearing dark because of preferential staining by RuO_4 vapor.

Figure 5.3 shows the temperature dependence of the lamellar spacings, D_x, determined by small angle X-ray measurement. The lamellar spacing decreased remarkably through the SmA_d temperature region. On the other hand, it was relatively constant in the crystalline and isotropic phases. The reduction is 25%, which is accountable with the conformational change of the main-chain from an extended form to random coil.

5.3.2. Thermal Behavior of PS-*b*-Poly(***lc1***)/Homopolystyrene Blends

Three blended systems were prepared by blending PS-*b*-Poly(***lc1***) with three homopolystyrenes, hPS37, hPS26, and hPS08; PS-*b*-Poly(***lc1***)/hPS37 in blend system **1**, PS-*b*-Poly(***lc1***)/hPS26 in system **2**, and PS-*b*-Poly(***lc1***)/hPS08 in system **3**. The systems **1**, **2**, and **3**, hence, have the values of r_s=1.4, 1.0, and 0.3, respectively (see Table 5.1). In each system, we prepared several blend samples with different weight fractions of LC segment; **a** with 0.35, **b** with 0.30, **c** with 0.25, **d** with 0.20, **e** with 0.15, and **f** with 0.10. According to

Table 5.1. Characterization of LC block copolymer and homopolystyrenes

Sample	M_n [a]	M_w/M_n [a]	F of Poly(***lc1***) segment [b]	r_s [c]
PS-*b*-Poly(***lc1***)	47,000	1.03	0.45	-
hPS37	37,000	1.06	-	1.4
hPS26	26,000	1.06	-	1.0
hPS08	8,200	1.09	-	0.3

a) Determined by GPC. b) Weight fraction of Poly(***lc1***) segment determined by ^{1}H NMR. c) The ratio of M_n of homopolystyrene to M_n of the polystyrene segment in PS-*b*-Poly(***lc1***).

Table 5.2. Characterization of the PS-*b*-Poly(***lc1***) / homopolystyrene blends[a)]

		F [b)] of hPS	F [b)] of Poly(***lc1***) segment	Transition temperature / °C (Enthalpy changes / kcal mol^{-1} [c)])			
				Heating		Cooling	
				T_1 (DH_1)	T_2 (DH_2)	T_1 (DH_1)	T_2 (DH_2)
PS-*b*-Poly(***lc1***)		-	0.47	108.2 (1.0)	132.6 (0.52)	102.8 (0.99)	133.4 (0.52)
PS-*b*-Poly(***lc1***) / hPS37	**1a**	0.24	0.35	106.8 (0.91)	126.3 (0.50)	101.0 (0.83)	125.4 (0.45)
	1b	0.35	0.30	109.3 (0.77)	133.2 (0.38)	103.5 (0.74)	133.2 (0.38)
	1d	0.55	0.20	109.3 (0.75)	135.5 (0.40)	103.5 (0.75)	134.8 (0.44)
	1f	0.78	0.10	108.6 (0.71)	134.1 (0.53)	102.6 (0.62)	133.2 (0.44)
PS-*b*-Poly(***lc1***) / hPS26	**2a**	0.24	0.35	106.8 (0.95)	129.4 (0.54)	101.9 (0.87)	130.7 (0.49)
	2b	0.35	0.30	105.5 (0.94)	129.9 (0.45)	99.9 (1.0)	124.0 (0.66)
	2c	0.45	0.25	105.5 (1.1)	125.6 (0.50)	100.1 (1.0)	124.3 (0.67)
	2d	0.55	0.20	107.0 (1.1)	130.0 (0.74)	101.4 (1.1)	129.6 (0.71)
	2e	0.66	0.15	107.0 (1.2)	128.9 (0.62)	101.4 (1.1)	129.1 (0.65)
	2f	0.78	0.10	107.0 (1.1)	128.9 (0.83)	101.4 (1.1)	128.5 (0.71)
PS-*b*-Poly(***lc1***) / hPS08	**3a**	0.24	0.35	106.5 (0.95)	129.1 (0.72)	101.2 (0.89)	128.9 (0.59)
	3b	0.35	0.30	107.1 (0.90)	129.9 (0.49)	101.7 (0.90)	130.3 (0.54)
	3c	0.45	0.25	106.6 (0.50)	127.6 (0.50)	101.2 (0.95)	127.4 (0.63)
	3d	0.55	0.20	107.4 (1.1)	129.4 (0.69)	101.8 (1.0)	129.1 (0.66)
	3e	0.66	0.15	107.7 (1.1)	130.5 (0.62)	102.1 (1.1)	129.3 (0.53)
	3f	0.78	0.10	108.3 (0.93)	132.3 (0.83)	102.5 (0.90)	131.6 (0.71)

a) Determined by DSC measurements at 2nd heating and cooling (2°C·min^{-1}). b) Weight fraction. c) Estimated per mole of LC Poly(***lc1***) segment.

these notations, the blend samples were named as **Xy** where **X** is the system number (**1**-**3**) and y is the alphabet (**a**-**f**) showing the weight fraction of Poly(***lc1***) (refer to Table 5.2).

Typical DSC thermograms of blend samples are shown in curves b-g of Figure 5.1. All blends exhibited two phase transitions similarly as PS-*b*-Poly(***lc1***)[10]. The phase sequence is also similar; the crystalline-SmA_d and SmA_d-isotropic phase transitions took place. The transition temperatures and enthalpies were summarized in Table 5.2. We can again find that the values of transition temperature and enthalpies are similar to those of the neat PS-*b*-Poly(***lc1***). Hence, it is concluded that the crystallinity and liquid crystallinity of the Poly(***lc1***) segment in its microdomain were not essentially affected by blending the hPS.

5.3.3. Morphology in Crystalline Phase of Poly(*lc1*) Segment in the Blends

Figure 5.4 shows TEM photographs for ultrathin sections cut out of the PS-*b*-Poly(***lc1***)/hPS blends. Here, the blend samples were initially heated up to the isotropic phase at 150°C, annealed for 24h, and then cooled down to the crystalline phase at a rate of $2°C \cdot min^{-1}$.

As found in Figure 5.4, no macroscopic phase segregation was involved for all the blends with the crystal Poly(***lc1***) segment. It is further found that the hPS did not significantly perturb the long-range spatial order of the lamellar microdomains. The expansion in the interlamellar spacing causes undulation of the lamellae or bending of the interface resulting in a broader distribution of the spacing between lamellae. Its most typical example can be seen in the micrographs of **1d** and **1f**. According to Hashimoto's work for PS-*b*-PI/hPS[11-13], the blends in a system **1** are evidently classified into the 'dry-brush' regime. Hence, it is expected that the hPS did not expand the distance between the neighboring junctions of PS-*b*-Poly(***lc1***) at the interface, but the interdomain distance by locating in the middle of the PS domain. Thus the observation is reasonable that the lamellar morphology in a series of **1** is strongly sustained with the variation of hPS content. On the other hand, some small pieces of lamellae coexist with long ranged lamellae in system **3** which surely in the 'wet-brush' regime, but the situation was essentially similar to that in system **1**. In the crystalline phase, thus, the hPS, even if it had the lower molecular weight, did not expand seriously the distance between the neighboring junctions at the interface.

When the content of hPS was relatively lower, the lamellar packing was somewhat regular

Table 5.3. Lamellar spacing of PS-*b*-Poly(***lc1***)/homopolystyrene blends

	$D_{obs.}$ / Å	$D_{calc.}$ / Å [a)]
1a	442	442
2a	434	442
2b	490	517
3a	418	442
3b	470	517

a) Calculated by assuming 'dry-brush' regime (see the text).

enough to allow the estimation of the lamellar spacing by the small-angle X-ray method. The lamellar spacings, D_x, are listed for **1a**, **2a**, **2b**, **3a**, and **3b** in Table 5.3 and are compared with the calculated values under the assumption of the perfect 'dry-brush'. D_x for **1a** was almost equal to the calculated one, but D_x for **3a** and **3b** were relatively smaller than the calculated values, implying that the hPS08 expands somewhat the distance between the neighboring chains of PS-*b*-Poly(***lc1***) at the interface of the microdomain although the degree of expansion was not so large.

Thus it seems that all the systems in a crystalline phase behave as in a 'dry-brush' regime irrespective of the molecular weight of mixed hPS.

5.3.4. Morphology in Isotropic Phase of Poly(*lc1*) Segment

Next, we tried to examine the morphology in the isotropic phase of Poly(***lc1***) segment. For this purpose, the materials were heated to 150°C, annealed for 24h, and then quenched to room temperature. Figure 5.5 shows the TEM photographs for the same materials as presented in Figure 5.4. By comparing Figure 5.4 and 5.5, one knows that for any blends in system **1** the lamellar morphology was similarly observed as in the crystalline phase. On the other hand, in some blends of system **2** and **3**, the morphology was drastically altered. The typical change can be seen in **2f** and **3f** where only the spherical microdomain can be seen. From a series of photographs in system **3**, the morphology was found to depend on the content of PS so that the lamellar microdomain in **3a** was altered to cylinder-like domain in **3d** and finally to the sphere domain in **3f** with the increase of the content of PS. This is just expected for the blends in the 'wet-brush' regime, *i.e.*, the low molecular weight hPH08 could swell the PS microdomain of block copolymer and spread the distance between the neighboring chains at

the interface of the microdomain of the block copolymer to yield the interface curvature of the cylindrical or spherical microdomain.

5.3.5. Morphological Changes on Phase Behavior of Poly(*lc1*) Segment

By composing the micrographs of **3f** in Figures 5.4 and 5.5, one can realize that the morphology in the blends strongly depends on the phase structure of Poly(***lc1***) segment[10]. To clarify OOT , the blend samples were annealed at the respective temperatures; at 135℃ in the isotropic phase for 24h, at 125℃ in the SmA_d temperature region near the isotropization temperature for 1 week, and at 115℃ in the SmA_d temperature region near the crystallization temperature for 1 week. All the annealed samples were then quenched to room temperature. Figure 5.6 represents the typical micrographs observed for **1f**, **2f**, and **3f**.

1f sustained to form the lamellar microdomain over the whole temperature region as expected from the data in Figures 5.4 and 5.5. In **2f** the spherical microdomain of the isotropic phase was altered to lamellar or cylindrical microdomain on the transition into SmA_d phase, which can be considered to be caused by the elastic energy of the aligned mesogens. This investigates in next chapter by using nematic LC block copolymers. In **3f**, spherical microdomain can be seen in the SmA_d phase at higher temperatures of 125℃ as well as in the isotropic phase, and transformed to the lamellar microdomain in the SmA_d phase at lower temperatures of 115℃. Thus the OOT was likely to take place when both the molecular weight of blended hPS and the weight fraction of Poly(***lc1***) segment were relatively lower. The OOT observed in system **3** is schematically illustrated as functions of the temperature and the fraction of Poly(***lc1***) segment in Figure 5.7b. This result was interestingly compared with that of Figure 5.7a, as observed for system **1**, where the lamellar microdomain was invariably formed in the whole region of temperature and Poly(***lc1***) content.

The OOT typically observed for the blends of system **3** with lower weight fraction of Poly(***lc1***) segment, for example, **3d**, **3e**, and **3f**, can be understood as following. At the isotropic temperatures, the hPS08 with r_s=0.3 spread strongly the distance between the neighboring chains at the interface of the microdomain of PS-*b*-Poly(***lc1***) because of the preferred swelling into the PS microdomain. This resulted in the morphological change from lamella to cylinder or sphere. On transition to the SmA_d of the Poly(***lc1***) segment, the

side-chain mesogens took up the uniaxial orientation to form the smectic layer, simultaneously the main-chain of Poly(***lc1***) segment changed from random coil to the extended form, and then the smectic layers were formed perpendicularly to the interface[10]. Considering that the radius of sphere or cylinder was around 200-300Å which was roughly ten times as large as the smectic layered thickness of 26Å, the smectic layers developing from the largely curved interface could not be packed effectively without layer deformation (see Figure 5.8b). Only the flat interface from the lamellar microdomains was comfortable for the smectic or crystalline layer structure (Figure 5.8c). Thus in SmA_d phase at lower temperatures or in crystalline phase, the lamellar microdomain was preferred by overcoming the entropic loss due to exclusion of homopolystyrene from the interface in the PS microdomain of block copolymer.

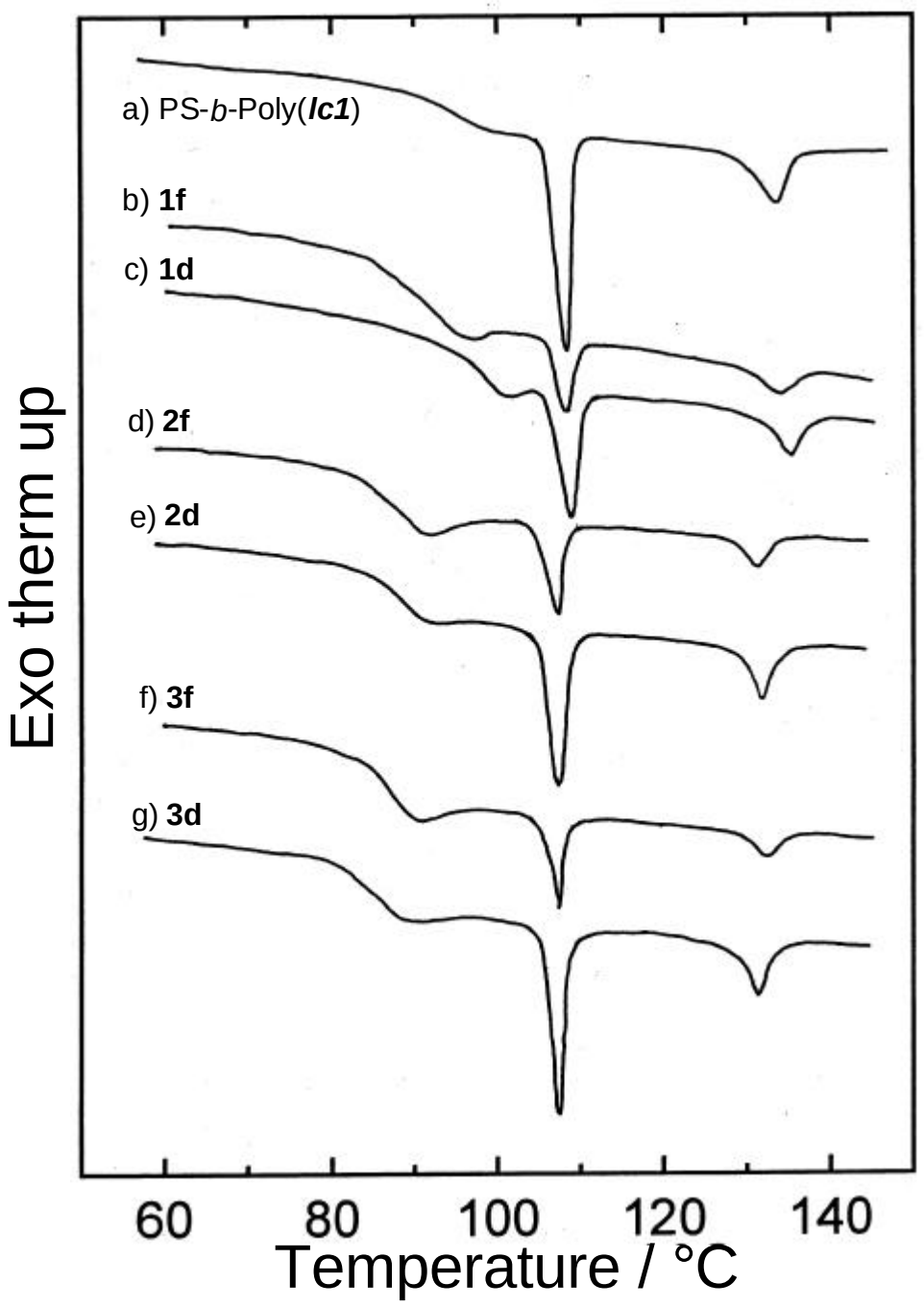

Figure 5.1. DSC thermograms of the neat block copolymer (curve a) and the blends (curve b-g) measured at a heating rate of 2°C·min^{-1}. Two peaks are attrributed to the crystal-SmA_d and SmA_d-isotropic phase transitions of Poly(***lc1***) segment.

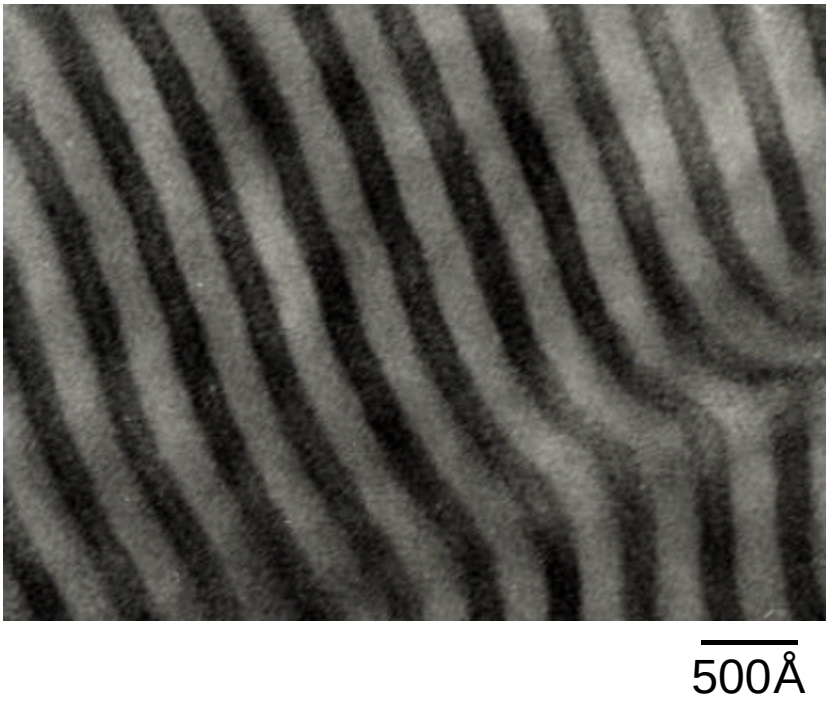

Figure 5.2. The transmission electron micrograph for the ultrathin section cut out of the neat PS-*b*-Poly(***lc1***) at crystalline phase. This shows a typical lamellar type microphase segregation. Dark area is the LC Poly(***lc1***) microdomain because of staining by RuO_4.

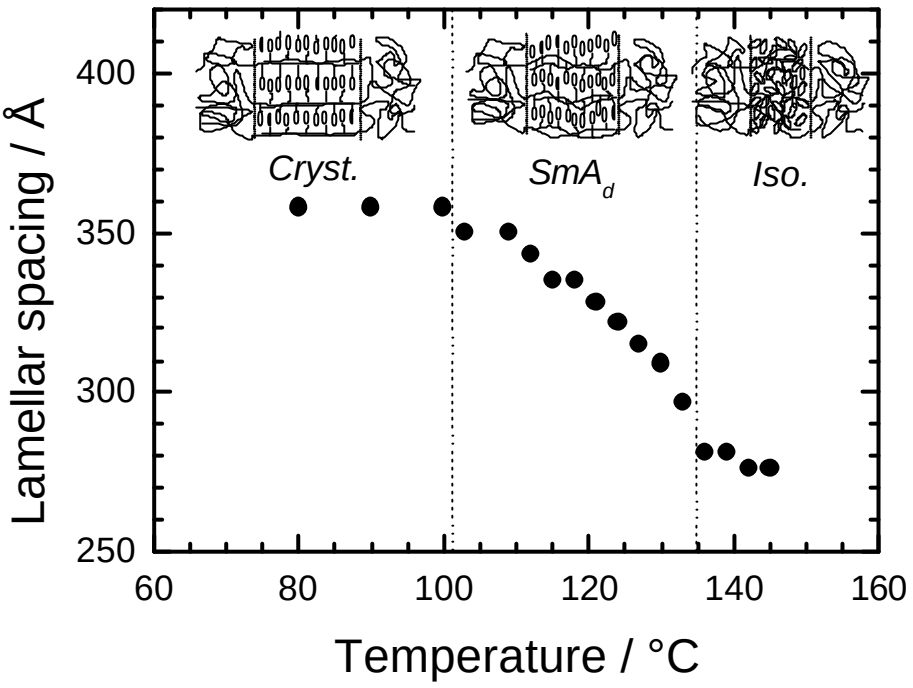

Figure 5.3. Temperature dependence of the lamellar spacing for neat PS-*b*-Poly(***lc1***) measured by small-angle X-ray scattering. Schematic illustration of the structure changes on crystal-SmA_d-isotropic phase transitions are inserted.

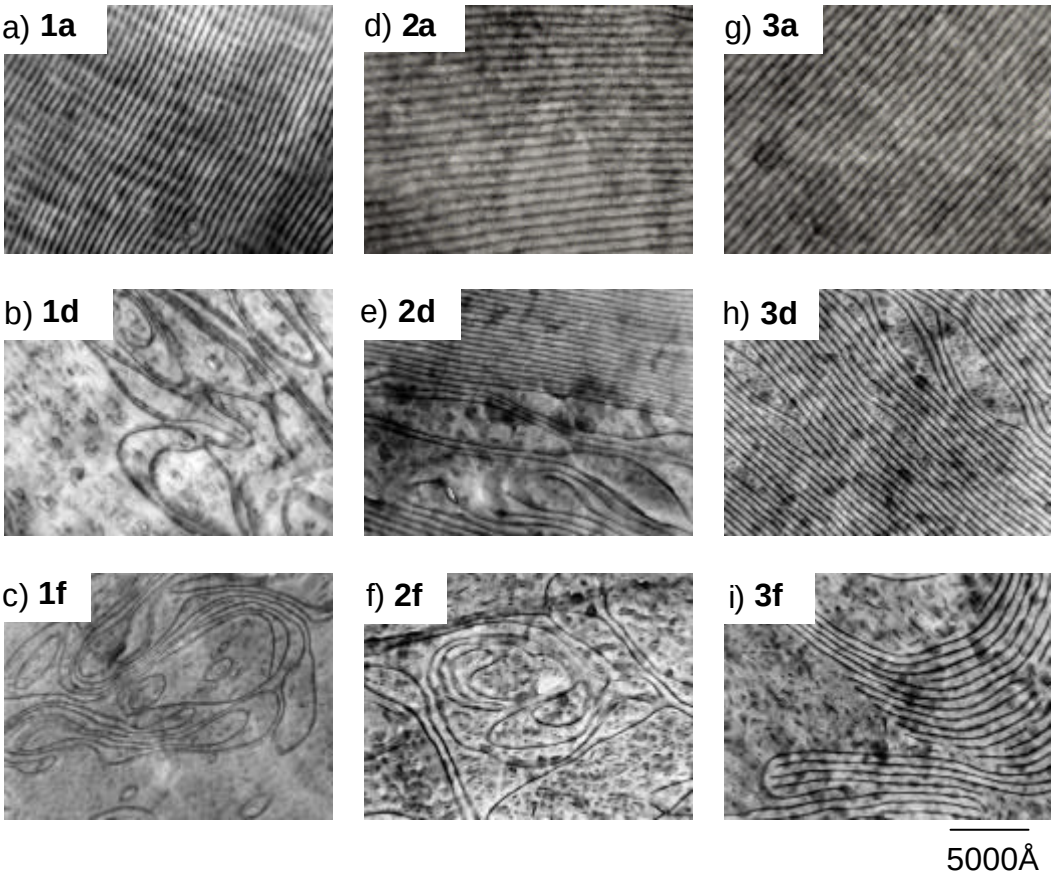

Figure 5.4. Transmission electron micrographs for the ultrathin section cut out of PS-*b*-Poly(***lc1***)/hPS blends at the crystalline phase; **1a**, **1d**, and **1f** in system **1**, **2a**, **2d**, and **2f** in system **2**, and **3a**, **3d**, and **3f** in system **3**.

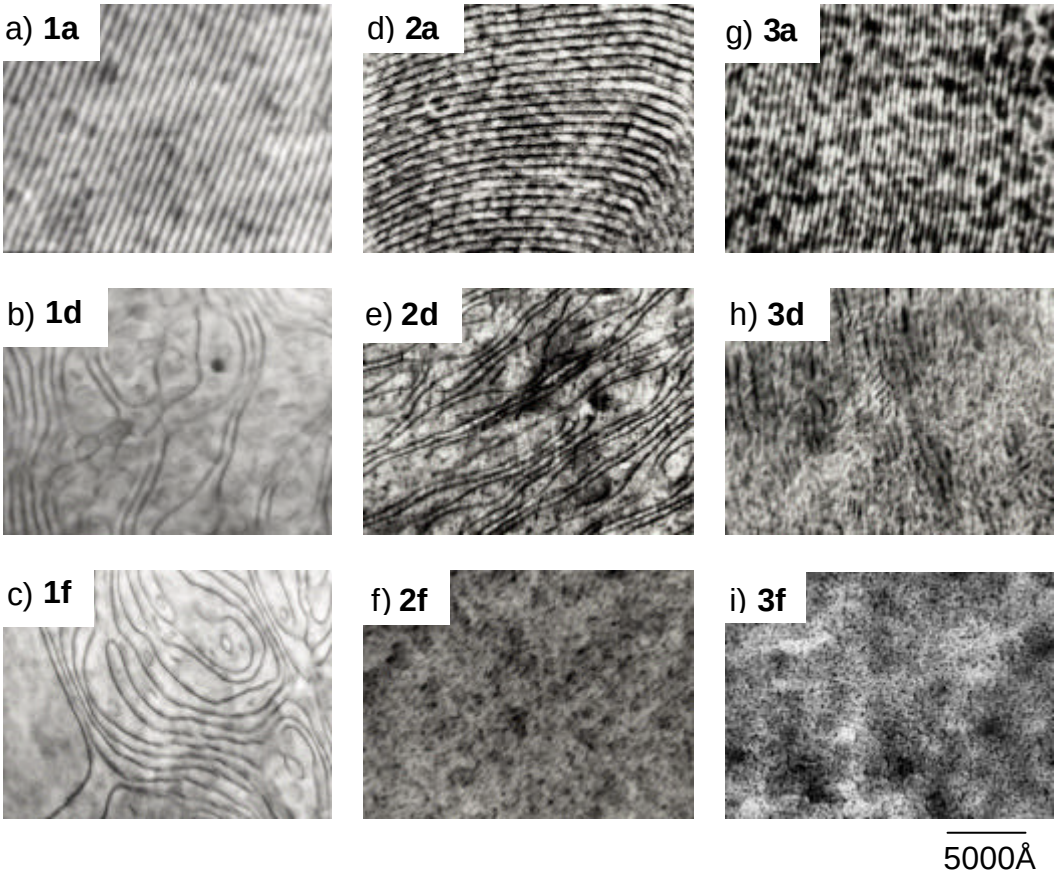

Figure 5.5. Transmission electron micrographs for the ultrathin section cut out of PS-*b*-Poly(***lc1***)/hPS blends which were quenched from the isotropic phase at 150°C after annealing for 24h; **1a**, **1d**, and **1f** in system **1**, **2a**, **2d**, and **2f** in system **2** and **3a**, **3d**, and **3f** in system **3**.

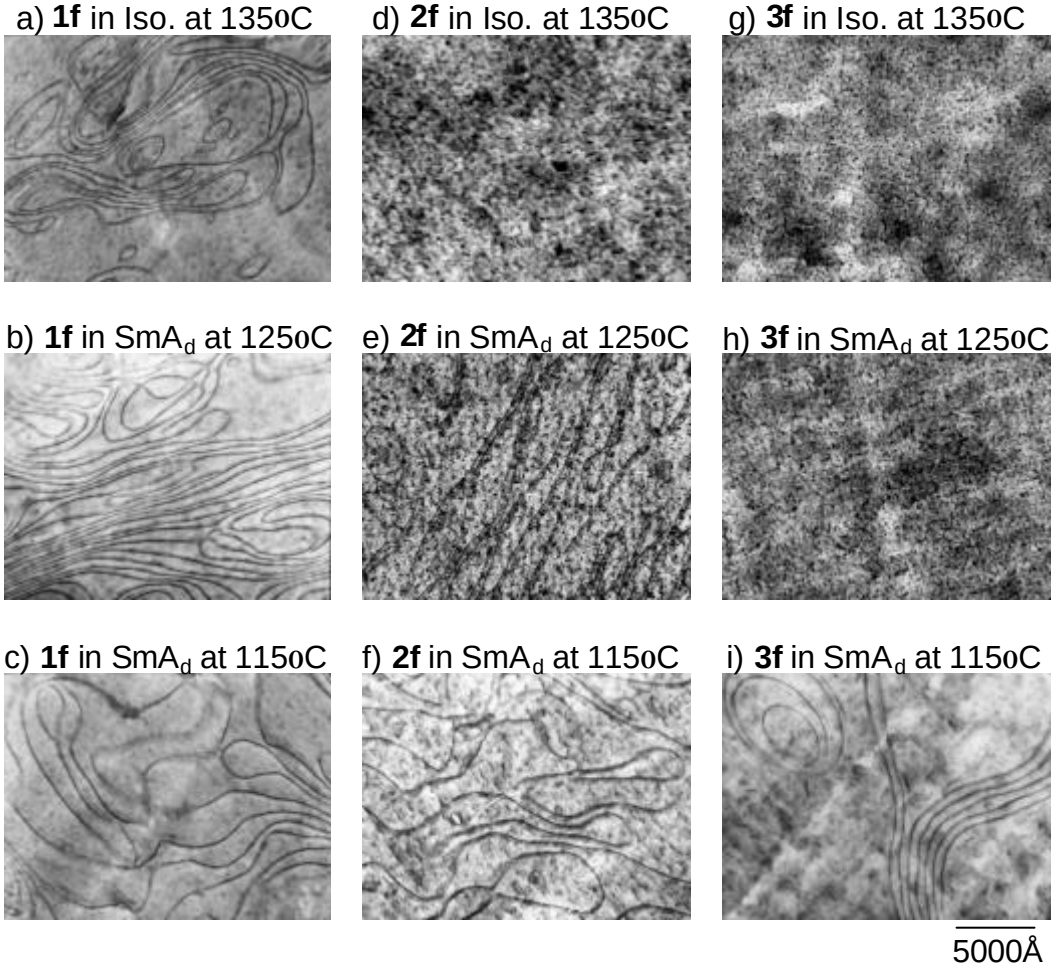

Figure 5.6. Transmission electron micrographs of **1f**, **2f**, and **3f** which were quenched from the SmA_d phase at 115°C, the SmA_d phase at 125°C and the isotropic phase at 135°C, respectively.

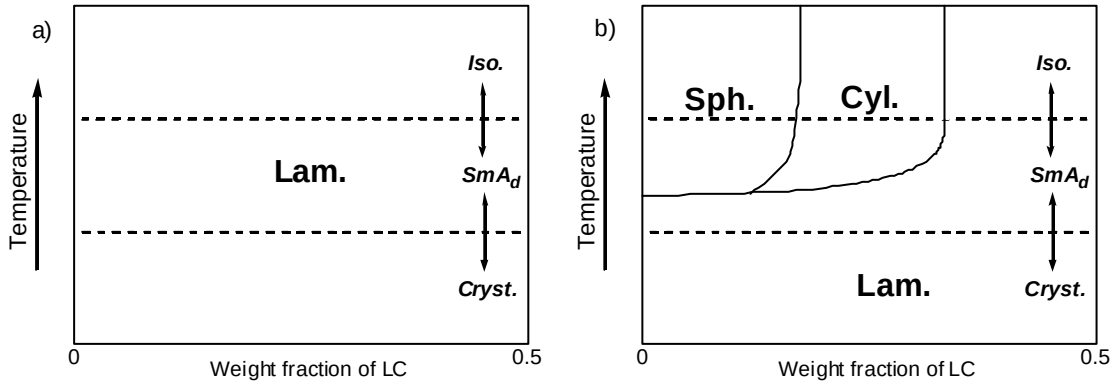

Figure 5.7. Variation of the microphase structures with the temperature and the weight fraction of LC segment; a) in system **1** and b) in system **3**.

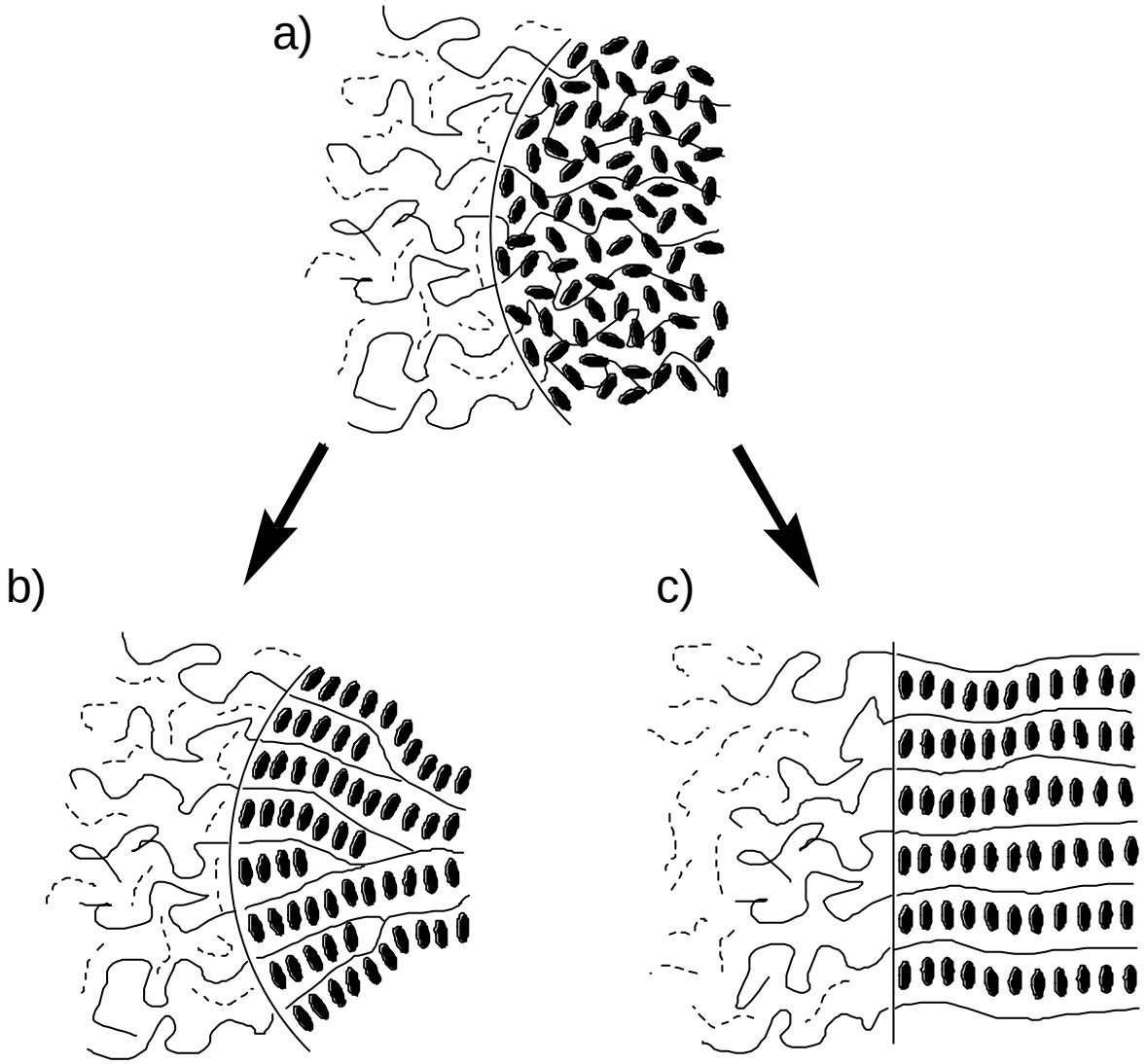

Figure 5.8. Schematical illustration of the microphase structure varying with the phase structure of LC segment; a) isotropic phase in spherical midrodomain, b) SmA_d in spherical microdomain, and c) SmA_d in lamellar microdomain.

5.4. Concluding Remarks

The interrelationship between the microdomain structure and the thermotropic phase structure of LC segment was studied in symmetric LC-coil block copolymer (PS-*b*-Poly(***lc1***))/homopolystyrene (hPS) blended samples. Neat block copolymer and all the blends with various weight fractions of LC content from 0.35 to 0.10 exhibited the microphase segregation and the LC segment in its microdomain underwent the well-defined crystalline-SmA_d-isotropic transitions. The hPS is thus soluble into the PS microdomain of the LC block copolymer.

The microdomain structure depends on both the molecular weight of hPS blended and the phase structure of LC segment. When the highest molecular weight of hPS with M_n=37000 was blended (so called 'dry-brush' regime), a lamellar type of microdomain was observed invariably even if the composition and temperature were varied. In contrast, when the lowest molecular weight of hPS with M_n=8200 was used (in a 'wet-brush' regime), the type of morphology was significantly varied. In the isotropic phase of LC segment, the lamellar morphology was observed for the blends with the weight fraction of LC contents from 0.45 to 0.35, but the cylindrical or spherical microdomain appeared with a decrease in the LC content. In the crystalline phase and SmA_d phase near the crystallization temperature, on the other hand, the lamellar microdomain was commonly formed. In some blends with the lower weight fractions of LC segment of 0.10 to 0.30, hence, there was seen order-order transition from sphere or cylinder to lamella on decreasing the temperature from isotropic to crystalline phase. This morphological transformation was caused by the formation of the layered structure that tends to orient perpendicularly to the interface of microdomain, leading to the reasonable conclusion that both the microdomain morphology and the solubility style of the homopolymer were dominated by the counterbalance between the energetic gain to the layer formation of LC segment and entropic loss due to the exclusion of the microdomain if the PS segment.

References in This Chapter

1. 1. M. Walther and H. Finkelmann, *Prog. Polym. Sci*., **21**, 951 (1996).
2. G. Mao and C. K. Ober, *Acta Polym*., **48**, 205 (1997).
3. S. Poser, H. Fischer, and M. Arnold, *Prog. Polym. Sci.*, **23**, 1337 (1998).
4. L. Leibler, *Macromolecules*, **13**, 1602 (1980).
5. A. K. Khandpur, S. Föster, F. S. Bates, I. W. Hamley, A. J. Ryan, W. Bras, K. Almdal, and K. Mortensen, *Macromolecules*, **28**, 8796 (1995).
6. J. Sänger, W. Gronski, S. Maas, B. Stühn, and B. Heck, *Macromolecules*, **30**, 6783 (1997).
7. M. Anthamatten and P. T. Hammond, *Macromolecules*, **32**, 8066 (1999).
8. a) Chapter 3 in this thesis

   b) T. Itoh, M. Yamada, A. Hirao, S. Nakahama, and J. Watanabe, *Mol. Cryst., Liq. Cryst.*, **347**, 211 (2000).
9. A. Schneider, J. J. Zanna, M. Yamada, H. Finkelmann, and R. Thomann, *Macromolecules*, **33**, 649 (2000).
10. a) Chapter 1 and Chapter 2 in this thesis.

    b) M. Yamada, T. Iguchi, A. Hirao, S. Nakahama. and J. Watanabe, *Macromolecules* **28**, 50 (1995).

    c)M. Yamada, T. Iguchi. A. Hirao, S. Nakahama, and J. Watanabe, *Polym. J.* **30**, 23 (1998).
11. H. Hasegawa and T. Hashimoto, 'Self-Assembly and Morphology of Block Copolymer System' in "Comprehensive Polymer Science", S. L. Aggarwal and S. Russo, Ed., Pergamon Press, Ltd., Oxford, 1996, Suppl. 2.
12. T. Hashimoto, H. Tanaka, and H. Hasegawa, *Macromolecules*, **23**, 4378 (1990)
13. S. Koizumi, H. Hasegawa, and T. Hashimoto, *Makromol. Chem., Macromol. Symp*., **62**, 75 (1992)

Chapter 6

Interrelation between Microdomain Structure and Liquid Crystalline Phase Behavior in AB Type Block Copolymers Containing Polystyrene and Nematic Side-Chain Liquid Crystalline Segment

Abstract: We synthesized well-defined AB type diblock copolymers, which contain polystyrene (PS) segment and side-chain liquid crystalline poly(6-[4-(4'-cyanophenyl) phenoxy]hexyl acrylate) segment with various compositions, by atom transfer radical polymerization. The thermotropic phase behavior and structures were examined for seven copolymers with the segmental composition of LC segment from 10wt% to 73wt%. All copolymers, except for the copolymer with 10wt% of LC segment, exhibited isotropic phase, nematic phase, and nematic glass. The block copolymers form lamellar, cylindrical, and spherical microdomains, and disordered state in the isotropic phase as expected by the weight fraction. Their microdomain spacings did not change on the isotropic-nematic phase transition and throughout all temperature region, which means that the conformation of the LC segment in the nematic phase was the same as that in the isotropic phase, so that random coil of LC segment can be considered. Some block copolymers showed order-disorder and order-order transition induced by nematic phase. The order-disorder transition was the morphological transformation between LC-cylinders in the nematic phase and disorder state in the isotropic phase, in which LC-spheres were not be observed. The order-order transition between PS-cylinders in the nematic phase and PS-spheres in the isotropic phase took place. This means that nematic phase was unstable in and out the spherical microdomain due to elastic energy of LC phase. Hence, the microdomains minimize the elastic energy rather than interfacial free energy. Moreover, 'transparent nematic' phase was indicated by the isotropic-nematic phase transition with PS-spheres.

6.1. Introduction

In previous chapters, we found morphological transformations induced by smectic liquid crystalline (LC) phase behavior in smectic A_d LC block copolymers (PS-*b*-Poly(***lc1***)s) prepared by anionic polymerization[1]. Yamada *et al.* reported that most distinct feature of PS-*b*-Poly(***lc1***) was the conformational changes from random coil to extended form with decrement of temperature in the smectic temperature region[2]. More properties were cleared for PS-*b*-Poly(***lc1***) in previous chapters of this thesis. At high temperature region in the smectic phase, the layered packing of mesogens enforced anisotropic chain conformation to counter amorphous polystyrene (PS) segment. In some case within narrow region of its segmental composition near the boundary of cylinders and lamellae, lamellar type of microphase segregated structure did not have the ability to stow anisotropic PS segment, which bent the interface of microdomain, and then lamellae altered into LC-cylinders (in Chapter 3). At low temperature region in the smectic phase, on the other hand, the highly anisotropic and nearly extended LC segment was unfavorable to the microdomain with bending interface, and then LC-spheres and LC-cylinders altered into lamellae (in Chapter 5).

More fundamentally, LC phase is simply composed by mesogenic alignment, namely nematic phase. It has elastic field of bend, spray, and twist due to the mesoenic alignment. On the other hand, block copolymers compose restricted spaces of microdomains which have characteristic shapes including lamellar, cylindrical, spherical, and bicontinuous morphologies with tens nano meters size. For a nematic LC block copolymer, it is easy to be considered that the one-dimensional mesogenic alignment is stable in lamellae, cylinders, and their matrix if the director of microdomains and mesogens are same. But it is difficult to be considered that the mesogenic alignment is stably stowed in spheres and their matrix because highly elastic energy of the nematic field is induced at the bent interface of spherical microdomains. In reality, Sänger *et al.* observed a morphological transformation from PS-spheres in isotropic temperature region to PS-cylinders in nematic temperature region for a PS-*b*-LC-*b*-PS triblock copolymer with a volume fraction of PS segment at 0.12[3]. This means that the nematic phase is stable with cylindrical microdomains rather than spheres.

On the other hand, we observed LC phase was allowed to take place in LC-spheres (in **3f** of Chapter 5) below the smectic-isotropic phase transition temperature which was determined by

a differential scanning calorimetric (DSC) measurement. Furthermore, Yamamoto and Tanaka reported 'transparent nematic' (TN) phase in which DSC thermograms showed its transitional peak but with optically isotropic phase in a study of a lyotropic inverse micelle composed of water, oil (thermotropic LC, pentylcyanobipnenyl, 5CB), and surfactant (didodecyl dimethyl ammonium bromide, DDAB)[4]. We expect similar phenomena in LC block copolymer system where nematic matrix with PS-spheres is allowed. To clarify them, we synthesized new LC block copolymer (PS-*b*-Poly(***lc2***)) containing PS segment and poly(6-[4-(4'-cyanophenyl) phenoxy]hexyl acrylate) (Poly(***lc2***)) segment in Chapter 2

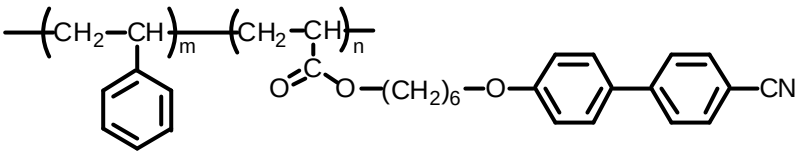

which shows nematic phase in the Poly(***lc2***) segment. Then we show the interrelations between the nematic LC phase behavior and the microdomain morphologies in current chapter.

6.2. Experimental Section

Materials The AB type block copolymers (PS-*b*-Poly(***lc2***)) containing PS and poly(6-[4-(4'-cyanophenyl)phenoxy]hexyl acrylate) (Poly(***lc2***)) were prepared by atom transfer radical polymerization (ATRP). Details were described in Chapter 2. The weight fractions of Poly(***lc2***) segment were varied from 0.10 to 0.73. The block copolymers were named **N1**-**N7** as shown in Table 6.1. The molecular weight (M_n) and the molecular weight distribution (M_w/M_n) were estimated from GPC profile based on the standard PS calibration. The composition of each segment was finally determined by ^{1}H NMR.

Methods Differential scanning calorimetric (DSC) measurements were carried out with Perkin-Elmer Pyris I at a scanning rate of 10°C·min^{-1}. X-ray measurements were performed by using Rigaku Denki X-ray generator with Ni-filtered Cu-Kα radiation. Reflection spacings were calibrated by using silicon standard or a chicken tendon. Temperature of the material was regulated within 1°C by using Mettler FP-82 hot stage. Polarized optical microscopic (POM) observations were carried out by using OLYMPUS BX50 equipped with Mettler FP-82 hot stage. Transmission electron microscopic (TEM) observation to clarify the morphology of block copolymers was performed by JEOL JEM-1010 transmission electron microscope with 80kV of accelerating voltage. For this observation, the block copolymer was cut into ultrathin sections (700-1000Å) by ultramicrotome with a glass knife. The sectioned specimens were stained with the vapor of ruthenium tetraoxide (RuO_4) for 10min before observation.

6.3. Results and Discussion

6.3.1. Phase Transition

DSC measurement was carried out on several heating and cooling cycles for **N1**-**N7**. The transition temperatures, enthalpy changes, and glass transition temperatures (T_g) are summarized in Table 6.1. As can be seen in Figure 6.1, **N3**-**N7** showed one dominant peak on heating and cooling, reversibly, which can be considered nematic-isotropic phase transition. No crystallization took place in all of this polymeric system, but glass transitions were clearly observed around 40°C and 90°C. PS segment has T_g about 90°C. Hence, the nematic phase in Poly(***lc2***) segment vitrified around 40°C.

N1 showed no peak and **N2** showed small peak on only heating in the DSC measurement, and their T_g were higher than those of **N3**-**N7** by 20-30°C. It can be considered that very slow nematic-isotropic phase transition took place in **N2**. The high T_g can be considered that the nematic phase was difficult to take place in this composition and easy to vitrify.

We also observed that **N5** and **N7** with the weight fraction of the Poly(***lc2***) segment at 0.73 showed broaden peaks, while other PS-*b*-Poly(***lc2***)s showed sharp peaks. The reason of it will discuss below.

Table 6.1. Characterization of LC block copolymers.

Run	M_n [a]	M_w/M_n [a]	Weight fraction of LC segment	T_i / °C [b] (ΔH /kcal• mol^{-1} [c])		T_g / °C [b]
				Heating	Cooling	
N1	16400	1.14	0.10	109 [d]	106 [d]	67
N2	17800	1.13	0.17	112.4 (0.070)	106 [d]	61
N3	32200	1.15	0.54	120.9 (0.12)	118.9 (0.14)	38
N4	43500	1.22	0.65	127.1 (0.17)	124.9 (0.16)	39
N5	53900	1.38	0.73	116.9 (0.11)	118.6 (0.10)	36
N6	20200	1.19	0.69	121.2 (0.12)	119.1 (0.12)	38
N7	23200	1.34	0.73	116.2 (0.12)	114.0 (0.12)	36

a) Determined by GPC. b) Transition temperature of Poly(***lc2***) segment determined by DSC at the heating and cooling rates of 10°C•min^{-1}. c) Corresponding enthalpy changes estimated per mole. d) No phase transitional peak in DSC measurement and determined with birefringence appearing and clearing in POM observation.

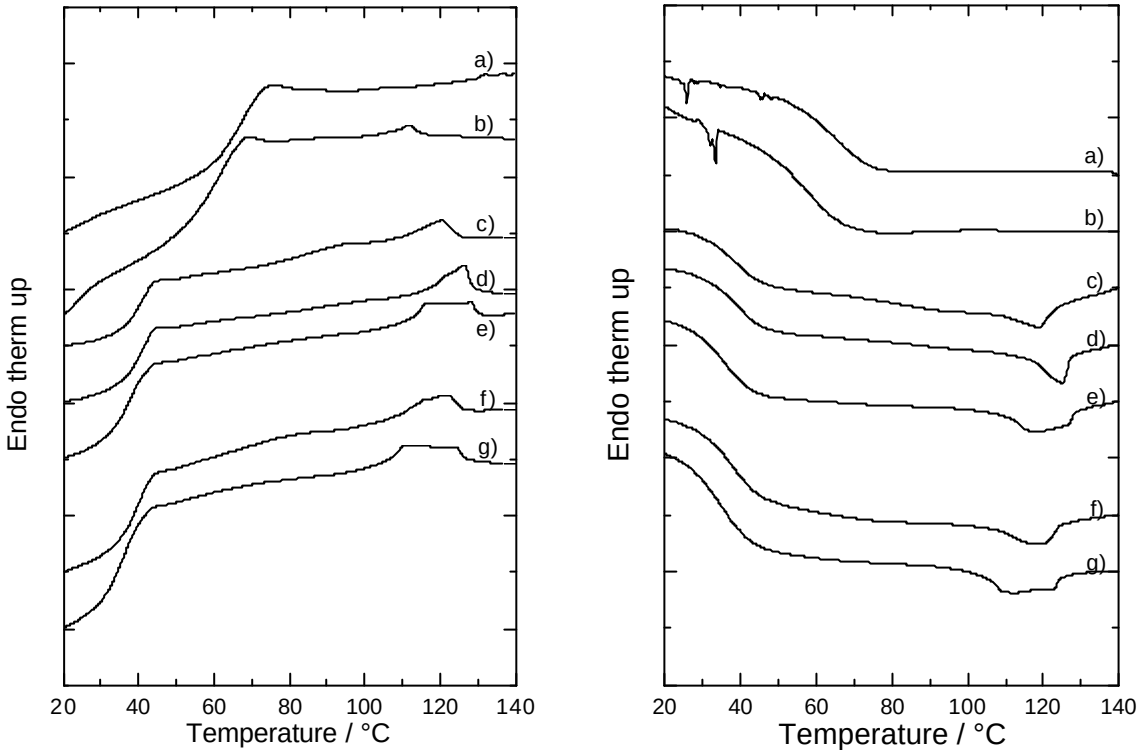

Figure 6.1. DSC thermograms on (left) heating and (right) cooling at the rate of 10°C·min^{-1} for a) **N1**, b) **N2**, c) **N3**, d) **N4**, e) **N5**, f) **N6**, and g) **N7**, respectively.

6.3.2. Phase Sequence in PS-*b*-Poly(*lc2*)

Figure 6.2 shows wide angle X-ray diffraction patterns for **N4** which were carried out to determine the LC phase. A oriented fiber drawn from LC phase at 90°C was used. Their axes was placed vertically. Above the transition temperature which was determined by the DSC measurement, **N4** showed isotropic broaden rings, although localized broaden diffractions on horizontal direction were shown below the transition. **N3** and **N5**-**N7** also showed these nematic patterns below the phase transition, while isotropic patterns were shown above their phase transitions. The nematic patterns remained below their T_g. Thus we conclude that **N3**-**N7** showed isotropic and nematic phases, and nematic glass in the microstructures of PS-*b*-Poly(***lc2***).

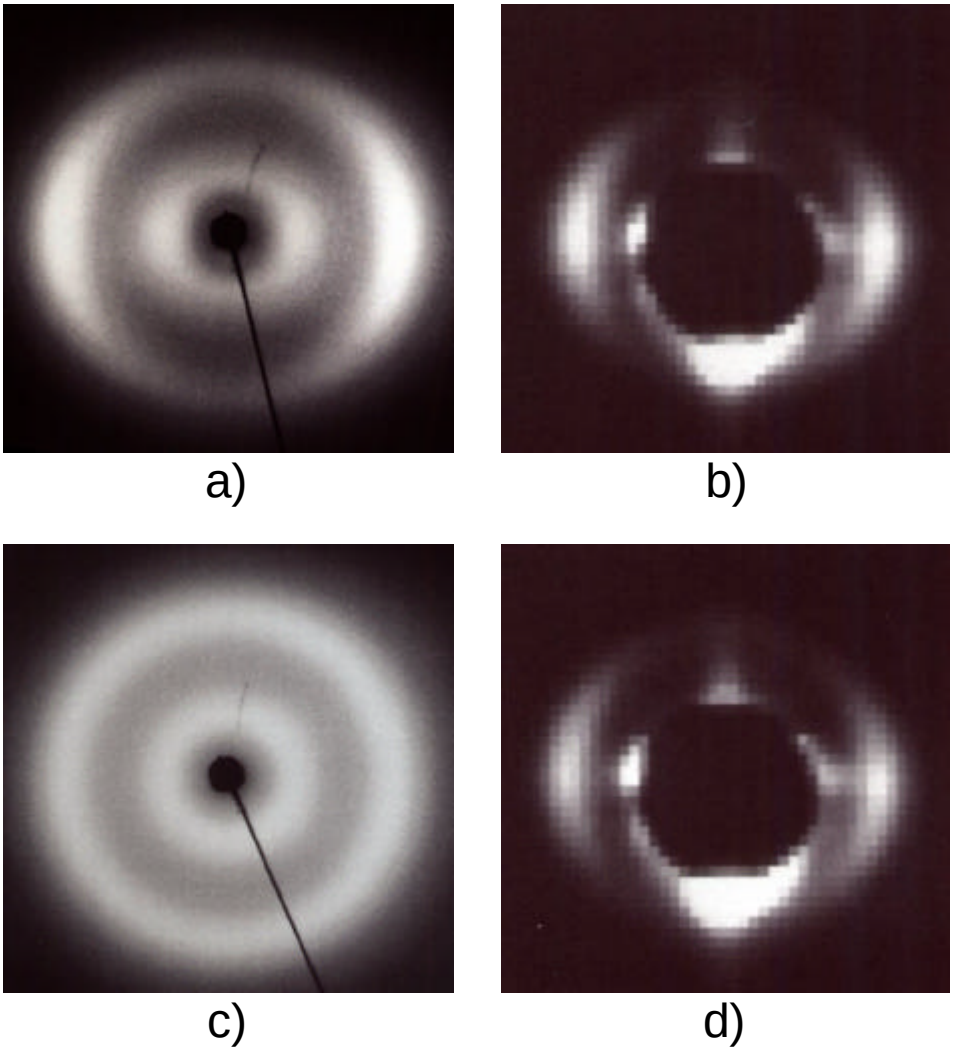

Figure 6.2. Wide angle X-ray diffraction photographs for the nematic and isotropic phases of PS-*b*-Poly(***lc2***) are given in a) and c), respectively. b) and d) are the corresponding small angle X-ray photographs. Here, the fiber specimen was drawn the nematic of **N4** and its axis was placed in the vertical direction. The oriented patterns observed here were invariable on heating and cooling.

Oriented fibers could not be obtained for **N1** and **N2**. Their bulk showed wide angle X-ray scattering patterns with broaden isotropic rings in whole temperature region. For **N2**, the broaden pattern under the phase transition which observed in DSC measurement indicates nematic phase. The phase sequence of **N1** was remained unknown.

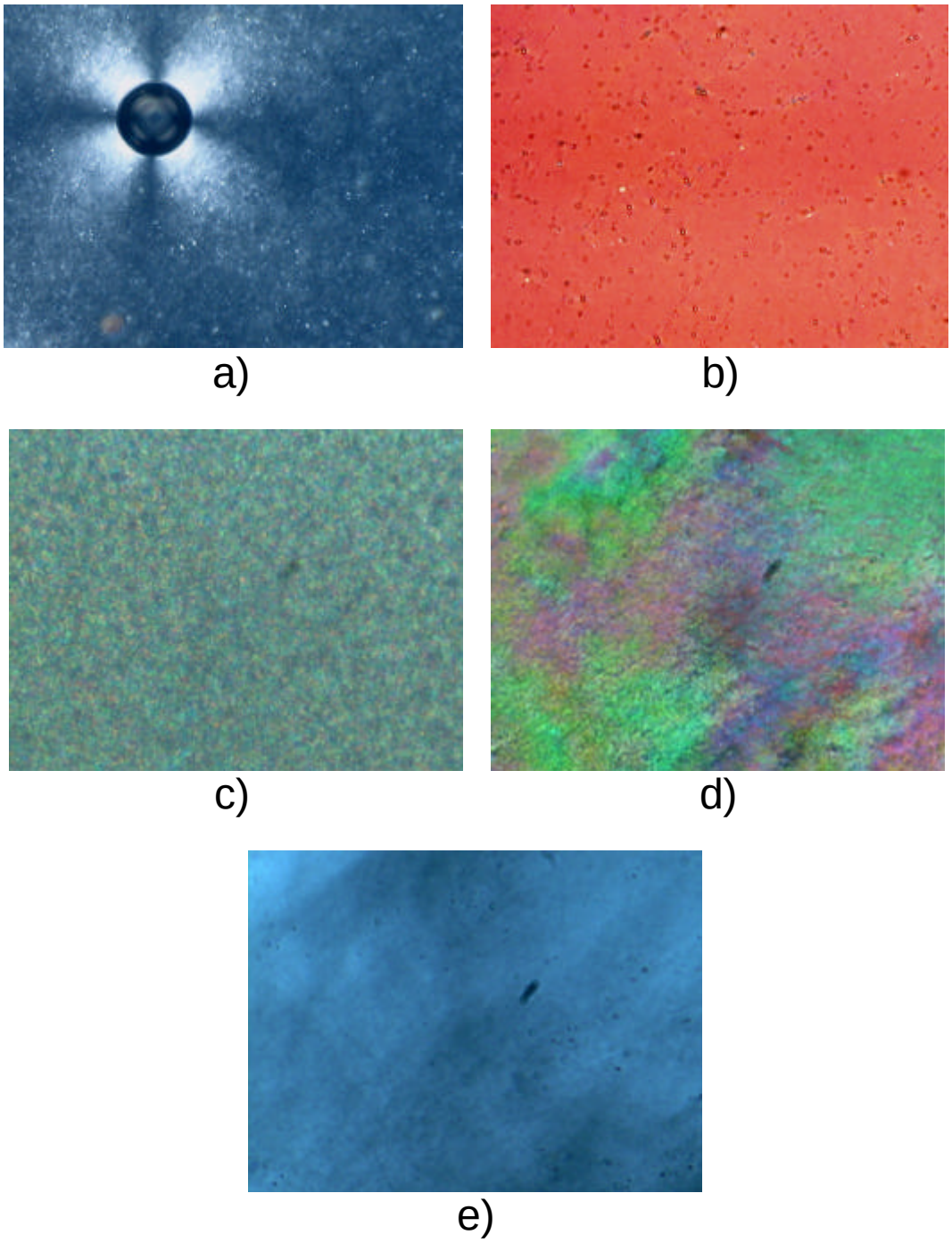

Figure 6.3. POM photographs for a) **N1,** b) **N2**, c) **N5**, and d) **N3** at room temperature, and e) **N3** at 140°C in the isotropic temperature. The birefringence disappeared above 106°C for **N1**. It disappeared above 110°C and 123°C for **N2** and **N5**, respectively, where the clearing temperatures were comparable to their nematic-isotropic phase transition temperature. For **N3**, the birefringence in the nematic phase became very weak in the isotropic phase, but it remained.

6.3.3. Microdomain Structures in the Nematic Block Copolymers

POM observations for **N1**-**N7** were carried out. If the microdomain is disordered or spherical, birefringence can not be observed under cross polarizers, while lamellae and cylinders show birefringence due to their anisotropy. Of course, it appears in LC phase, too.

N1 showed birefringence below 106°C, while it disappeared above the temperature. This indicates that its microdomain morphology was spherical or disordered above 106°C, but not below 106°C.

N3, **N4**, and **N6** showed birefringence in whole temperature region of the nematic phase and the isotropic phase. On the phase transition, the birefringence in the nematic phase drastically changed very weak and colorless but remained in the isotropic phase. This indicates that lamellae or cylinders existed in their isotropic phase.

N2, **N5**, and **N7** also showed birefringence below their transition temperatures, while did not show above the temperature. This indicates that their morphologies in the isotropic phase were spheres or disordered.

TEM observation was carried out for ultrathin sections cut out of the **N1**-**N7** to clarify their morphologies. Here, all copolymers were initially heated up to 140°C, annealed overnight, and then (i) quenched to room temperature in order to vitrify the microdomain morphologies

Table 6.2. Domain spacings and microdomain morphology.

	Domain Spacing [a] / Å		Morphology [d]	
	nematic [b]	isotropic	nematic [b]	isotropic [c]
N1 [e]	224	224 [f]	Poly(***lc2***)-Cyl.	Disorder
N2	233	233 [f]	Poly(***lc2***)-Cyl.	Disorder
N3	284	284	Lam.	Lam.
N4	381	381	PS-Cyl.	PS-Cyl.
N5	448	448	PS-Cyl.	PS-Sph.
N6	191	191	PS-Cyl.	PS-Cyl.
N7	227	227	PS-Cyl.	PS-Sph.

a) Determined by small angle X-ray measurement and calculated from first-order reflection. b) Cooled to room temperature after annealed at 110°C. c) Annealed at 140°C, and then quenched to room temperature. d) Determined by TEM observation. Lam., Cyl., and Sph. denotes alternative lamella, cylinder, and sphere, respectively. e) Its phase sequence was unknown. But the **N1** obtained by same thermal treatment as b and c. f) Calculated from disordered broaden reflection.

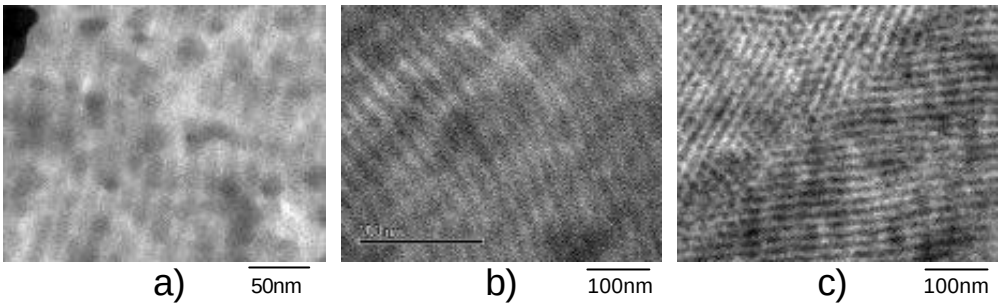

Figure 6.4. Typical transmission electron micrographs for ultrathin section cut out of a) **N1**, b) **N3**, and c) **N6** stained by RuO_4. Dark regions are the PS microdomain. All materials listed in this figure were slowly cooled down from the isotropic phase to room temperature.

at the temperature or (ii) cooled down to room temperature at the rate of 2°C·min^{-1}. Their morphologies are listed in Table 6.2. **N3** showed lamellae, and **N4** and **N6** showed PS-cylinders, which were comparable to their segmental compositions, in the isotropic and nematic phase, respectively. Microdomain morphologies for **N1**, **N2**, **N5**, and **N7** are described below.

6.3.4. Order-Disorder Transition Induced by Nematic Phase

We could not see any aspects even spheres for **N2** in the isotropic phase, while Poly(***lc2***)-cylinders could be seen in the nematic phase in TEM observation (Figure 6.4). According to the result in POM observation, order-disorder transition (ODT) was induced by the nematic-isotropic phase transition. **N2** showed disordered state in the isotropic phase because **N2** had highly asymmetric segmental composition and small M_n. It was reported that symmetric smectic LC block copolymers with low molecular weight composed lamellar type microdomain in the smectic phase but disordered in the isotropic phase[2,5]. ODT induced by nematic phase have not been reported and current study is the first report.

It was expected that the mesogens in Poly(***lc2***)-cylinders aligned along the direction of the cylinders because of elastic energy due to the mesogenic orientation in the nematic phase. This is supported by the fact that Poly(***lc2***)-spheres were not observed. However, we could not confirm it here.

N1 was also treated thermally with the same as (i) and (ii), and observed by TEM. We observed no aspects in the **N1** quenched from 140°C, while Poly(***lc2***)-cylinder in it cooled

down to room temperature. This also shows ODT. The ODT temperature was considered to be 106°C at which birefringence appeared in POM observation. Probably it is also induced by the nematic phase as same as **N2** because Poly(***lc2***)-spheres could not observed. But its phase sequence was not clear, thus we could not determined that the ODT was induced either by some phase transition or *c* dependency of temperature.

6.3.5. Chain Conformation in Nematic Phase

Small angle X-ray scattering measurement was carried out to determine microdomain spacings at the isotropic and the nematic phase by using their fiber specimens. Figure 6.2 shows diffraction patterns for **N4**, in which its fiber axis was placed along vertical direction. A clear first order reflection corresponding microdomain structures can be seen on its horizon in whole temperature region. Localized reflection means that the microdomains aligned along the fiber. **N3** and **N6** also showed same diffraction patterns in the nematic and the isotropic phases, respectively.

The spacings which were calculated from their first-order reflections are summarized in Table 6.2. The microdomain morphologies in **N3**, **N4**, and **N6** did not change throughout all temperature region. Previously, on the other hand, symmetric smectic A_d LC block copolymer, PS-*b*-Poly(***lc1***), which composed lamellar type microdomains, changed the microdomain spacings in the smectic A_d temperature region because of a conformational change in the Poly(***lc1***) segment from a extended form to a random coil[1,2]. On the other hand, the domain spacings of **N3**, **N4**, and **N6** did not change in whole temperature region even if the nematic-isotropic phase transition took place. Compared to the result in PS-*b*-Poly(***lc1***), the unchanged domain spacing in current study means that the conformation of the Poly(***lc2***) segment was the same or hardly changed throughout the phase transition. In the isotropic phase, the main-chain was considered as random coil because of no LC structure. Hence, the random coil of the Poly(***lc2***) segment could be considered to take place also in the nematic phase.

Oriented fiber could not be obtained for **N1** and **N2** but their bulks also showed reflections which was corresponded to microdomain structures or composition fluctuations. **N5** and **N7**

also showed sharp reflections due to their microdomain structures. However, trends of scattering patterns were different from that of **N3**, **N4**, and **N6** as described below.

6.3.6. Order-Order Transition Induced by Matrix of Nematic Phase

Small angle X-ray scattering measurement was carried out for fiber of **N5** as shown in Figure 6.5. In the nematic phase, the reflection was localized at the horizontal direction, which means that the microdomains were aligned along the fiber axis and indicates the microdomain was cylinder or lamella. Moreover, the microdomain morphology was not sphere because it does not show such a localized reflection due to its isotropy. In the isotropic phase at 135°C, on the other hand, the reflection became an isotropic ring. This can be considered either that the orientation of the microdomains was isolated or that the microdomains were altered into spheres or disordered. Again after the fiber was cooled into the nematic phase at 90°C, the reflection was localized at the past position on the horizon. The isolation and localization of the scattering patterns were reversibly on several heating and cooling. Moreover, wide angle X-ray diffraction patterns also showed that the mesogenic director aligned along the fiber axis again as shown in Figure 6.5. This mesogenic orientation is considered to be induced by the orientation of the microdomains. Hence, the isolated reflection in the isotropic phase means that the microdomains lost their alignment due to alteration into spheres or disordered.

To clarify the microdomain morphology, TEM observation was carried out for ultrathin section in two states of **N5**. One was annealed at 140°C overnight, then quenched to room temperature. The other was annealed at 110°C overnight, and then slowly cooled to room temperature at the cooling rate of $1°C \cdot min^{-1}$. Figure 6.6 shows the micrographs of them. In the isotropic phase, dark droplets, which correspond to PS-microdomain, could be seen. As expected in small angle X-ray scattering measurement, the microdomains could be determined as PS-sphere in the isotropic phase. In the nematic phase, on the other hand, some dark lines and ellipsoids could be seen. They can not be regarded as spherical microdomains. Hence, the microdomain morphology was determined as PS-cylinders. In the case of **N7**, TEM photograph shows PS-cylinders in the nematic phase, while PS-spheres could be seen in the isotropic phase as well as **N5**.

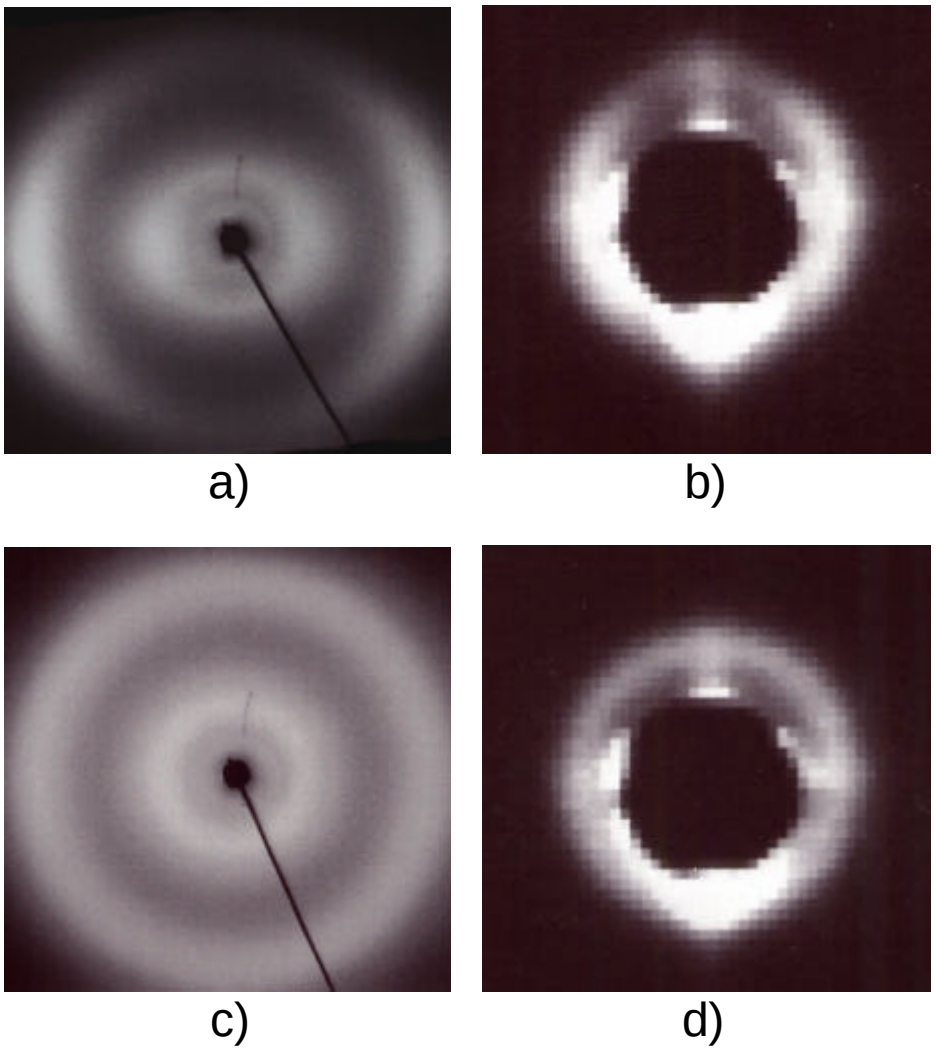

Figure 6.5. Wide angle X-ray diffraction photographs for **N5** in the nematic at 90°C and isotropic phases at 135°C of PS-*b*-Poly(***lc2***) are given in a) and c), respectively. b) and d) are small angle X-ray scattering photographs the corresponding to a) and c), respectively. Here, a fiber specimen was drawn from the nematic and its axis was placed in the vertical direction. The microdomains aligned along the nematic directors in the nematic phase. On the other hand, anisotropy of microdomains disappeared in the isotropic phase.

These results clearly show that the nematic phase altered PS-spheres into PS-cylinders. Additionally, the direction of the PS-cylinders coincided with the nematic director in X-ray studies as described above. In the case of nematic phase, conformation of Poly(***lc2***) segment did not changed through the phase transition as described above. Hence, it is enough to considered only the effect of side-chain mesogenic orientation on the morphological

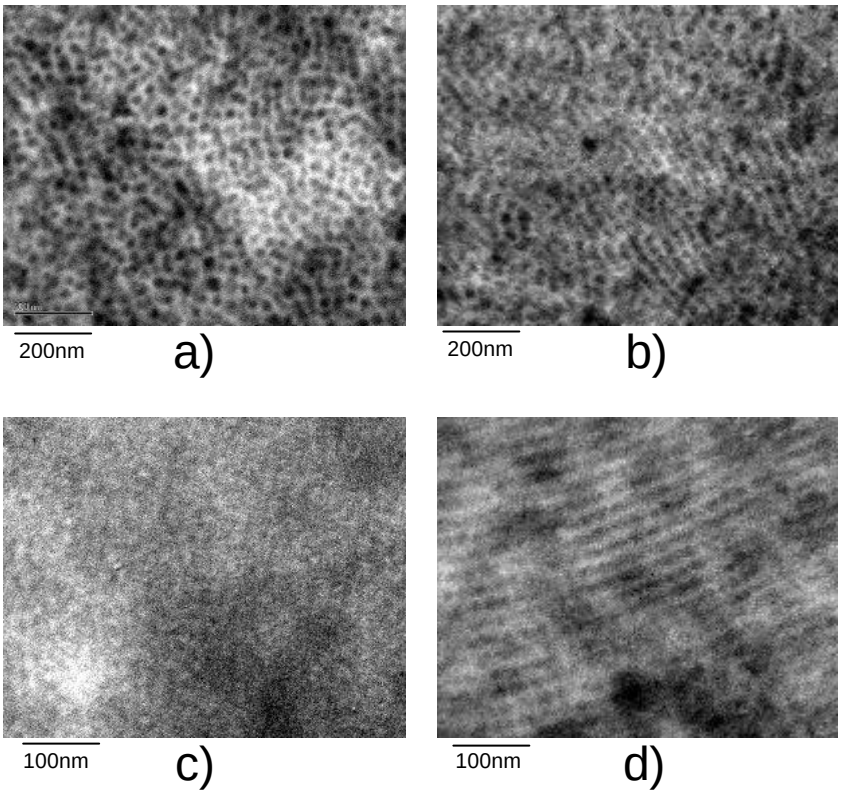

Figure 6.6. Transmission electron microscopic photographs for the ultrathin section cut out of the block copolymers stained by RuO_4. Dark area is the PS microdomain. a) **N5** and c) **N7** quenched from the isotropic phase, respectively. b) **N5** and d) **N7** annealed at 110°C in the nematic phase and then slowly cooled to room temperature, respectively.

transformation. When Poly(***lc2***) segment shows the isotropic phase, PS-*b*-Poly(***lc2***) can be regarded as conventional amorphous-amorphous block copolymer such as polystyrene-*b*-polyisoprene. Hence, **N5** and **N7** had PS-spheres in the isotropic phase as expected from the segmental composition of each segment. On the other hand, PS-spheres had their diameters around 10nm. They were considered to be large defects of the nematic field, while PS-cylinders can be stowed stably in nematic matrix when the mesogens aligned along the same direction of PS-cylinders (Figure 6.8). Thus the PS-spheres in the isotropic phase were altered into PS-cylinders by the elastic energy in the nematic phase. Similar results has already reported by Sänger *et al.* in a PS-*b*-LC-*b*-PS triblock copolymer by TEM observation[3].

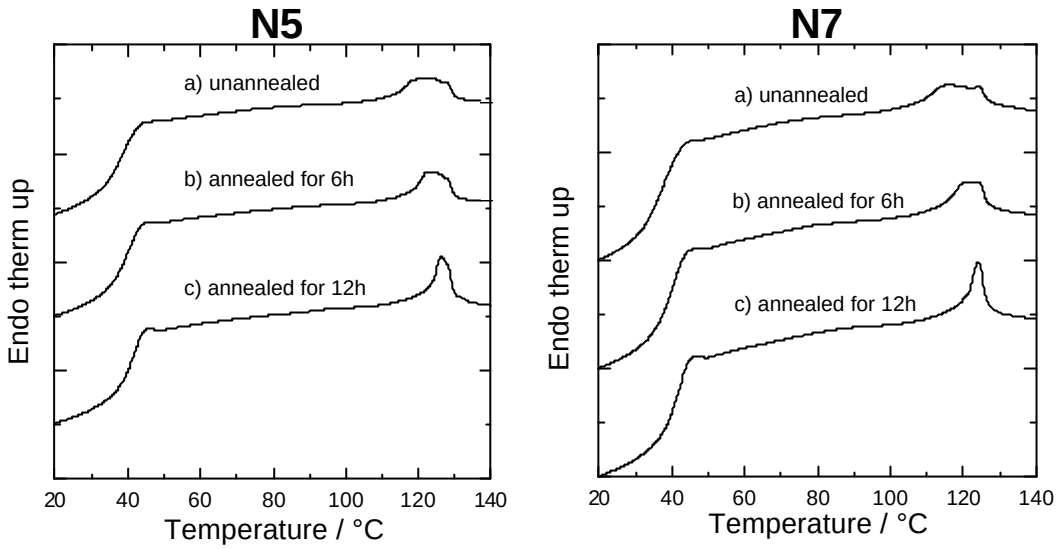

Figure 6.7. DSC thermograms on heating at the rate of 10°C·min^{-1} for **N5** and **N7** after annealed at 115°C for a) 0h, b) 6h, and c) 12h, respectively.

6.3.7. Phase Stability in Microdomain Morphology

N5 and **N7** showed broaden phase transition in DSC measurement as shown in Figure 6.1. The reason is considered due to the morphological transformation on the phase transition. Some researchers reported that LC phase transition temperature depended on their microdomain morphology in smectic LC block copolymers. Yamada *et al.*[6] and Ober *et al.*[7] separately observed that the smectic-isotropic phase transition temperature in cylinder type microdomain was higher than that in lamellae. The reason for the stabilized smectics has not been clarified, but Thomas *et al.* pointed out that the elastic energy in the LC field may change the interfacial energy of the microdomain[8]. In other words, the microdomain morphology in LC block copolymer will also changed the stability of the LC phase, and then will raise the transition temperature. In the same reference, it was also pointed out that the conformational changes of smectic segment may affect the stability of the LC phase in microdomains. We also found the effects of it on microdomains in Chapter 5. On the other hand, such conformational change was not observed in current study for nematic PS-*b*-Poly(***lc2***)s. Hence, only the effect of nematic elastic energy was taken into account.

DSC thermograms of **N5** and **N7** clearly showed annealing effect on the nematic-isotropic

Table 6.3. Thermal behavior dependency of annealing in the nematic phase[a)]

Annealing time[b)]	T_i / °C (ΔH / kcal·mol^{-1})[c)]	
	N5	**N7**
unannealed	116.9 (0.11)	116.2 (0.12)
6h	123.3 (0.16)	121.0 (0.18)
12h	126.4 (0.18)	124.1 (0.18)

a) Thermal data corresponding in Figure 6.7. b) Placement in the nematic phase at 115°C.
c) Transition temperature and corresponding enthalpy changes estimated per mole.

phases transition temperature. **N5** and **N7** were heated to 150°C in the isotropic phase, placed isotherm for 1h in order to eliminate prethermal history, cooled to 115°C in the nematic phase, placed for predetermined hours at the temperature, cooled to 0°C in the glassy nematic state, and then heated. All of heating and cooling rates were 10°C·min^{-1}. The last heated thermograms are exhibited in Figure 6.7. With the annealing, the transitional peak became sharper, and the peak temperature localized at the higher region. The enthalpy changes also slightly enlarged with the annealing as shown in Table 6.3, which means increment of stability of the nematic phase. This indicates that the nematic phase was unstable and difficult to take place with PS-sphere due to increment of elastic energy of nematic.

Interestingly, this also means that the nematic phase can take place within the matrix of PS-spheres. The phase transition corresponded to PS-spheres was obviously exhibited with the reduction of the nematic-isotropic phase transition temperature, which means that the PS-spheres were large defects and that the nematic phase was difficult to take place. Yamamoto and Tanaka reported 'transparent nematic' (TN) phase in which DSC thermograms showed its transitional peak but optically isotropic phase was observed in POM observation in the study of a lyotropic inverse micelle phase composed of water, oil (thermotropic LC, pentylcyanobipnenyl, 5CB), and surfactant (didodecyl dimethyl ammonium bromide, DDAB)[4]. They illustrated the mesogens were perpendicular to the domain boundary in the TN phase. In our case, however, it can be considered that the mesogens lied on the interface because Poly(***lc2***) segment must spread perpendicular to the interface at the domain boundary as illustrated in Figure 6.8a. In this study, we could not obtain true transparent state because the morphological transformation took place at the same time. It needs more investigation of TN phase in LC block copolymers.

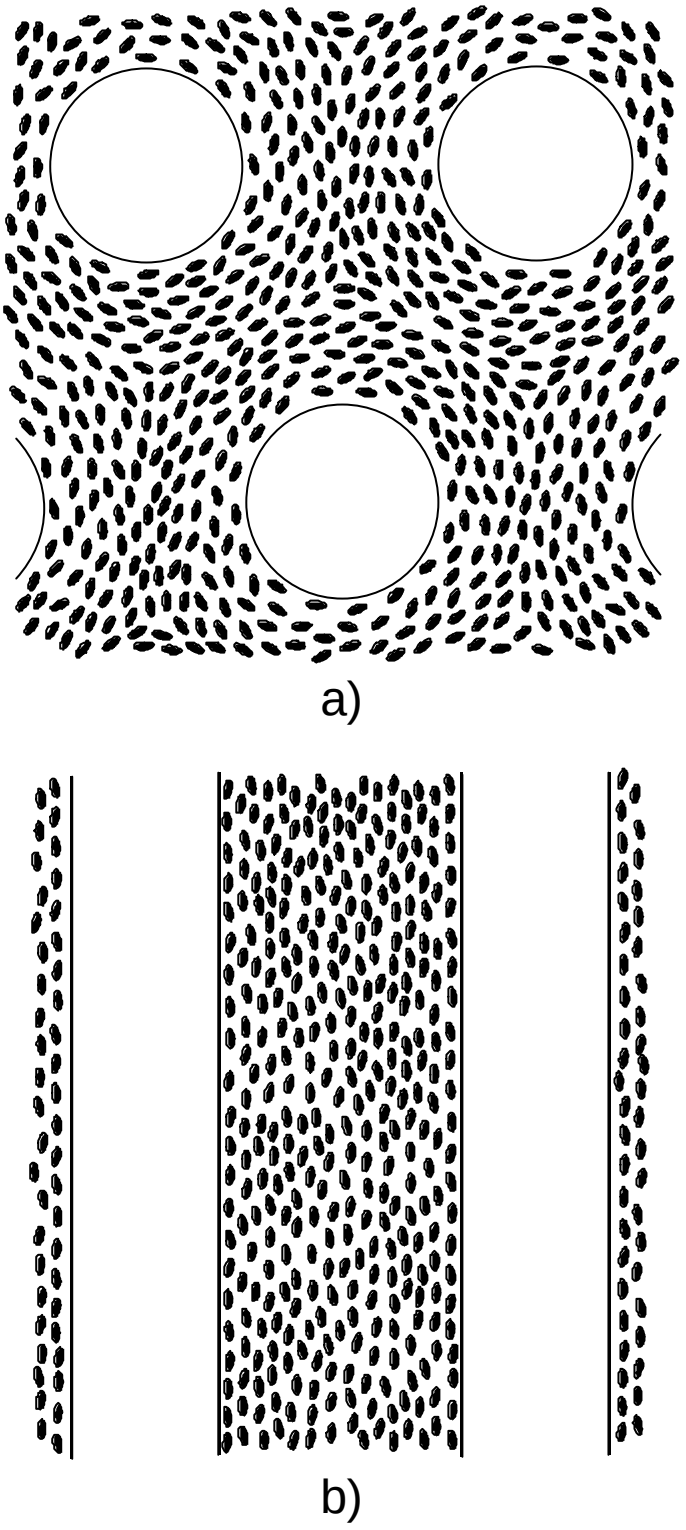

Figure 6.8. Schematic illustrations of the nematic phase with a) PS-spheres (namely ‘transparent nematic’) and b) PS-cylinders.

6.4. Concluding Remarks

We studied seven nematic LC block copolymers (PS-*b*-Poly(***lc2***)s) containing polystyrene (PS) and poly(6-[4-(4'-cyanophenyl)phenoxy]hexyl acrylate) (Poly(***lc2***)) with various compositions and molecular weights synthesized by atom transfer radical polymerization. Phase sequence of a PS-*b*-Poly(***lc2***) with 10wt% of Poly(***lc2***) segment could not be determined. Poly(***lc2***) segments in the other materials showed isotropic phase, nematic phase, and vitrified nematic phase. The microdomain spacings in the isotropic phase remained in the nematic phase, which indicates that conformation of Poly(***lc2***) segment was random coil in the nematic phase. Order-disorder transition induced by the nematic-isotropic phase transition can be seen in a PS-*b*-Poly(***lc2***) with 17wt% of Poly(***lc2***) segment where the disordered microdomain in the isotropic phase was altered into Poly(***lc2***)-cylinderes in the nematic phase. Two PS-*b*-Poly(***lc2***)s with the 73wt% of Poly(***lc2***) segments showed PS-spheres in the isotropic phase as expected from the composition, while PS-cylinders were formed in the nematic phase and their directors were the same as mesogenic directors. This means the elastic energy in the nematic field induced the director of PS-microdomains with transforming microdomain morphology. Additionally, the nematic-isotropic transition temperature was higher and sharper in PS-cylinders than that of PS-spheres. Corresponding enthalpy also enlarged in PS-cylinders compared with in PS-spheres. This means that the PS-spheres reduce the stability of the nematic phase due to disturbance of the mesogenic alignment and increment the elastic energy at the interface of PS-spheres. Moreover, we obtained a result that 'transparent nematic' phase was indicated in the matrix of the PS-spheres.

References in This Chapter

1. M. Yamada, T. Iguchi, A. Hirao, S. Nakahama, and J. Watanabe, *Macromolecules*, **28**, 50 (1995).
2. M. Yamada, T. Iguchi. A. Hirao, S. Nakahama, and J. Watanabe, *Polym. J.*, **30**, 23 (1998).
3. J. Sänger, W. Gronski, S. Maas, B. Stühn, and B. Heck, *Macromolecules*, **30**, 6783 (1997).
4. J. Yamamoto and H. Tanaka, *Nature*, **409**, 321 (2001).
5. W. Y. Zheng, R. J. Albalak, and P. T. Hammond, *Macromolecules*, **31**, 2686 (1998).

6. M. Yamada, T. Itoh, R. Nakagawa, A. Hirao, S. Nakahama, and J. Watanabe, *Macromolecules*, **32**, 282 (1999).
7. G. Mao, J. Wang, S. R. Clingman, C. K. Ober, J. T. Chen, and E. L. Thomas, *Macromolecules*, **30**, 2556 (1997).
8. C. O. Osuji, J. T. Chen, G. Mao, C. K. Ober, and E. L . Thomas, *Polymer*, **41**, 8897 (2000).

Chapter 7

Summary

The main subject of this thesis is establishment of new techniques to control of molecular structure, liquid crystalline (LC) structure, and microdomain structure throughout the study in LC block copolymer containing amorphous polymer segment and side-chain LC polymer (SCLCP) segment. For this purpose, three parts including synthesis of LC block copolymers, effects of the microdomain structure on the phase behavior, and effects of the LC phase behavior on the microdomain structures were investigated by using two LC species of nematic and smectic A_d and using two systems including neat LC block copolymer and blends with corresponding homopolymer. Obtaining results throughout this thesis are reconstituted and summarized in the last chapter.

7.1. Synthesis of LC Block Copolymer (Control of Molecular Structure)

We can use some techniques to synthesize LC block copolymers, which have some advantages and disadvantages. It is one of the important area to investigate better method of synthesis. We have discussed and determined currently the best method of synthesis for LC block copolymer as following.

7.1.1. Polymer Analogous Reaction

Polymer analogous reactions were widely used because of its ability to obtain well-controlled LC block copolymers with wide range of molecular weight and narrow molecular weight distribution (MWD). A functionalized segment in some block copolymer combines mesogenic materials to prepare LC block copolymer. But a fatal disadvantage is that LC block copolymers have some defects in their LC segment owing to the incomplete conversion to introduce the mesogenic moiety in the precursor. Hence, we can not discuss behaviors of the main-chain in the LC segment, which has an important role to compose

microdomain structures. (reference 1-4 in Chapter 2)

7.1.2.Living Anionic Polymerization

Other techniques are direct polymerizations of mesogenic monomers by some living systems. Living anionic polymerization is the best method to obtain a well-defined block copolymer with a controlled molecular weight and a very narrow MWD. It enables us to discuss the role of the main-chain in the LC segment which is an important factor of determining microdomain morphologies. Using living anionic polymerization, we synthesized and successfully obtained smectic A_d LC block copolymers containing polystyrene segment and poly(6-[4-(4'methoxyphenyl)phenoxy]hexyl methacrylate) segment with various compositions, various molecular weights, and narrow MWDs (<1.05). However, living anionic polymerization also has some disadvantages. Styrenic and methacrylic LC monomers are available but acrylic LC monomers currently can not be used. Furthermore, functional groups are limited. Hence, living anionic polymerization can not prepare LC block copolymers with various LC moieties. Moreover, the LC block copolymers can not have large molecular weight with various compositions in some case. (M. Yamada *et al.*, *Macromolecules*, **28**, 50 (1995) and in Chapter 2)

7.1.3.Atom Transfer Radical Polymerization

Living radical polymerizations dissolve the problems in living anionic polymerization, because it hardly has these limitations for LC monomer species and functional groups. In Chapter 2, atom transfer radical polymerization (ATRP) has been able to produce LC block copolymers with conventional SCLCP with controlled molecular weights and various compositions. MWD is generally rather wide than living anionic polymerization (M_w/M_n=1.1~1.3). However, we can discuss the role of the main-chain in the LC segment. Moreover, thermally stable polymers can be synthesized by this technique, while thermally unstable polymers are obtained by other living radical system of nitroxide mediated radical polymerization (NMP) and reversible addition-fragmentation chain transfer (RAFT). If the living propagation end is transformed and stabilized thermally, methacrylates are not available in NMP and PS-precursor is not available in RAFT. We synthesized and successfully obtained

nematic LC block copolymers containing polystyrene segment and poly(6-[4-(4'-cyanophenyl)phenoxy]hexyl acrylate) segment by ATRP. (in Chapter 2)

7.2. Effects of Block Copolymer on LC Phase Behavior (Control of Nanometers Ordered LC Structure)

It has been clarified that LC phase behavior strongly depends on microdomain morphologies in the LC block copolymers. Additionally we note the conformation of main-chain back bone of LC segment, which is not an effect of the microdomain but is clarified through LC block copolymer with its domain size.

7.2.1. Microdomain Morphologies

Previously it was found that smectic structure is stable in cylinders rather than lamellae and spheres. Nematic phase also clarified to be stable in cylinders rather than spheres because spherical microdomains inhibit one-dimensional mesogenic alignment. However, the nematic phase can take place at the matrix of spheres ('transparent nematic' phase) with reduction of its stability. (in Chapter 6)

Microdomains strongly affect on the mechanism of phase transition. Throughout kinetic studies in the isothermal crystallization quenched from LC phase, microdomain interfaces dominate the nucleation mechanism, which is homogeneous in LC homopolymer and heterogeneous in LC block copolymer. It has been also clarified that the growth of the crystallization drives within its microdomain and is not carried into neighboring LC microdomain beyond intermediary microdomain of its counter segment. (in Chapter 4)

7.2.2. Composition Fluctuation

Most of researchers are interested in the LC phase behavior only in microphase segregated structures. But we clarified and pointed out that composition fluctuations also play an important role throughout the study in isothermal crystallization kinetics and orientational behavior in fibers. LC phase behaviors are strongly affected by the composition fluctuation because of a disturbance LC structure. It reduces stability of LC phase, which was observed in

thermal measurement. At the same time, the composition fluctuation behaves like microphase segregated structures even if the interface of microdomains is smeared. The composition fluctuation was elongated in a fiber drawn from the isotropic phase, and then side-chain mesogenic layers sprayed perpendicular to the fiber axis, while side-chain mesogenic layers in a fiber of corresponding LC homopolymer were aligned parallel to the fiber axis. Moreover, crystallization mechanism was different from the homopolymer because the composition fluctuation behaved as nuclei of crystallization. (in Chapter 4)

7.2.3. Main-Chain Back Bone Behavior

In smectic A_d temperature region, the main-chain conformation of LC segment in smectic A_d LC block copolymer continuously changed from random coil in the isotropic phase to extended form in the crystalline phase. The reason for the conformational change is a counterbalance between entropic gain of the main-chain conformation and energetic loss of the mesogenic layered structure (M. Yamada *et al.*, *Polym. J.*, **30**, 23 (1998)). The kinetic study indicates that the same conformational changes took place in corresponding LC homopolymer (in Chapter 4).

On the other hand, nematic LC block copolymer shows invariant microdomain spacings throughout the isotropic and nematic phases, which indicates that the nematic LC segment retains random coil in the nematic phase. (in Chapter 6)

7.3. Morphological Transformation in LC Block Copolymer Induced by LC Phase Behavior (Control of Tens Nanometers Ordered Microdomain Structure)

It is also clarified that LC phase behavior strongly influences microdomain structure in LC block copolymer. It can change sizes and morphologies of microdomain. The factors of the changes are nematic elastic energy, smectic layered packing, and conformational changes of its LC segment. Another technique, for example, blending homopolymer, is also available.

7.3.1. Nematic Elastic Energy

Nematic phase is difficult to take place with spherical microdomains without vitrification

or blend. We showed a morphological order-disorder transformation in nematic LC block copolymer. Microdomains are disordered in the isotropic phase, while LC-cylinder is induced by the nematic phase. LC-sphere can not be observed in the neat nematic LC block copolymer. (in Chapter 6)

We also showed a morphological order-order transformation in nematic LC block copolymer induced by nematic elastic energy. Spherical microdomains in the isotropic phase altered into cylindrical microdomains in the nematic phase. The directors of the cylinders and mesogens are the same. This clearly means that the nematic mesogenic directors do not prefer spherical microdomains because they disturb the nematic fields, and that cylindrical microdomains allow nematic director alignments along the cylindrical axis. (in Chapter 6)

7.3.2. Anisotropic Chain Conformation in Smectic

LC segment in smectic LC block copolymer has anisotropic chain conformation in the smectic phase due to the smectic layered packing. It ceases anisotropic chain conformation to its counter segment. If the counter segment can not hold the anisotropy in lamellae, the interface of the microdomain is bent and the counter segment fills matrix of LC-cylinders in order to relax the anisotropy. (in Chapter 3)

7.3.3. Conformational Change in LC segment

Sizes of microdomains in smectic A_d LC block copolymer are continuously changed by the conformational changes of LC segment in smectic A_d temperature region. This property enables to control the size of microdomains. (M. Yamada *et al.*, *Polym. J.*, **30**, 23 (1998))

Microdomain morphologies are also altered by the extension of the LC segment. We have studied blends of symmetric smectic A_d LC block copolymer which composed lamellar type of microdomains and corresponding amorphous homopolymer. In wet-brush regime, we observed LC-spheres at high temperature near the isotropization temperature in the smectic phase, while LC-lamellae can be seen at low temperature near the crystallization temperature. This can be explained that spherical and cylindrical microdomains can not stow the extended segmental chains, but only LC-lamellae can do. At the same time, the solution style was also altered from wet-brush regime into dry-brush regime where the homopolymer was excluded

from the interface of the block copolymer. (in Chapter 5)

7.4. Future Works

In this thesis, we have studied AB type of diblock copolymers containing amorphous segment and LC segment in which smectic A_d phase and nematic phase take place. On the other hand, LC phase has more variable structures and properties such as helical cholesteric structure, ferroelectric chiral smectic, mesogenic alignment with magnetic or electric field, and so on. We have succeeded in living radical polymerization of LC block copolymer, thus it is enable us to obtain LC block copolymers containing variable LC species, while past methods could not. We need more studies to clarify the effects of the microdomain structures on LC phase behaviors and those of the microdomains on LC phase behavior in the study of various LC block copolymers.

We treated neat LC block copolymer and its blends with corresponding homopolymer. Other systems such as blends with low molecular weight and various LC moieties are also an interesting study which is a branch of this thesis, which will be a typical wet-brush regime in the area of polymer blends. Moreover, mechanical analysis should clarify more property of LC block copolymers, but it has not been studied well.

It is also an interesting study in ability of LC block copolymers in applications such as devices. Referring to the study of blend system in this thesis, we also note that LC block copolymer can be used as a surfactant (compatibilizer). Applying to polymer dispersed LC system, for example, LC block copolymer will reduce surface free energy between polymer and other LC moieties. Stable and tailor-made particles and nano-structures can be expected with this technique. Moreover, surface grafting SCLCP can be obtained by using LC block copolymer. It will dissolve a problem of an interaction between surface and low molecular weight LC moieties in LC display. Living radical polymerization can be also produce directly surface grafting SCLCP. We believe that obtaining results and aspects in this thesis are useful for applications.

LC block copolymer system is interesting from views of studies in both block copolymer field and LC (not limited in LC polymer) field. Some black boxes and difficulties have been

remained. However, we believe that LC block copolymers have enormous potential of clarifying fundamental problems in block copolymer field and LC field. Furthermore, we also believe, expect, and propose that LC block copolymer is one of the great materials in nano-technologies.

List of Publications

1. ‘Side-chain LC block copolymers with well defined structures prepared by living anionic polymerization. 2: Effect of the glass transition temperature of amorphous segments on the phase behavior and structure of the LC segment’

   M. Yamada, **T. Itoh**, A. Hirao, S. Nakahama, and J. Watanabe, *High Perform. Polym*., **10**, 131 (1998).

2. ‘Synthesis of Side-Chain Liquid Crystalline Homopolymers and Block Copolymers with Cyanobiphenyl Moieties as the Mesogen by Living Anionic Polymerization and Their Thermotropic Phase Behabior’

   M. Yamada, **T. Itoh**, R. Nakagawa, A. Hirao, S. Nakahama, and J. Watanabe, *Macromolecules*, **32**, 282 (1999).

3. ‘Side-Chain LC Block Copolymers with Well Defined Structures Prepared by Living Anionic Polymerization. 3: Effect of the Composition on the Microdomain Structure and the Phase Behavior of the LC Segment’

   T. Itoh, M. Yamada, A. Hirao, S. Nakahama, and J. Watanabe, *Mol. Cryst. Liq. Cryst*., **347**, 211 (2000).

4. ‘Side-Chain LC Block Copolymers with Well Defined Structures Prepared by Living Anionic Polymerization IV. Microphase Morphology in Blends with Coil Homopolystyrenes’

   T. Itoh, N. Tomikawa, M. Yamada, M. Tokita, A. Hirao, and J. Watanabe, *Polym. J.*, **33**, 783 (2001).

(out of this thesis)

1. ‘Aromatic Polyesters with Flexible Side Chains. 8. Studies on Long Periodical Structure Observed in Layered Crystalline Phase’

   K. Fu, T. Nematsu, M. Sone, **T. Itoh**, T. Hayakawa, M. Ueda, M. Tokita, and J. Watanabe, *Macromolecules*, **33**, 8367 (2000).

Acknowledgements

The investigations described in this thesis were carried out at the Department of Polymer Chemistry, Tokyo Institute of Technology.

I wish to express his science gratitude to Professor Junji Watanabe for his invaluable guidance, stimulating discussions and encouragements throughout this work.

Grateful acknowledgement is due to Dr. Masayuki Yamada for his teaching and encouragement.

I am sincerely grateful to Dr. Jun Yamamoto (ERATO), Dr. Susumu Kawauchi, and Dr. Masatoshi Tokita in all around of this work, Dr. Tsuneo Chiba in TEM observations, Professor Takeshi Fukuda (Kyoto University) in synthesis of materials for their helpful suggestions.

Sincere appreciation is due to all of my colleagues for their kind helps, particularly, to Mr. Naoki Tomikawa and Mr. Yusuke Okazaki, for their active collaborations in a part of this work.

This dissertation work was supported in part by a Research Fellowship of Japan Society of Promotion of Science for Young Scientists (2001-), which is gratefully acknowledged.

Finally, I heartily wish to express my thanks to my parents, Tadaatsu Itoh and Ikuko Itoh, my sisters, Yasuyo Itoh and Mutsumi Itoh, and to my grandmother, Masae Itoh, for their devoted support.

March, 2002

Tomomichi Itoh